SIMNRA User's Guide

Matej Mayer
Max-Planck-Institut für Plasmaphysik
Boltzmannstr. 2
D-85748 Garching
Germany
email: Matej.Mayer@ipp.mpg.de
Tel.: ++49 89 32991639
Fax.: ++49 89 32992279
www.rzg.mpg.de/∼mam

This manual describes SIMNRA version 5.0

Additional publications about SIMNRA (You can use the first as general reference for the program):

- M. Mayer, *SIMNRA User's Guide*, Report IPP 9/113, Max-Planck-Institut für Plasmaphysik, Garching, Germany, 1997
- M. Mayer, *SIMNRA, a Simulation Program for the Analysis of NRA, RBS and ERDA*, Proceedings of the 15th International Conference on the Application of Accelerators in Research and Industry, J. L. Duggan and I.L. Morgan (eds.), American Institute of Physics Conference Proceedings **475**, p. 541 (1999)
- W. Eckstein and M. Mayer, *Rutherford Backscattering from layered Structures beyond the Single Scattering Model*, Nucl. Instr. Meth. **B153** (1999) 337
- M. Mayer, *Ion Beam Analysis of Rough Thin Films*, In print at Nucl. Instr. Meth. **B**

SIMNRA IS NOT FREE. IT IS A SHAREWARE PROGRAM AND COSTS BETWEEN 200-300 US$. YOU CAN USE SIMNRA FOR A TRIAL PERIOD OF THIRTY (30) DAYS WITHOUT FEE. IF YOU WANT TO USE SIMNRA AFTER THIS PERIOD, YOU HAVE TO PAY THE REGISTRATION FEE AND YOU HAVE TO REGISTER THE PROGRAM.

The pricing is as follows:

200 US$	for a single researcher
250 US$	for a university research laboratory
300 US$	for an industry research laboratory

Registered users of any previous version of SIMNRA can upgrade their registration for a reduced fee:

100 US$	registered users of any previous version of SIMNRA

Please pay the registration fee to

Max-Planck-Institut für Plasmaphysik
Account: 5804058488
Bank: Hypobank München
Bank Routing Code: 70020001

Please indicate on the remitance that the money is intended for SIMNRA.

To register the program and get a registration number either send an email, a letter by surface mail, or send a fax to Dr. Matej Mayer. The address can be found on the title page of this manual. You will receive your registration number within a few days. Run the program and click HELP:REGISTER... to enter the registration number.

Most cross-section data files included with SIMNRA have been taken from SigmaBase (http://ibaserver.physics.isu.edu/sigmabase). These cross-section data files are not included in the shareware fee, but are freely available from SigmaBase. See the file //ibaserver.physics.isu.edu/sigmabase/newuser.html for more information about SigmaBase. The stopping power data files SCOEF.95A and SCOEF.95B have been taken from the SRIM 97 distribution. These files are not included in the shareware fee, but are freely available for scientific purposes.

SIMNRA was developed at the Max-Planck-Institut für Plasmaphysik, Garching, Germany.

NOTICE TO USERS: CAREFULLY READ THE FOLLOWING LEGAL AGREEMENT. THIS LICENSE AGREEMENT IS PART OF SIMNRA. USE OF SIMNRA PROVIDED WITH THIS AGREEMENT CONSTITUTES YOUR ACCEPTANCE OF THESE TERMS. IF YOU DO NOT AGREE TO THE TERMS OF THIS AGREEMENT, PROMPTLY REMOVE SIMNRA TOGETHER WITH ALL COPIES FROM YOUR COMPUTER. THE CROSS SECTION DATA FILES IN R33 AND RTR FILE FORMAT (*.R33 AND *.RTR FILES) STORED IN THE CRSEC SUBDIRECTORY ARE EXCLUDED FROM THIS AGREEMENT: THESE FILES HAVE BEEN TAKEN FROM SIGMABASE AND ARE SUBJECT TO THE TERMS LISTED IN http://ibaserver.physics.isu.edu/sigmabase/newuser.html. THE FILES SCOEF.95A and SCOEF.95B STORED IN THE STOP DIRECTORY ARE EXCLUDED FROM THIS AGREEMENT: THESE FILES HAVE BEEN TAKEN FROM THE SRIM 97 CODE AND ARE SUBJECT TO THE TERMS LISTED IN THE SRIM MANUAL, WHICH MAY BE OBTAINED FROM www.research.ibm.com/ionbeams.

PRODUCT LICENSE AGREEMENT

1. You have the right to use SIMNRA freely for thirty (30) days for the purpose of evaluation. After thirty days you must either buy SIMNRA or remove it from your computer and stop using it.

2. You may upload SIMNRA to any electronic bulletin board or demonstrate the software and its capabilities. If you copy or upload SIMNRA you must copy or upload it together with all files, including this license. You may not reproduce or distribute SIMNRA for resale or other commercial purposes, including bundling with any product that is offered for sale.

3. Copyright: SIMNRA is protected by international copyright law. The owner of the copyright is the Max-Planck-Institut für Plasmaphysik. You agree that any copies of SIMNRA will contain the same proprietary notices which appear on and in the software. You are not alowed to distribute any modified versions of SIMNRA.

4. Warranty: SIMNRA is provided AS IS AND WITH ALL FAULTS. The author and the Max-Planck-Institut für Plasmaphysik make no warranties with respect to the program and the program data. The author and the Max-Planck-Institut für Plasmaphysik do not warrant that the program or any of its data is error free. The author and the Max- Planck-Institut für Plasmaphysik disclaim all warranties with respect to the software or its data, either express or implied, including but not limited to implied warranties of merchentability, fitness for a particular purpose, and nonfringement of third-party rights. No liability is assumed for damages, direct or consequential, which may result from the use of this software.

Contents

Chapter 1

Overview

This report describes the use of the program SIMNRA and the physical concepts implemented therein. SIMNRA is a Microsoft Windows program for the simulation of back- or forward scattering spectra for ion beam analysis with MeV ions. SIMNRA is mainly intended for the simulation of spectra with non-Rutherford backscattering cross-sections, nuclear reactions and elastic recoil detection analysis (ERDA). About 300 different non-Rutherford and nuclear reaction cross-sections for incident protons, deuterons, ^{3}He and ^{4}He-ions are included. SIMNRA can calculate spectra for any ion-target combination including incident heavy ions and any geometry including transmission geometry. Arbitrary multi-layered foils in front of the detector can be used. SIMNRA uses the Ziegler-Biersack values for the electronic stopping powers of swift and heavy ions and the universal ZBL-potential for the calculation of nuclear stopping. Alternatively the Andersen-Ziegler values for electronic stopping powers may be used. Energy loss straggling is calculated including the corrections by Chu to Bohr's theory. Energy loss straggling propagation in thick layers is considered correctly. Additionally the effects of plural large angle scattering and surface roughness can be calculated approximately. Data fitting (layer thicknesses, compositions etc.) is possible by means of the Simplex algorithm. OLE automation allows automated analysis of large numbers of spectra.

In contrast to other programs for the simulation of backscattering spectra SIMNRA is easy to use due to the Microsoft Windows user interface. SIMNRA makes full use of the graphics capacities of Windows.

This manual is organised in the following way:

- System requirements and the installation of the program are described in chapter 2.
- The use of the program is described in chapter 3. A quick overview about the steps necessary to calculate a spectrum is given in chapter 3.1. More details are found in the rest of chapter 3.
- The physical concepts implemented in the program are described in detail in chapter 4.

- Some examples for the abilities of the program are shown in chapter 5.

Chapter 2

Installation

2.1 System requirements

- SIMNRA requires Windows 95, 98, NT, 2000 or XP.
- Super-VGA resolution of 800 × 600 pixels or higher is recommended.
- SIMNRA requires about 5 MB free hard disk space.
- The User's Guide and help system require Adobe Acrobat or Acrobat Reader. See section 3.11 for more details.
- Reading spectrum data in Canberra's CAM-file format requires the Genie-2000 software package. See section 3.2 for more details.

2.2 Installation

The installation of SIMNRA on Windows NT or Windows 2000 systems requires administrator privileges. SIMNRA is distributed with a setup program. To install SIMNRA simply run the setup program and follow the instructions. After running the setup program you should have obtained the files listed in table 2.1.

To register run SIMNRA, click `About:Register...` and enter your registration number in the appropriate field.

2.3 Uninstalling SIMNRA

SIMNRA is shipped with an automatic uninstall program. Refer to your Microsoft Windows documentation on how to uninstall programs.

Directory	Files	
	SIMNRA.EXE	executable program
	README.TXT	Readme file
	CHANGES.TXT	Describes the changes since version 3.0
	LICENSE.TXT	Product license agreement
	MANUAL.PDF	This manual
\ATOM	ATOMDATA.DAT	atomic data
\STOP	STOPH.DAT	electronic stopping power data (Andersen/Ziegler)
	STOPHE.DAT	
	LCORRHI.DAT	
	SCOEF.95A	electronic stopping power data (Ziegler/Biersack)
	SCOEF.95B	
	CHU_CORR.DAT	Chu correction data to Bohr straggling
\CRSEC	CRSDA.DAT	cross-section data
	*.R33	
	*.RTR	
\DLL	*.DLL	dynamic link libraries used by SIMNRA
\SAMPLES	*.NRA	examples
\LAYERS	*.LAY	predefined materials (mylar, stainless steel)
\DEFAULT	SETUP.NRA	default experimental setup
\USERDLL	SAMPLE*.DPR	Code examples in Pascal for user supplied dynamic link libraries, see Section 3.13

Table 2.1: Directory structure and files used by SIMNRA.

Chapter 3

Using SIMNRA

3.1 Basic steps

This section gives a quick overview about the basic steps necessary to calculate a backscattering spectrum.

Three steps must be performed before a backscattering spectrum can be calculated: In a first step the experimental situation (incident ions, geometry) has to be defined, then the target must be created, and in a third step the cross-sections used for the calculation have to be chosen.

1. Click `Setup:Experiment`. Here you choose the incident ions, the ions energy, define the scattering geometry (see fig. 3.2), and you enter the energy calibration of the experiment.

2. Click `Target:Target`. Here you create the target. Each target consists of *layers*. Each layer consists of different elements with some atomic concentration, which does not change throughout the layer, and each layer has a thickness.

3. If there is a foil in front of the detector, then click `Target:Foil` for the definition of a foil. The default is no foil in front of the detector. Like the target, the foil can consist of different layers, and the layers can have different compositions.

4. Click `Reactions`. Here you have to choose which cross-section data should be used for the simulation. The default are Rutherford cross-sections for all elements. You can select non-Rutherford cross-sections instead and you can add nuclear reactions.

5. Now the spectrum can be calculated. Click `Calculate:Calculate Spectrum` for a simulation of the spectrum.

6. With `Setup: Calculation` the parameters for the calculation can be altered. The default values are normally sufficient, and you should change these values only if you know what you are doing.

7. With `File:Read Spectrum Data` a measured spectrum can be imported for comparison with the simulated one and for data fitting.

3.2 `File` menu

In the `File` menu all necessary commands for reading and saving files and data, printing spectra and terminating the program are located.

- `New`: This menu item resets the program to its starting values. All calculated spectra, target, foil and setup definitions are deleted.
- `Open...`: This menu item reads a saved calculation from disk.
- `Save`: This menu item saves all current parameters, target and foil definitions, experimental and simulated data to disk. The data are saved as an ASCII file. The default file extension is NRA.
  Depending on the settings in `Options: Preferences: Saving` (see section 3.10) the old NRA-file can be saved to a file named BACKUP.NRA. In the case of erraneous overwriting of a file you can recover the old data from this file.
- `Save as...`: Like `Save`, but you will be prompted for the name of the file.
- `Read Spectrum Data`: This menu item allows the import of experimental data. The availability of menu items depends on the settings in `Options: Preferences`.

  `Read Spectrum Data: ASCII...`: Allows the import of experimental data in ASCII format.

  The data file format must be as follows: The file may contain an arbitrary number of comment lines at the beginning of the file. A comment line is a line that contains any non-numeric character. These lines will be ignored. The first line that contains only numeric characters will be treated as the first line of data. Each data line must consist of two columns: In the first column the channel number must be given (Integer), in the second column the number of counts must be given (Double). The two columns are separated by an arbitrary number of blanks or tabs. Each line must end with <CR><LF>[1]. The data file may contain up to 8192 channels. An example for a valid data file is given in fig. 3.1.

  `Read Spectrum Data: Canberra...`: Allows the import of spectral data stored in Canberra's CAM file format.

  SIMNRA uses Canberra's Genie-2000 software package for reading CAM files. The Genie-2000 package is not part of SIMNRA and must be obtained separately from Canberra Industries. This package must be installed correctly before you can read CAM files. The dynamic link libraries sad.dll etc. must be in the search path, and the virtual data manager (VDM) must be installed. SIMNRA has been tested with Genie-2000 versions 1.3 and 1.4.

  Note: SIMNRA reads only spectral data stored in CAM files. Any other information which may be stored in the CAM file, like energy calibration etc., is ignored.

[1] <CR> means Carriage Return (#13 decimal), <LF> means Line Feed (#10 decimal).

`Read Spectrum Data: IPP...`: Reads experimental data stored in the data file format used at the IPP Garching, Germany. This data file format will not be described here.

`Read Spectrum Data: ISI...`: Reads experimental data stored in the data file format used at ISI, Jülich, Germany. This data file format will not be described here.

`Read Spectrum Data: User...`: Allows to read experimental data stored in any user defined format. A dynamic link library (dll) has to be supplied by the user, which reads the data and passes them to SIMNRA. See Section 3.13 for more details.

- `Write Spectrum Data...`: This menu item exports the experimental and simulated data as columns into an ASCII file. You can import this file easily into any plot program, such as Excel, Origin or Mathematica.

  The file format is as follows: The first line is a comment line which contains information about the contents of the different columns. The first column is the channel number, the second column contains the experimental data (This column is set to zero if experimental data are not available), the third column contains the simulated data (This column is set to zero if simulated data are not available). If the `Element spectra` option in `Setup: Calculation...` is checked, then the next columns will contain the simulated spectra for each element in the target. The columns are separated with blanks.

- `RUMP: Read RBS File...`: This menu item allows to read a binary RBS-file produced by RUMP containing experimental parameters (Type of incident particles, incident energy, scattering geometry, etc.) and spectral data.

  Note 1: RUMP stores the description of the sample and the absorber foil in sample description files (*.LCM). You can read sample description files with `RUMP:Read Sample Description File...`.

  Note 2: The RBS-file may contain only one experimental spectrum. Compression level 3 (zero compression) is not implemented. See section 3.12 for more details.

- `RUMP: Read Sample Description File...`: This menu item allows to read a sample description file produced by RUMP or the IBA data furnace NDF. The default file extension of sample description files is *.LCM.

  Note 1: RUMP stores the description of the sample and the absorber foil in sample description files (*.LCM). The experimental parameters (Type of incident particles, incident energy, scattering geometry, etc.) and spectral data are stored in files with extension *.RBS. You can read RBS-files with `RUMP:Read RBS File...`.

  Note 2: SIMNRA supports only a subset of the RUMP sample description commands. Especially the RUMP commands `Equation`, `Species` and `Fuzz` are not supported. If your sample description file contains these commands, they will be neglected and a warning will be shown. See section 3.12 for more details.

```
This line may contain any comment <CR><LF>
This line may contain any comment as well <CR><LF>
 Channel  Counts <CR><LF>
       1    1000 <CR><LF>
       2  1000.0 <CR><LF>
       3   1.0E3 <CR><LF>
       4  +1.0E3 <CR><LF>
  <EOF>
```

Figure 3.1: Example for a valid data file which can be imported with `File: Read Data: ASCII...`. The first three lines will be ignored by the program. The channel number must be an integer number, counts may be integer or floating point numbers.

- `RUMP: Write Sample Description File...`: This menu item allows to store the structure of the target and the absorber foil in a sample description file in RUMP format. The default file extension is *.LCM. These files can be read by RUMP or the IBA data furnace NDF.

  Note: SIMNRA allows to define a correction factor for the stopping power of each layer for each ion species. The correction factors are not stored in the sample description file.

- `Print...`: This menu item will print all parameters of the calculation and plot the experimental and simulated curves. See also the print preferences on the `Options: Preferences` tab.

  Note 1: SIMNRA is not intended to produce high quality graphics. If you want to obtain these, you should use a graphics program such as Excel or Origin. You can exchange data between SIMNRA and any graphics program by file with `File: Write Data...` and via the clipboard with `Edit: Copy Data`.

- `Exit`: Terminates the program.

3.3 `Edit` menu

- `Copy Data`: Copies experimental and simulated data in ASCII format to the clipboard. They can be pasted into any spreadsheet program.

  The format of the data in the clipboard is as follows: The data are organised in three columns. The first column contains the channel number, the second column contains the experimental data, and the third column contains the simulated data. The columns are separated with tabs. Spectra of individual elements or isotopes are not copied to the clipboard. Use `File: Write Spectrum Data...` to export spectra of individual elements or isotopes to a file.

- `Copy Page`: Copies the visible graphics to the clipboard (in enhanced metafile format). You can paste the graphics into any word processing program such as Microsoft Word.

3.4 `Setup` menu

3.4.1 `Setup: Experiment...`

In the `Setup: Experiment...` menu the global parameters of the backscattering experiment are defined.

- `Incident ion`: Selects the incident ions. For incident protons (H), D, T, ^{3}He or ^{4}He ions, the ions are selected by clicking the appropriate radio button.

  For incident heavy ions select `Other` and enter the ions name in `Other ion: Element` (for example Si, Cl, I). Lowercase and uppercase letters in the ions name are treated similar, you can enter silicon as Si, si, SI or sI. The ions mass is selected from the drop down box.

- `Energy`: Energy of the incident ions (in keV).

- `Geometry`: Geometry of the experiment: Incident angle α, exit angle β and scattering angle θ. α and β are measured towards the surface normal, see fig 3.2. All angles in degrees.

  Note 1: $0° \leq \alpha < 90°$.

  Note 2: $0° \leq \beta \leq 180°$. If $90° < \beta \leq 180°$ then transmission through the target is calculated.

- `Detector geometry`: Click the button to enter the detailed geometry of the detector (beam diameter, detector diaphragm width, distance sample-detector and shapes of incident beam and detector diaphragm). This is only necessary if geometrical straggling due to the finite widths of the incident beam and detector diaphragm shall be calculated. For RBS geometrical straggling usually is negligeable. See section 3.4.2 for details.

- `Calibration`: Conversion from channels to energy. To account for detector nonlinearities, SIMNRA can use a non-linear energy calibration with a quadratic term of the form

$$E\,[\text{keV}] = A + B \times \text{channel} + C \times \text{channel}^2. \tag{3.1}$$

  E is the particle energy in keV. The calibration offset A must be entered in the `Calibration Offset` field, A in keV. The energy per channel B must be entered in the `Energy per Channel` field, B in keV/channel. C is the quadratic correction term, C in keV/channel^2. For a linear energy calibration $C = 0.0$. A linear calibration is appropriate in most cases, and only if a high accuracy is intended a non-linear calibration should be used.

- `More energy calibration options`: An individual energy calibration may be used for each ion species. This is mainly useful for ERDA measurements with incident heavy ions, where each recoil species may require an individual calibration. By clicking the button an individual nonlinear energy calibration for each ion species

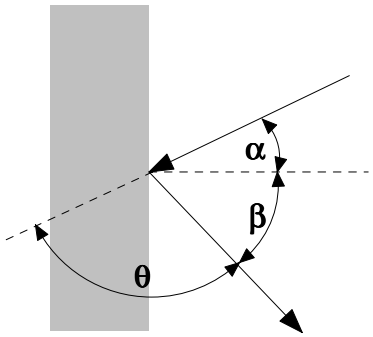

Figure 3.2: Geometry of a scattering experiment. Incident angle α, exit angle β and scattering angle θ.

may be supplied. If no individual energy calibration is defined, the major energy calibration entered in the `Calibration` fields of the `Setup: Experiment` form (see above) is used.

Attention: The energy scale, which is plotted at the top of the plot, is obtained with the major energy calibration from the `Calibration` fields of the `Setup: Experiment` form. The energy scale is not valid for particles with individual energy calibrations.

- `Particles*sr`: Number of incident particles times the solid angle of the detector. Solid angle in steradians. The number of incident particles is obtained from the collected charge and the charge state. `Calculate: Particles*sr...` can be used for the calculation.

- `Detector Resolution`: Energy resolution of the detector (in keV). The energy resolution is measured as full width at half maximum (FWHM). This energy resolution is used for all ion species, if no specific resolution for that ion is supplied (see below).

  SIMNRA can use different detector energy resolutions for different ion species. By pressing the button detector energy resolutions for each ion species may be entered. If no energy resolution for an ion species is supplied, the default resolution (see above) is used.

  Note: SIMNRA uses a constant, energy independent detector resolution for each ion species. This is (more or less) true for swift ions (protons and He), but for heavy ions the detector resolution depends on the particle energy. Currently energy dependent detector resolutions are not implemented in SIMNRA.

- `Energy spread of incident beam`: Usually the incident ion beam is not monoenergetic but has an energy distribution. SIMNRA assumes a gaussian energy distribution of the incident beam with a full width at half maximum which can be entered in the `Energy spread of incident beam` field. If this field is set to 0.0 SIMNRA assumes a monoenergetic incident beam.

The `File`-menu allows to save experimental setups to disk and read experimental setups from disk. All information contained in the `Setup Experiment` form, the `Detector`

`geometry` form, all energy calibrations and all detector resolutions are saved. The NRA data file format is used for saving.

- `Save as Default`: The current experimental setup is stored as startup default for SIMNRA in the file `DEFAULT\SETUP.NRA`.
- `Save Setup as`: Save the current experimental setup to file.
- `Read Setup`: Reads an experimental setup from file.
  Note: You can read any NRA-file with `Read Setup`. Only the setup information will be read, any other information (such as target composition, experimental spectra etc.), which may be present in the NRA file, will be ignored.

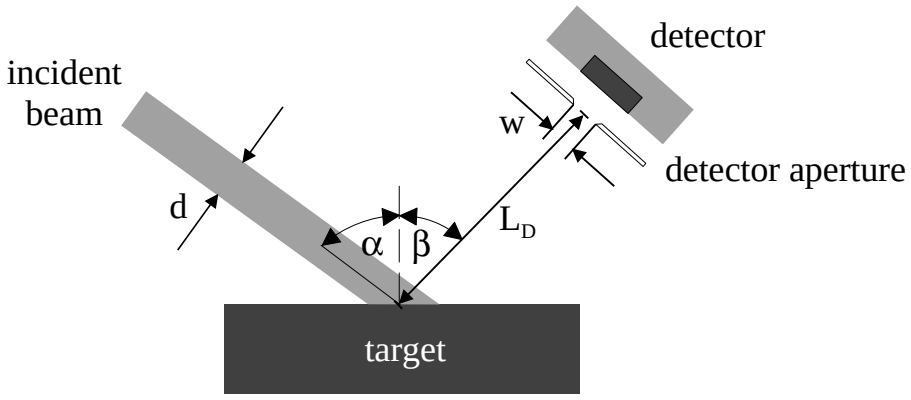

Figure 3.3: Detector geometry. d is the diameter of the incident beam, w the width of the detector aperture and L_D the distance between sample and the detector aperture. Incident angle α and exit angle β.

3.4.2 `Detector geometry`

In this menu the detailed geometry of the detector is entered. This is only necessary if geometrical straggling is calculated. Usually, geometrical straggling is small for RBS, but may be considerable for ERDA. Set all numbers to zero if geometrical straggling shall be neglected. This is the program default. See fig. 3.3 for details.

- `Diameter of incident beam`: Diameter of the incident beam in mm. Please note that the size of the beam spot on the sample surface is $d/\cos\alpha$.
- `Shape of incident beam`: Circular or rectangular beams may be selected. A homogeneous current distribution of the incident beam is assumed.
- `Diameter of detector aperture`: Diameter of the detector aperture in mm.
- `Shape of detector aperture`: Circular or rectangular apertures may be selected. Use rectangular also for long narrow slits.
- `Distance sample-detector aperture`: Distance between the sample surface and the detector aperture in mm.

Note: If `Straggling` in the `Setup: Calculation` menu is unchecked, then geometrical straggling (and electronic energy loss straggling) are neglected.

3.4.3 `Setup: Calculation...`

In the `Setup: Calculation...` menu the calculation parameters can be altered. This affects the accuracy of the calculation, but also the time necessary to calculate a simulated spectrum.

- `Stepwidth incident ions`: Stepwidth of the incident ions used in the calculation. See chapter 4 for details. `Automatic` or `Fixed` can be selected. If `Automatic` is selected, the program will choose the stepwidth automatically. This is usually the best choice for obtaining high accuracy and small computing times. `Automatic` is the program default. The automatically determined stepwidth is kept always below the resolution of the experiment. Because the resolution in larger depths degrades due to energy loss straggling the program uses a small stepwidth near the surface and a larger stepwidth in larger depths.

  `Fixed` stepwidth: The program uses a fixed stepwidth for the calculation. If `Fixed` is selected the default for the stepwidth is 10 keV. For incident heavy ions with energies in the range of several ten MeV this stepwidth can be increased to several 100 keV.

  The stepwidth used for incident ions affects the time T necessary to perform a calculation strongly. T depends on the stepwidth of the incoming ion ΔE roughly as $T \propto 1/\Delta E$: Decreasing the stepwidth by a factor of two will roughly double the computing time.

  Note 1: The stepwidth of the incident ions is an important parameter for the accuracy of a simulation. If the stepwidth of the incident ion is too high, especially if the exit angle β is close to 90° or the detector resolution is below 10 keV, unwanted oscillations or steps in the simulated spectra may occur. This is due to rounding errors in the routine which calculates the contents of each channel. If these oscillations occur you have to decrease the stepwidth of the incident ions. If `automatic` stepwidth control is selected, these problems should never occur: The program always selects a stepwidth which is small enough.

  Note 2: If the backscattering cross-section contains narrow resonances, the stepwidth of the incoming ions should be lower than the width of the resonance. `Automatic` stepwidth control should not be used with narrow resonances.

- `Stepwidth outgoing ions`: Stepwidth of outgoing particles used in the calculation. See chapter 4 for details. `Automatic` or `Fixed` can be selected. If `automatic` is selected, the program will choose the stepwidth automatically. This is usually the best choice for obtaining high accuracy and small computing times. `Automatic` is the program default. The automatically determined stepwidth is large at high energies, where the stopping power shows only small variations to decrease computing time. The step width is decreased near the stopping power maximum and at low energies, where the stopping power varies strongly, to increase accuracy.

  `Fixed` stepwidth: The program uses a fixed stepwidth for the calculation of outgoing particles. The stepwidth will remain constant at all energies and for all outgoing

particles. If `Fixed` is selected the default for the stepwidth is 200 keV. For incident heavy ions with energies in the range of several ten MeV this stepwidth can be increased.

If a small `fixed` stepwidth is used this may increase the accuracy of the calculation, but will slow down the calculation. A very small `fixed` stepwidth may be even more accurate than `automatic` stepwidth control. In contrast a large `fixed` stepwidth decreases the accuracy of the calculation, but will speed up the calculation. There is no easy recipe for the best choice of a `fixed` stepwidth. Usually the best compromise between speed and accuracy is `automatic` stepwidth control.

- `Cutoff Energy`: All particles are calculated until their energy has decreased below the cut-off energy. You may speed up the calculation if you increase the cut-off energy. The lowest possible value for the cut-off energy is 10 keV.

- `Isotopes`: If checked, backscattering from all isotopes of all elements in the target is calculated. Especially for heavy elements with many isotopes this will slow down the calculation significantly. If unchecked, the program will use only the mean masses of the elements. Default is checked.

  Important: Non-Rutherford cross-sections and nuclear reactions are only available if `Isotopes` is checked.

- `Straggling`: If checked, electronic energy loss straggling and geometrical straggling (if selected, see section 3.4.2) is taken into account. Default is checked.

- `Multiple Scattering`: If checked, straggling due to multiple small angle scattering will be calculated. Default is unchecked.

- `Dual Scattering`: Most particles are scattered into the detector with only one scattering event with large scattering angle. However, some particles may suffer more than one scattering event with large scattering angle before they reach the detector, see fig. 3.4. This is called plural scattering and results for example in the low background behind the low energy edge of high Z layers on top of low Z elements. The deviations at low energies between simulated and measured spectra are also mainly due to plural scattering.

  SIMNRA can calculate all trajectories with two scattering events. If `Dual Scattering` is unchecked, then only one scattering event is calculated. This is the default. If `Dual Scattering` is checked, additionally trajectories with two scattering events will be calculated.

  Warning: The calculation of dual scattering is a very time consuming process. If `Dual Scattering` is checked, this will slow down the calculation of a spectrum by a factor of about 200 (!), increasing the computing time from several seconds to *at least* several minutes.

  Note 1: Dual scattering should be used *only* if all cross-sections are Rutherford. For the calculation of dual scattering the cross-sections for all possible scattering

angles between $\approx 0°$ and 180° must be known. This is only the case for Rutherford cross-sections.

Note 2: SIMNRA calculates dual scattering *only* for incident ions and not for recoils or reaction products of nuclear reactions. Additional scattering in a foil in front of the detector (if any) is neglected.

Note 3: If `Dual Scattering` is checked, then `Straggling` must be checked too. SIMNRA will check `Straggling` automatically, if `Dual Scattering` is checked. As long as `Dual Scattering` is checked, `Straggling` cannot be unchecked.

- `Stopping power data`: The selection of stopping power data has a large influence on the shape of the simulated spectra. SIMNRA can use two different sets of electronic stopping power data for the stopping of swift and heavy ions in all elements: The well known electronic stopping power data by Andersen and Ziegler [1, 2, 3] or the electronic stopping power data by Ziegler, Biersack and Littmark [3]. The Ziegler-Biersack data are also used by Ziegler's SRIM (formerly TRIM) program in calculations of stopping powers and ranges. The difference between these two data sets is typically $< 5\%$, but may be larger in some cases. According to Ziegler [4] the Ziegler-Biersack data are more accurate and reliable than the Andersen-Ziegler data. The use of the Ziegler-Biersack data is recommended and the program default. The energy ranges in which the different stopping power formulas are valid are listed in table 3.1.

  Note: If the stopping power data by Andersen-Ziegler are used for incident hydrogen isotopes or heavy ions near 1 MeV/amu artificial steps or kinks may appear in the simulated spectra. This is due to a jump of the stopping power at 1 MeV/amu. See the description of the `High energy stopping` switch for a work-around. This problem does not appear if the Ziegler-Biersack data are used.

- `High energy stopping`: This switch is only available if Andersen-Ziegler electronic stopping power data are used. If checked, the program will use the correct high energy stopping formula by Andersen and Ziegler for incident protons and heavy ions for $E > 1$ MeV/amu. If unchecked, the program will use the medium energy formula, which is valid only in the range 10 keV/amu–1 MeV/amu, also at higher energies $E > 1$ MeV/amu. The difference between the two formulas usually is small. This switch is necessary because the two stopping power formulas do not fit smoothly together at 1 MeV/amu: The stopping power jumps at 1 MeV/amu resulting in artificial kinks and steps in the simulated spectra. This problem is overcome if `High energy stopping` is unchecked, however this will result in less accurate stopping powers for energies > 1 MeV/amu. A better solution is to use the Ziegler-Biersack stopping powers, where this problem does not occur.

  This switch does not have any influence on the calculation of the stopping power of helium ions and is disabled. For helium ions always the medium energy formula is used, which is valid for all energies below 10 MeV. The default is checked.

- `Number of thickness steps`: Used for the calculation of layer roughness. A rough

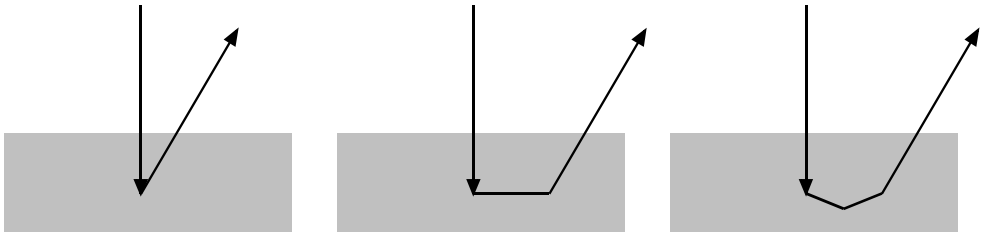

Figure 3.4: Examples of ion trajectories with one, two and three scattering events.

layer is approximated by the superposition of N spectra with different layer thicknesses, where N is the number of thickness steps. If N is small, the superposed spectrum may contain steps. Larger values of N result in smoother spectra, but slow down the calculation considerably. Default is $N = 10$.

Note: One rough layer requires the calculation of N spectra, two rough layers of N^2 spectra, three rough layers of N^3 spectra etc.

- `Number of angular steps`: Used for the calculation of substrate roughness. A rough substrate is approximated by the superposition of M spectra with different incident and exit angles, where M is the number of angular steps. If M is small, the superposed spectrum may contain steps. Larger values of M result in smoother spectra, but slow down the calculation considerably. Default is $M = 20$.

  Note: Substrate roughness requires the calculation of M spectra, one rough layers combined with substrate roughness of $N \times M$ spectra, where N is the `Number of thickness steps`, two rough layers combined with substrate roughness of $N^2 \times M$ spectra etc.

- `Element Spectra`: If checked, individual spectra for each element in the target are calculated and plotted. If unchecked, only the total spectrum is calculated and plotted. Default is unchecked.

- `Isotope Spectra`: If checked, individual spectra for each isotope in the target are calculated and plotted. Default is unchecked.

  Note: The number of individual spectra is limited to 20. If the target contains many isotopes, not all will be displayed.

- `Logfile`: If checked, a file named SIMNRA.LOG is created. This file contains additional information about each step of the calculation. The logfile is intended for debugging the program. Default is unchecked.

Incident ion	Andersen-Ziegler (keV/amu)	Ziegler-Biersack (keV/amu)
Hydrogen (H, D, T)	1–100000	1–100000
Helium (^{3}He, ^{4}He)	0.25–2500[a]	1–100000
Heavy ions	1–100000	1–100000

Table 3.1: Energy ranges in which the different stopping power formulas are valid.

[a]High energy electronic stopping formula for energies > 2.5 MeV/amu from [1] not implemented.

3.5 `Target` menu

3.5.1 `Target: Target...`

In this menu the target is created. A target consists of *layers*. Each layer consists of different elements and has some thickness. The composition of a layer does not change throughout his thickness. To simulate a concentration profile you have to use multiple layers.

The layer number 1 is at the surface of the target, the layer number 2 is below layer 1 and so on, see fig. 3.5.

- `Thickness`: Thickness of the layer (in 10^{15} atoms/cm^2). The conversion factor from μg/cm^2 or μm to atoms/cm^2 can be determined with `Calculate: Density...` for pure elements.

- `Number of Elements`: Number of different elements in this layer. The maximum number of different elements in a layer is 20.

- `Element`: Name of the element, for example Si, W, Au. Lowercase and uppercase letters in elements names are treated similar, you can enter silicon as Si, si, SI or sI. XX means that this element is unknown. The special symbols D for deuterium, T for tritium and A for ^{4}He can be used.

- `Concentration`: Atomic concentration of the element in the actual layer. The concentration c must be $0.0 \le c \le 1.0$. The sum of the concentrations of all elements in one layer must be equal to 1 ($0.999 \le \sum c_i \le 1.001$). If the sum of concentrations is not equal to 1, the word concentration is written in red colour, if the sum of concentrations is equal to 1, the word concentration is written in black colour. You can use the small buttons to set the concentration of the element i to 1 minus the sum of concentrations of all other elements, $c_i = 1 - \sum_{i \neq j} c_j$.

- `Isotopes`: These buttons can be used to change the concentrations of isotopes of that element in the actual layer. You will need this only if this element does not have the natural composition of isotopes. You can create for example a layer of enriched ^{13}C on top of ^{12}C, or the like. The sum of concentrations of all isotopes of one element must be equal to 1.

  Note: The `Isotopes` check-box in the `Setup: Calculation...` menu must be checked to manipulate individual isotopes.

- `Correction factor(s) for stopping power`: SIMNRA uses Bragg's rule to calculate the stopping power of a layer, see Section 4.6.3 for more details. However, it has been shown experimentally that for several compounds like hydrocarbons or oxides deviations from Bragg's rule occur. To account for deviations from Braggg's rule a correction factor f can be used, and the program will use the stopping power $S(E)$ as function of energy E

$$S(E) = f\, S_{\mathrm{Bragg}}(E) \tag{3.2}$$

$S_{\mathrm{Bragg}}(E)$ is the stopping power according to Bragg's rule. Note that the factor f is energy independent. An individual factor f for each ion species and each layer may be defined. If no factor f is given the program uses $f = 1$, i.e. uses Bragg's rule.

- `Layer and substrate roughness`: Click the button if the current layer or the substrate is rough. See section 3.5.2 for details.

To manipulate layers use the buttons in the `Layer manipulation` box. Additionally layers can be copied and pasted from the clipboard and layers can be saved and read from file.

- `Add`: Adds a layer. The added layer will be the last layer. The maximum number of different layers is 100.
- `Ins`: Inserts a layer in front of the current layer. The maximum number of different layers is 100.
- `Del`: Deletes the current layer.
- `Prev`: Go to the previous layer.
- `Next`: Go to the next layer.

A layer can be copied to the clipboard with `Edit: Copy Layer` (or by pressing Ctrl C). A layer can be pasted from the clipboard with `Edit: Paste Layer` (or by pressing Ctrl V).

A layer can be saved to file with `File: Save Layer`. A layer can be read from file with `File: Read Layer`.

Attention: If a layer is pasted from the clipboard or read from file, the current layer is overwritten.

The whole target (or foil) with all layers can be saved to file with `File: Save Target`. A target (or foil) can be read from file with `File: Read Target`.

`Show: Target summary` displays the total amounts (in atoms/cm^2) of all elements in the target. This is mainly useful if the target consists of plural layers composed of the same elements in different concentrations. The total amount of each element is the sum of this element in all layers.

3.5.2 Layer and substrate roughness

In this menu the roughnesses of the current layer and of the substrate are defined.

- `Has thickness distribution`: Check, if the current layer is rough, i.e. if the layer thickness is not uniform, but varies from point to point. A rough layer is described by a distribution of layer thicknesses. The distribution is divided into N steps. The step number N can be adjusted by the `Number of thickness steps` in the `Setup: Calculation...` menu, see section 3.4.3.

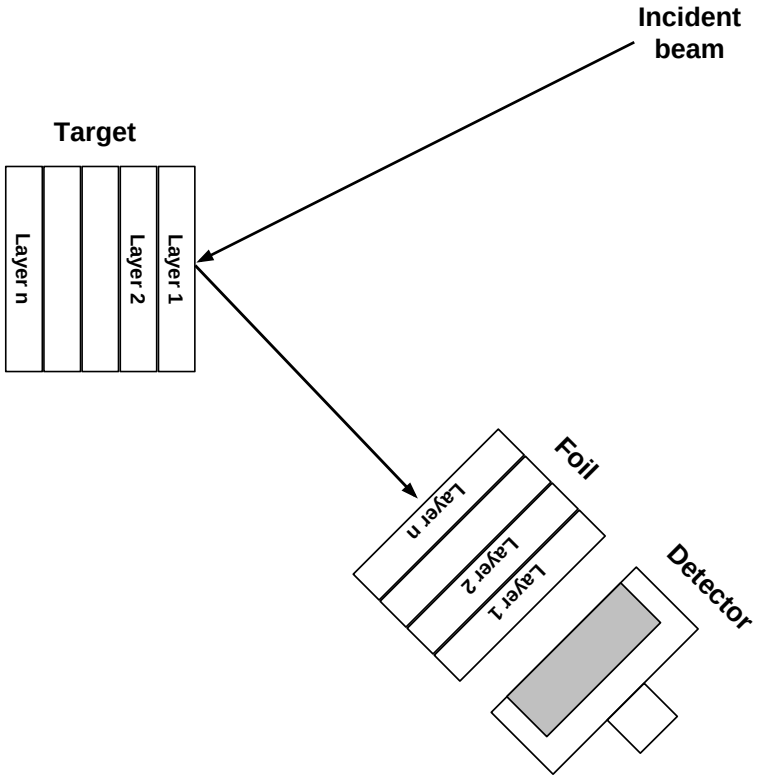

Figure 3.5: Layer structure of target and foil. For the target, layer 1 is at the surface, the layer with the highest number is the deepest layer. Backscattered particles first penetrate the foil layer with the highest number, the foil layer 1 is in front of the detector.

Filename	Material	Common name
INCON600.LAY	Inconel 600	
INCON625.LAY	Inconel 625	
SS14301.LAY	Stainless steel 1.4301, AISI 304 (US)	
SS14541.LAY	Stainless steel 1.4541	V2A
SS14571.LAY	Stainless steel 1.4571	V4A
SS316.LAY	Stainless steel 316 (US)	
MYLAR.LAY	Polyethylenterephthalat	Mylar, Hostaphan

Table 3.2: Predefined materials for stopper foils stored in the \LAYERS directory.

- `FWHM of thickness distribution`: SIMNRA assumes a Gamma distribution of layer thicknesses, see section 4.9 for details, with the layer thickness as mean value. The width and shape of the distribution is determined by the full width at half maximum (FWHM), with

$$\mathrm{FWHM} = 2.35482\,\sigma \tag{3.3}$$

  where σ is the standard deviation [2]. FWHM in 10^{15} atoms/cm^2.

- `Has substrate roughness`: Check if the layers are on top of a rough substrate. A rough substrate is described by a distribution of incident and exit angles and has no other influence. Only one substrate can exist for all layers, i.e. the substrate parameters are identical for all layers. Substrate roughness is not available for foils. The distribution of incident and exit angles is divided into M steps. The step number M can be adjusted by the `Number of angular steps` in the `Setup: Calculation...` menu, see section 3.4.3.

- `FWHM of substrate roughness`: SIMNRA assumes a Lorentz distribution of angles. Enter the full width at half maximum (FWHM) of the angle distribution, in deg.

3.5.3 `Target: Foil...`

In this menu a foil in front of the detector can be created. Like the target a foil can consist of multiple layers with different compositions. See the previous section for details. If the foil consists of multiple layers, then backscattered particles first will penetrate layer n, then layer $n-1$ etc., layer 1 is directly in front of the detector (see fig. 3.5).

The default is no foil in front of the detector.

Some common materials used as stopper foils are already stored in the \`LAYERS` directory. The materials and files are listed in table 3.2. These files can be imported in the `Target` menu with `File: Read layer`.

[2] Strictly speaking, the Gamma distribution has only a standard deviation σ, while the full width at half maximum (FWHM) is undefined. However, the Gamma distribution resembles a Gaussian distribution in many cases, which justifies the use of the FWHM. Internally, SIMNRA uses only the standard deviation σ, which is derived from the FWHM through eq. 3.3.

3.6 `Reactions` menu

In the `Reactions` menu the cross-sections used for the calculation of the simulated spectrum are chosen. Rutherford cross-sections for backscattering of projectiles and creation of recoils are available for all ion-target combinations, if kinematically possible. For heavy projectiles backscattered from light target nuclei two different solutions may be kinematically possible, see eq. 4.5 in section 4.3. The solution with the minus sign appears as `Rutherford cross-section (low energy solution)` in the `Reactions` menu.

Additionally SIMNRA can handle non-Rutherford cross-sections for backscattering and recoil production and can use nuclear reactions cross-sections. SIMNRA is able to read three different file formats with cross-section data:

1. The file CRSDA.DAT. This file was developed in the years 1985–1995 at the IPP Garching and contains fitting coefficients to various cross-section data. A documentation is not available, and no guarantee is provided that the fits agree with the original data. The use of these data is highly discouraged and they should be used only if no other data are available.

2. The R33 file format. Cross-sections for nuclear reaction are stored in the R33 file format in the SigmaBase data repository for ion beam analysis[3]. Most files with this extension have been taken from SigmaBase, a few ones were added by the author. The majority of these files has been digitised from the original publications by G. Vizkelethy from Idaho State University. No guarantee is provided for agreement with the original publication. The references of the original publications are found in the file headers.

3. The RTR (Ratio To Rutherford) file format. These files contain non-Rutherford cross-sections for backscattering of protons and α-particles. The files contain the ratio of measured to Rutherford cross-sections. The majority of the data has been digitised from the original publications by R.P. Cox, J.A. Leavitt and L.C. McIntyre, Jr. from Arizona University. These cross-section data have been published in [5]. All files with this extension have been taken from SigmaBase. The references of the original publications are found in [5].

SIMNRA distinguishes between three different types of scattering events for each isotope:

1. Backscattering of projectiles

2. Creation of recoils

3. Nuclear reactions.

[3] http://ibaserver.physics.isu.edu/sigmabase. This server is mirrored in New Zealand at http://pixe.gns.cri.nz/.

The chosen cross-sections for each type of scattering event must be unambiguous: You can choose, for example, Rutherford cross-section for backscattering in the energy range from 0.000–0.999 MeV, some non-Rutherford cross-section for backscattering in the energy range from 1.000-1.999 MeV and a different cross-section for backscattering in the energy range from 2.000–3.000 MeV. You cannot choose, however, Rutherford cross-section for backscattering in the range 0.000–2.000 MeV and another cross-section for backscattering in the energy range from 1.000–2.000 MeV: In this case the program does not know which cross-section it should use in the range from 1.000–2.000 MeV, and you will get the error message 'Energy overlap in cross-sections'.

All available cross-section data are listed in tables 3.3, 3.4 and 3.5. If you want to add new cross-section data files, see section 3.14.

Note 1: Some files contain total cross-section data $\sigma(E)$. In these cases the differentiell cross-section $d\sigma/d\Omega$ is obtained by SIMNRA for all kinematically allowed angles by assuming angular independence of the cross-section in the center of mass system:

$$\left(\frac{d\sigma}{d\Omega}\right)_{CM}(E,\theta) = \frac{1}{4\pi}\sigma(E) \tag{3.4}$$

This cross-section is then transformed from the center of mass to the laboratory system. The assumption of angular independence in the center of mass system is well fulfilled for the ^{3}He(D,p)α-reaction for incident energies below about 1.2 MeV and for the D(^{3}He,p)α-reaction for incident energies below about 1.8 MeV.

Note 2: Use the data files that came with SIMNRA. Some of the original data files at SigmaBase contain small format errors, such as additional blank lines, which confuse the program.

Note 3: Non-Rutherford cross-sections and nuclear reactions are only available if `Isotopes` in the `Setup:Calculation...` menu is checked.

Table 3.3: Non-Rutherford backscattering cross-sections.

	θ **(Lab)**	**Energy (keV)**	**File**	**Reference**
D(p,p)D	151	1800–3000	PH_LA76A.RTR	Langley 1976
T(p,p)T	163.2	2500–3500	PH_LA76B.RTR	Langley 1976
^{3}He(p,p)^{3}He	159.2	2000–3000	PHELA76A.RTR	Langley 1976
^{4}He(p,p)^{4}He	161.4	1500–3700	PHELA76B.RTR	Langley 1976
^{4}He(p,p)^{4}He	165	1500–3000	CRSDA.DAT, No. 5	?
^{6}Li(p,p)^{6}Li	164	1200–3100	PLIBA51A.RTR	Bashkin 1951
^{7}Li(p,p)^{7}Li	156.7	373–1398	PLIWA53A.RTR	Warters 1953
^{7}Li(p,p)^{7}Li	164	1700–3500	PLIBA51B.RTR	Bashkin 1951
^{7}Li(p,p)^{7}Li	165	1300–2800	PLIMA56A.RTR	Malmberg 1956
^{9}Be(p,p)^{9}Be	142.4	1600–3000	PBEMO56A.RTR	Mozer 1956
^{9}Be(p,p)^{9}Be	158.7	200–1700	PBEMO56B.RTR	Mozer 1956
^{9}Be(p,p)^{9}Be	170.5	2400–2700	PBELE94A.RTR	Leavitt 1994
^{10}B(p,p)^{10}B	154	1000–3000	PB_OV62A.RTR	Overley 1962
^{11}B(p,p)^{11}B	150	500–2000	PB_TA56A.RTR	Trautfest 1956
^{11}B(p,p)^{11}B	155	2200–3300	11BPPB_1.R33	Symons 1963
^{11}B(p,p)^{11}B	161.4	1100–3800	11BPPB.R33	Segel 1965
C(p,p)C	150	1000–3500	12CPPC_1.R33	Amirikas 1993
C(p,p)C	165	1000–3500	12CPPC.R33	Amirikas 1993
C(p,p)C	170	300–700	PC_LI93A.RTR	Liu 1993
C(p,p)C	170	700–2800	PC_LI93B.RTR	Liu 1993
C(p,p)C	170	300–3000	PC_LI93C.RTR	Liu 1993
C(p,p)C	170	700–2500	PC_RA85A.RTR	Rauhala 1985
C(p,p)C	170	996–3498	PC_AM93A.RTR	Amirikas 1993
C(p,p)C	170	1000–3500	12CPPC_2.R33	Amirikas 1993
^{12}C(p,p)^{12}C	179.2	4000–6600	12CPP179.R33	Tosaki 2000
^{12}C(p,p)^{12}C	168.2	400–4500	PC_JA53A.RTR	Jackson 1953
^{14}N(p,p)^{14}N	150	800–1900	PN_TA56A.RTR	Tautfest 1956
^{14}N(p,p)^{14}N	152	1035–1075	PN_HA57A.RTR	Hagedorn 1957
^{14}N(p,p)^{14}N	152	1450–1625	PN_HA57B.RTR	Hagedorn 1957
^{14}N(p,p)^{14}N	152	650–1800	PN_HA57E.RTR	Hagedorn 1957
^{14}N(p,p)^{14}N	155.2	1850–3000	PN_LA67A.RTR	Lambert 1967
^{14}N(p,p)^{14}N	158.7	1735–1760	PN_HA57C.RTR	Hagedorn 1957
^{14}N(p,p)^{14}N	158.7	1785–1815	PN_HA57D.RTR	Hagedorn 1957
^{14}N(p,p)^{14}N	159.5	600–4000	PN_BA59A.RTR	Bashkin 1959
^{14}N(p,p)^{14}N	165	1850–3000	PN_LA67B.RTR	Lambert 1967
^{14}N(p,p)^{14}N	167.2	3600–4100	PN_OL58A.RTR	Olness 1958
^{14}N(p,p)^{14}N	170	1450–2300	PN_RA85A.RTR	Rauhala 1985
^{16}O(p,p)^{16}O	149.5	2450–2850	PO_GO65A.RTR	Gomes 1965
^{16}O(p,p)^{16}O	170	1000–3580	PO_AM93A.RTR	Amirikas 1993
^{16}O(p,p)^{16}O	170	700–4000	16OPPO.R33	Gurbich 1997
^{19}F(p,p)^{19}F	150	2000–5000	PF_BO93A.RTR	Bogdanovic 1993
^{19}F(p,p)^{19}F	160	500–1300	PF_DE56A.RTR	Dearnaly 1956
^{19}F(p,p)^{19}F	160	1300–2064	PF_DE56B.RTR	Dearnaly 1956
^{19}F(p,p)^{19}F	160	500–1300	PF_DE56C.RTR	Dearnaly 1956
^{19}F(p,p)^{19}F	160	1300–1550	PF_DE56D.RTR	Dearnaly 1956
^{19}F(p,p)^{19}F	165	850–1010	PF_KN89A.RTR	Knox 1989
^{19}F(p,p)^{19}F	165	1000–1875	PF_KN89B.RTR	Knox 1989
^{19}F(p,p)^{19}F	165	1350–1550	PF_KN89C.RTR	Knox 1989

	θ (Lab)	Energy (keV)	File	Reference
^{19}F(p,p)^{19}F	158.7	600–1800	PF_WE55A.RTR	Webb 1955
^{19}F(p,p)^{19}F	158.7	1300–1500	PF_WE55B.RTR	Webb 1955
^{20}Ne(p,p)^{20}Ne	166 (CM)	1500–2800	PNELA71A.RTR	Lambert 1971
^{23}Na(p,p)^{23}Na	156.5	550–1450	PNABA56A.RTR	Bauman 1956
^{24}Mg(p,p)^{24}Mg	164	400–4000	PMGMO51A.RTR	Mooring 1951
^{24}Mg(p,p)^{24}Mg	164	792–856	PMGMO51E.RTR	Mooring 1951
^{24}Mg(p,p)^{24}Mg	164	1466–1501	PMGMO51F.RTR	Mooring 1951
^{24}Mg(p,p)^{24}Mg	164	1642–1671	PMGMO51G.RTR	Mooring 1951
^{24}Mg(p,p)^{24}Mg	164	1991–2026	PMGMO51H.RTR	Mooring 1951
^{24}Mg(p,p)^{24}Mg	164	2393–2431	PMGMO51I.RTR	Mooring 1951
^{24}Mg(p,p)^{24}Mg	170	700–2540	PMGRA88A.RTR	Rauhala 1988
^{27}Al(p,p)^{27}Al	170	1000–2450	PALRA89A.RTR	Rauhala 1989
^{28}Si(p,p)^{28}Si	167.2	1300–4000	PSIVO59A.RTR	Vorona 1959
Si(p,p)Si	170	1000–3580	PSIAM93A.RTR	Amirikas 1993
Si(p,p)Si	170	1470–2200	PSIRA85A.RTR	Rauhala 1985
^{31}P(p,p)^{31}P	165	1000–2000	PP_CO63A.RTR	Cohen-Ganouna 1963
^{32}S(p,p)^{32}S	167.4	1300–4000	PS_OL58A.RTR	Olness 1958
S(p,p)S	170	1500–2690	PS_RA88A.RTR	Rauhala 1988
Cl(p,p)Cl	150	2000–5000	PCLBO93A.RTR	Bogdanovic 1993
^{40}Ar(p,p)^{40}Ar	159.5	1800–3600	PARBK61A.RTR	Barnhard 1961
^{40}Ar(p,p)^{40}Ar	166 (CM)	1000–2000	PARCO63A.RTR	Cohen-Ganouna 1963
^{40}Ar(p,p)^{40}Ar	166 (CM)	1825–1950	PARCO63B.RTR	Cohen-Ganouna 1963
^{40}Ar(p,p)^{40}Ar	155	1750–2750	PARFR58A.RTR	Frier 1958
^{40}Ca(p,p)^{40}Ca	160	1800–3000	PCAWI74A.RTR	Wilson 1974
^{48}Ti(p,p)^{48}Ti	160	1800–2150	PTIPR72A.RTR	Prochnow 1972
^{48}Ti(p,p)^{48}Ti	160	2150–2500	PTIPR72B.RTR	Prochnow 1972
^{48}Ti(p,p)^{48}Ti	160	2500–2800	PTIPR72C.RTR	Prochnow 1972
^{48}Ti(p,p)^{48}Ti	160	2900–3040	PTIPR72D.RTR	Prochnow 1972
^{48}Ti(p,p)^{48}Ti	170	1000–2600	PTIRA89A.RTR	Rauhala 1989
^{12}C(^{3}He,^{3}He)^{12}C	159.4	1800–5400	12CTTC.R33	Kuan 1964
^{6}Li(α,α)^{6}Li	112	2500–4500	ALIBO72A.RTR	Bohlen 1972
^{7}Li(α,α)^{7}Li	121	2500–4500	ALIBO72B.RTR	Bohlen 1972
^{9}Be(α,α)^{9}Be	136	6000–20000	ABETA65A.RTR	Taylor 1965
^{9}Be(α,α)^{9}Be	157.5	1500–6000	ABEGO73A.RTR	Goss 1973
^{9}Be(α,α)^{9}Be	170.5	575–4200	ABELE94A.RTR	Leavitt 1994
^{10}B(α,α)^{10}B	170.5	975–3275	AB_MC92A.RTR	McIntyre 1992
^{11}B(α,α)^{11}B	150.8	2000–4000	AB_RA72A.RTR	Ramirez 1972
^{11}B(α,α)^{11}B	160.5	4000–8000	AB_OT72A.RTR	Ott 1972
^{11}B(α,α)^{11}B	170.5	980–3300	AB_MC92B.RTR	McIntyre 1992
C(α,α)C	149	4000–12000	AC_MS72A.RTR	Marvin 1972
C(α,α)C	165	1810–9050	AC_FE94A.RTR	Feng 1994
C(α,α)C	167	4000–7500	AC_BI54A.RTR	Bittner 1954
C(α,α)C	170	5000–9000	AC_CH94A.RTR	Cheng 1994
C(α,α)C	170.5	1560–5000	AC_LE89A.RTR	Leavitt 1989
^{12}C(α,α)^{12}C	30	2000–4800	12CAA12C30.R33	Bogdanović Radović 2002
^{12}C(α,α)^{12}C	45	2000–4800	12CAA12C45.R33	Bogdanović Radović 2002

	θ (Lab)	Energy (keV)	File	Reference
$^{12}C(\alpha,\alpha)^{12}C$	60	2100–4800	12CAA12C60.R33	Bogdanović Radović 2002
$^{12}C(\alpha,\alpha)^{12}C$	135	2100–4800	12CAA12C135.R33	Bogdanović Radović 2002
$^{12}C(\alpha,\alpha)^{12}C$	150	2100–4800	12CAA12C150.R33	Bogdanović Radović 2002
$^{13}C(\alpha,\alpha)^{13}C$	165	2000–3500	AC_BA65A.RTR	Barnes 1965
$^{13}C(\alpha,\alpha)^{13}C$	165	3300–6500	AC_KE68A.RTR	Kerr 1968
$^{14}N(\alpha,\alpha)^{14}N$	163.7	2600–4700	AN_KA58A.RTR	Kashy 1958
$^{14}N(\alpha,\alpha)^{14}N$	165	2000–6200	AN_FE94A.RTR	Feng 1994
$^{14}N(\alpha,\alpha)^{14}N$	167	4550–6550	AN_FO93A.RTR	Foster 1993
$^{14}N(\alpha,\alpha)^{14}N$	167	7090–9070	AN_FO93B.RTR	Foster 1993
$^{14}N(\alpha,\alpha)^{14}N$	167	8650–9000	AN_FO93C.RTR	Foster 1993
$^{14}N(\alpha,\alpha)^{14}N$	167.2	2000–4000	AN_HE58A.RTR	Herring 1958
$^{15}N(\alpha,\alpha)^{15}N$	165.2	1600–2600	AN_SM61A.RTR	Smothich 1961
$^{15}N(\alpha,\alpha)^{15}N$	165.2	2400–3800	AN_SM61B.RTR	Smothich 1961
$^{15}N(\alpha,\alpha)^{15}N$	165.2	3800–4800	AN_SM61C.RTR	Smothich 1961
$^{15}N(\alpha,\alpha)^{15}N$	165.2	4700–5600	AN_SM61D.RTR	Smothich 1961
$^{15}N(\alpha,\alpha)^{15}N$	165.2	1600–5600	AN_SM61E.RTR	Smothich 1961
$^{15}N(\alpha,\alpha)^{15}N$	165.2	1600–5600	AN_SM61F.RTR	Smothich 1961
$^{15}N(\alpha,\alpha)^{15}N$	165.2	3800–4800	AN_MO72A.RTR	Mo 1972
$^{16}O(\alpha,\alpha)^{16}O$	158.6	6000–10500	AO_HU67A.RTR	Hunt 1967
$^{16}O(\alpha,\alpha)^{16}O$	165	2050–9000	AO_FE94A.RTR	Feng 1994
$^{16}O(\alpha,\alpha)^{16}O$	165	9200–9900	AO_CA85A.RTR	Caskey 1985
$^{16}O(\alpha,\alpha)^{16}O$	165	9600–10500	AO_CA85B.RTR	Caskey 1985
$^{16}O(\alpha,\alpha)^{16}O$	165	10320–10700	AO_CA85C.RTR	Caskey 1985
$^{16}O(\alpha,\alpha)^{16}O$	165	10650–11100	AO_CA85D.RTR	Caskey 1985
$^{16}O(\alpha,\alpha)^{16}O$	165	11050–11600	AO_CA85E.RTR	Caskey 1985
$^{16}O(\alpha,\alpha)^{16}O$	165	11500–12500	AO_CA85F.RTR	Caskey 1985
$^{16}O(\alpha,\alpha)^{16}O$	165	12150–12750	AO_CA85G.RTR	Caskey 1985
$^{16}O(\alpha,\alpha)^{16}O$	165	12500–13500	AO_CA85H.RTR	Caskey 1985
$^{16}O(\alpha,\alpha)^{16}O$	165	9150–12750	AO_CA85I.RTR	Caskey 1985
$^{16}O(\alpha,\alpha)^{16}O$	165.7	5000–12500	AO_JO69A.RTR	John 1969
$^{16}O(\alpha,\alpha)^{16}O$	170	2000–9000	AO_CH93A.RTR	Cheng 1993
$^{16}O(\alpha,\alpha)^{16}O$	170	1770–5000	AO_LE90A.RTR	Leavitt 1990
$^{18}O(\alpha,\alpha)^{18}O$	160	2400–3500	AO_PO64A.RTR	Powers 1964
$F(\alpha,\alpha)F$	165	1500–5000	AF_CH93A.RTR	Cheng 1993
$^{19}F(\alpha,\alpha)^{19}F$	170	1500–2300	AF_CS84A.RTR	Cseh 1984
$^{19}F(\alpha,\alpha)^{19}F$	170	2300–3700	AF_CS84B.RTR	Cseh 1984
$^{19}F(\alpha,\alpha)^{19}F$	170	1500–4000	AF_CS84C.RTR	Cseh 1984
$Ne(\alpha,\alpha)Ne$	167.3	2400–3200	ANEGO54A.RTR	Goldberg 1954
$Ne(\alpha,\alpha)Ne$	167.3	3200–4000	ANEGO54B.RTR	Goldberg 1954
$Ne(\alpha,\alpha)Ne$	167.3	2400–4000	ANEGO54C.RTR	Goldberg 1954
$Na(\alpha,\alpha)Na$	165	2000–6000	ANACH91A.RTR	Cheng 1991
$Mg(\alpha,\alpha)Mg$	165	2000–9000	AMGCH93A.RTR	Cheng 1993
$^{24}Mg(\alpha,\alpha)^{24}Mg$	162.5	3150–3900	AMGCS82A.RTR	Cseh 1982
$^{24}Mg(\alpha,\alpha)^{24}Mg$	162.5	4200–4900	AMGCS82B.RTR	Cseh 1982
$^{24}Mg(\alpha,\alpha)^{24}Mg$	164	3150–3900	AMGKA52A.RTR	Kaufmann 1952
$^{24}Mg(\alpha,\alpha)^{24}Mg$	165	5900–6250	AMGIK79A.RTR	Ikossi 1979
$^{24}Mg(\alpha,\alpha)^{24}Mg$	165	6080–6140	AMGIK79B.RTR	Ikossi 1979
$Si(\alpha,\alpha)Si$	170	2000–6000	ASICH93A.RTR	Cheng 1993

	θ (Lab)	Energy (keV)	File	Reference
Si(α,α)Si	170	6000–9000	ASICH93B.RTR	Cheng 1993
^{28}Si(α,α)^{28}Si	165	2400–4000	ASILE72A.RTR	Leung 1972
^{28}Si(α,α)^{28}Si	165	4000–5000	ASILE72B.RTR	Leung 1972
^{28}Si(α,α)^{28}Si	165	5100–6000	ASILE72C.RTR	Leung 1972
^{28}Si(α,α)^{28}Si	165	2400–5000	ASILE72D.RTR	Leung 1972
^{27}Al(α,α)^{27}Al	170	2000–9000	AALCH93A.RTR	Cheng 1993
Cl(α,α)Cl	165	2000–9000	ACLCH93A.RTR	Cheng 1993
Ar(α,α)Ar	170	1800–5200	AARLE86A.RTR	Leavitt 1986
^{39}K(α,α)^{39}K	175.5	6000–8000	AK_FR82A.RTR	Frekers 1982
Ca(α,α)Ca	166	2200–8800	ACAHU90A.RTR	Hubbard 1990
^{40}Ca(α,α)^{40}Ca	145	5000–9000	ACASE87A.RTR	Sellschop 1987

C(^{6}Li,^{6}Li)C	165	1800–4700	C6LiLiC.R33	Mayer 2001
^{19}F(^{6}Li,^{6}Li)^{19}F	150	2500–7000	19F6LiLiF.R33	Pastuović 1998
^{27}Al(^{6}Li,^{6}Li)^{27}Al	140	4000–8000	Nurmela-6Li-Al_140.R33	Nurmela 1999
^{27}Al(^{6}Li,^{6}Li)^{27}Al	170	4000–8000	Nurmela-6Li-Al_170.R33	Nurmela 1999
Si(^{6}Li,^{6}Li)Si	140	4500–7750	Nurmela-6Li-Si_140.R33	Nurmela 1999
Si(^{6}Li,^{6}Li)Si	170	4500–7750	Nurmela-6Li-Si_170.R33	Nurmela 1999
Ti(^{6}Li,^{6}Li)Ti	140	5000–11000	Nurmela-6Li-Ti_140.R33	Nurmela 1999
Ti(^{6}Li,^{6}Li)Ti	170	5000–11000	Nurmela-6Li-Ti_170.R33	Nurmela 1999

C(^{7}Li,^{7}Li)C	165	2900–5400	C7LiLiC.R33	Mayer 2001
^{16}O(^{7}Li,^{7}Li)^{16}O	170	2750–6250	16O7LiLiO.R33	Rauhala 1988
^{27}Al(^{7}Li,^{7}Li)^{27}Al	140	4000–7900	Nurmela-7Li-Al_140.R33	Nurmela 1999
^{27}Al(^{7}Li,^{7}Li)^{27}Al	170	3460–7960	27Al7LiLiAl.R33	Räisänen 1993
Si(^{7}Li,^{7}Li)Si	140	4500–7800	Nurmela-7Li-Si_140.R33	Nurmela 1999
Si(^{7}Li,^{7}Li)Si	170	4450–7710	Si7LiLiSi.R33	Räisänen 1993
Ti(^{7}Li,^{7}Li)Ti	140	5250–11000	Nurmela-7Li-Ti_140.R33	Nurmela 1999
Ti(^{7}Li,^{7}Li)Ti	170	4950–11460	Ti7LiLiTi.R33	Räisänen 1993

Table 3.4: Non-Rutherford ERDA cross-sections.

	θ **(Lab)**	**Energy (keV)**	**File**	**Reference**
H(^{3}He,H)^{3}He	20	2000–3000	1HTP1X1.R33	Terwagne 1996
H(^{3}He,H)^{3}He	30	1900–3000	1HTP1X2.R33	Terwagne 1996
H(α,H)α	30	2500–4500	1HAP4HE30.R33	Bogdanović Radović 2001
H(α,H)α	40	2500–4500	1HAP4HE40.R33	Bogdanović Radović 2001
H(α,H)α	45	2500–4500	1HAP4HE45.R33	Bogdanović Radović 2001
H(α,H)α	50	2500–4500	1HAP4HE50.R33	Bogdanović Radović 2001
H(α,H)α	55	2500–4500	1HAP4HE55.R33	Bogdanović Radović 2001
H(α,H)α	60	2500–4500	1HAP4HE60.R33	Bogdanović Radović 2001
H(α,H)α	10	600–4800	HHEHHE10_KIM.R33	Kim 1999
H(α,H)α	15	600–4800	HHEHHE15_KIM.R33	Kim 1999
H(α,H)α	20	600–4800	HHEHHE20_KIM.R33	Kim 1999
H(α,H)α	25	600–4800	HHEHHE25_KIM.R33	Kim 1999
H(α,H)α	30	600–4800	HHEHHE30_KIM.R33	Kim 1999
H(α,H)α	35	600–4800	HHEHHE35_KIM.R33	Kim 1999
H(α,H)α	40	600–4800	HHEHHE40_KIM.R33	Kim 1999
H(α,H)α	10	1000–2500	ERD10H.R33	Quillet 1994
H(α,H)α	20	1000–2500	ERD20H.R33	Quillet 1994
H(α,H)α	30	1000–2500	ERD30H.R33	Quillet 1994
H(α,H)α	20	1000–3000	HHEHHE20.R33	Baglin 1992
H(α,H)α	25	1000–3000	HHEHHE25.R33	Baglin 1992
H(α,H)α	30	1000–3000	HHEHHE30.R33	Baglin 1992
H(α,H)α	35	1000–3000	HHEHHE35.R33	Baglin 1992
H(α,H)α	30	900–3000	CRSDA.DAT, No. 125	Baglin 1992
H(α,H)α	30	2000–7000	CRSDA.DAT, No. 3	?
D(α,D)α	10	1000–2500	ERD10D.R33	Quillet 1994
D(α,D)α	20	1000–2500	ERD20D.R33	Quillet 1994
D(α,D)α	30	1000–2500	ERD30D.R33	Quillet 1994
D(α,D)α	20	1000–3000	DHEDHE20.R33	Kellock 1993
D(α,D)α	25	1000–3000	DHEDHE25.R33	Kellock 1993
D(α,D)α	30	1000–3000	DHEDHE30.R33	Kellock 1993
D(α,D)α	35	1000–3000	DHEDHE35.R33	Kellock 1993
D(α,D)α	40	1000–3000	DHEDHE40.R33	Kellock 1993
D(α,D)α	30	2200–3000	CRSDA.DAT, No. 4	?
D(α,D)α	30	1000–2070	CRSDA.DAT, No. 130	Besenbacher 1986
D(α,D)α	30	2070–2180	CRSDA.DAT, No. 131	Besenbacher 1986
D(α,D)α	30	2180–2800	CRSDA.DAT, No. 132	Besenbacher 1986

Table 3.5: Nuclear reactions cross-sections. *Total* means that the data file contains total cross-section data.

	θ **(Lab)**	**Energy (keV)**	**File**	**Reference**
D(d,p)T	Total	5–5000	2DDP.R33	Bosch 1992
D(d,t)p	Total	5–5000	2DDT.R33	Bosch 1992
D(d,^{3}He)n	Total	1–5000	2DD3HE.R33	Bosch 1992
D(t,^{4}He)n	Total	1–1370	2DTA_3.R33	Bosch 1992
D(^{3}He,α)p	Total	380–1000	CRSDA.DAT, No. 1	?
D(^{3}He,α)p	Total	700–2000	CRSDA.DAT, No. 111	?
D(^{3}He,α)p	Total	300–2000	CRSDA.DAT, No. 129	?
D(^{3}He,α)p	Total	100–2500	2DTA_1.R33	Möller 1980
D(^{3}He,α)p	Total	10–2240	2DTA_2.R33	Bosch 1992
D(^{3}He,p)α	Total	380–1000	CRSDA.DAT, No. 28	?
D(^{3}He,p)α	Total	210–2150	2DTP_1.R33	Möller 1980
D(^{3}He,p)α	Total	280–2400	2DTP_2.R33	Bonner 1952
D(^{3}He,p)α	Total	100–2500	2DTP_3.R33	Möller 1980
D(^{3}He,p)α	Total	10–2240	2DTP_4.R33	Bosch 1992
T(d,^{4}He)n	Total	1–910	3TDA.R33	Bosch 1992
^{3}He(D,α)p	Total	250–660	CRSDA.DAT, No. 2	?
^{3}He(d,α)p	Total	10–1500	3HEDA_1.R33	Bosch 1992
^{3}He(D,p)α	Total	250–660	CRSDA.DAT, No. 46	?
^{3}He(D,p)α	Total	190–1600	3HEDP_1.R33	Bonner 1952
^{3}He(d,p)α	Total	10–1500	3HEDP_2.R33	Bosch 1992
^{6}Li(p,^{3}He)^{4}He	60	650–2900	6LIP3HE.R33	Marion 1956
^{6}Li(p,α)^{3}He	60	650–2900	6LIPA.R33	Marion 1956
^{6}Li(D,α)^{4}He	150	400–1900	6LIDA_1.R33	Maurel 1981
^{6}Li(^{3}He,p$_0$)^{8}Be	165	900–5100	6LITP0.R33	Schiffer 1956
^{6}Li(^{3}He,p$_1$)^{8}Be	165	900–5100	6LITP1.R33	Schiffer 1956
^{7}Li(p,α)^{4}He	150	500–1500	7LIPA.R33	Maurel
^{9}Be(p,α)^{6}Li	Total	30–700	9BEPA.R33	Sierk 1973
^{9}Be(p,D)^{8}Be	Total	30–700	9BEPD.R33	Sierk 1973
^{9}Be(p,D)^{8}Be	135	780–3000	9BEPD_1.R33	Weber 1956
^{9}Be(p,D)^{8}Be	165	1400–1500	9BEPD_2.R33	Mayer 2001
^{9}Be(D,α_0)^{7}Li	165	500–1900	9BEDA0.R33	Biggerstaff 1962
^{9}Be(D,α_1)^{7}Li	165	500–1600	9BEDA1.R33	Biggerstaff 1962
^{9}Be(^{3}He,p$_0$)^{11}B	90	1800–5100	9BETP0_1.R33	Wolicki
^{9}Be(^{3}He,p$_1$)^{11}B	90	1800–5100	9BETP1_1.R33	Wolicki
^{9}Be(^{3}He,p$_0$)^{11}B	150	1800–5100	9BETP0_2.R33	Wolicki
^{9}Be(^{3}He,p$_1$)^{11}B	150	1800–5100	9BETP1_2.R33	Wolicki
^{10}B(p,α_0)^{7}Be	50	1800–10800	10BPA0_1.R33	Jenkin 1964
^{10}B(p,α_1)^{7}Be	50	2350–10100	10BPA1_1.R33	Jenkin 1964
^{10}B(p,α_0)^{7}Be	90	1800–9500	10BPA0_2.R33	Jenkin 1964
^{10}B(p,α_1)^{7}Be	90	2650–7100	10BPA1_2.R33	Jenkin 1964
^{10}B(D,α_0)^{8}Be	156	980–1800	10BDA0.R33	Purser 1963
^{10}B(D,α_1)^{8}Be	156	980–1800	10BDA1.R33	Purser 1963
^{10}B(^{3}He,p$_0$)^{12}C	90	2050–4000	10B3HEP0_90.R33	McIntyre 1996
^{10}B(^{3}He,p$_1$)^{12}C	90	2050–4000	10B3HEP1_90.R33	McIntyre 1996
^{10}B(^{3}He,p$_0$)^{12}C	135	2050–4000	10B3HEP0_135.R33	McIntyre 1996
^{10}B(^{3}He,p$_1$)^{12}C	135	2050–4000	10B3HEP1_135.R33	McIntyre 1996
^{10}B(^{3}He,p$_0$)^{12}C	90	1300–5000	10BTP0.R33	Schiffer 1956

	θ (Lab)	Energy (keV)	File	Reference
^{10}B(^{3}He,p$_1$)^{12}C	90	1300–5000	10BTP1.R33	Schiffer 1956
^{10}B(α,p$_0$)^{13}C	135	4000–5000	10BAP0.R33	Giorginis 1995
^{10}B(α,p$_1$)^{13}C	135	4000–5000	10BAP1.R33	Giorginis 1995
^{11}B(p,α_0)^{8}Be	155	700–6000	11BPA0.R33	Symons 1963
^{11}B(^{3}He,p$_0$)^{13}C	90	2050–4000	11B3HEP0_90.R33	McIntyre 1996
^{11}B(^{3}He,p$_0$)^{13}C	135	2050–4000	11B3HEP0_135.R33	McIntyre 1996
^{11}B(^{3}He,p$_0$)^{13}C	90	3000–5400	11BTP0.R33	Holmgren 1959
^{11}B(^{3}He,p$_{1,2,3}$)^{13}C	90	3000–5400	11BTP123.R33	Holmgren 1959
^{11}B(^{3}He,D$_0$)^{12}C	90	3000–5400	11BTD0.R33	Holmgren 1959
^{12}C(D,p)^{13}C	135	520–2950	12CDP_1.R33	Jarjis 1979
^{12}C(D,p)^{13}C	165	800–1950	12CDP_2.R33	Kashy 1960
^{12}C(^{3}He,p$_0$)^{14}N	90	2100–2300	12CTP0.R33	Tong 1990
^{12}C(^{3}He,p$_1$)^{14}N	90	2100–2400	12CTP1.R33	Tong 1990
^{12}C(^{3}He,p$_2$)^{14}N	90	2100–2400	12CTP2.R33	Tong 1990
^{12}C(^{3}He,p$_0$)^{14}N	159.4	1800–5400	12CTP0_1.R33	Kuan 1964
^{12}C(^{3}He,p$_1$)^{14}N	159.4	1800–5400	12CTP1_1.R33	Kuan 1964
^{12}C(^{3}He,p$_2$)^{14}N	159.4	1800–5400	12CTP2_1.R33	Kuan 1964
^{12}C(^{3}He,α_0)^{11}C	159.4	1800–5400	12CTA0.R33	Kuan 1964
^{13}C(D,p)^{14}C	135	600–2950	13CDP.R33	Marion 1956
^{14}N(D,α_0)^{12}C	150	600–1400	14NDA0_1.R33	Amsel 1969
^{14}N(D,α_1)^{12}C	150	600–1400	14NDA1_1.R33	Amsel 1969
^{14}N(D,p$_0$)^{15}N	150	500–1900	14NDP0_1.R33	Simpson 1984
^{14}N(D,p$_{1,2}$)^{15}N	150	600–1400	14NDP12.R33	Amsel 1969
^{14}N(D,p$_3$)^{15}N	150	800–1400	14NDP3.R33	Amsel 1969
^{14}N(D,p$_{4,5}$)^{15}N	150	600–1400	14NDP45.R33	Amsel 1969
^{14}N(D,p$_5$)^{15}N	150	600–1400	14NDP45.R33	Amsel 1969
^{14}N(^{3}He,p$_0$)^{16}O	90	2100–4000	14N3HEP0_90.R33	McIntyre 1996
^{14}N(^{3}He,p$_0$)^{16}O	135	2100–4000	14N3HEP0_135.R33	McIntyre 1996
^{14}N(^{3}He,p$_{1,2}$)^{16}O	90	2100–4000	14N3HEP12_90.R33	McIntyre 1996
^{14}N(^{3}He,p$_{1,2}$)^{16}O	135	2100–4000	14N3HEP12_135.R33	McIntyre 1996
^{14}N(^{3}He,p$_{3,4}$)^{16}O	90	2100–4000	14N3HEP34_90.R33	McIntyre 1996
^{14}N(^{3}He,p$_{3,4}$)^{16}O	135	2100–4000	14N3HEP34_135.R33	McIntyre 1996
^{14}N(^{3}He,p$_{1,2}$)^{16}O	90	1600–2800	14NTP1X1.R33	Terwagne 1994
^{14}N(^{3}He,p$_{1,2}$)^{16}O	135	1600–2800	14NTP1X2.R33	Terwagne 1994
^{14}N(^{3}He,p$_3$)^{16}O	90	1600–2800	14NTP3X1.R33	Terwagne 1994
^{14}N(^{3}He,p$_3$)^{16}O	135	1600–2800	14NTP3X2.R33	Terwagne 1994
^{14}N(^{3}He,p$_4$)^{16}O	90	1600–2800	14NTP4X1.R33	Terwagne 1994
^{14}N(^{3}He,p$_4$)^{16}O	135	1600–2800	14NTP4X2.R33	Terwagne 1994
^{14}N(^{3}He,p$_5$)^{16}O	90	1600–2800	14NTP5X1.R33	Terwagne 1994
^{14}N(^{3}He,p$_5$)^{16}O	135	1600–2800	14NTP5X2.R33	Terwagne 1994
^{14}N(^{3}He,p$_7$)^{16}O	90	1600–2800	14NTP7X1.R33	Terwagne 1994
^{14}N(^{3}He,p$_7$)^{16}O	135	1600–2800	14NTP7X2.R33	Terwagne 1994
^{14}N(^{3}He,α_0)^{13}N	90	1600–2800	14NTA0X1.R33	Terwagne 1994
^{14}N(^{3}He,α_0)^{13}N	135	1600–2800	14NTA0X2.R33	Terwagne 1994
^{14}N(α,p$_0$)^{17}O	135	4000–5000	14NAP1.R33	Giorginis 1995
^{15}N(p,α)^{12}C	140	900–2860	15NPA.R33	Hagedorn 1957
^{15}N(D,α)^{13}C	90	400–1600	15NDA90.R33	Vickridge 1996
^{15}N(D,α)^{13}C	135	400–2000	15NDA135.R33	Vickridge 1996

	θ (Lab)	Energy (keV)	File	Reference
^{15}N(D,α)^{13}C	150	400–2000	15NDA150.R33	Vickridge 1996
^{15}N(D,α)^{13}C	150	800–1300	15NDA_1.R33	Sawicki 1985
^{16}O(D,α)^{14}N	135	800–2000	16ODA_2.R33	Amsel 1964
^{16}O(D,α)^{14}N	145	760–950	16ODA_1.R33	Turos 1973
^{16}O(D,α)^{14}N	165	800–2000	16ODA_3.R33	Amsel 1964
^{16}O(D,p$_0$)^{17}O	135	20–3000	16ODP0_1.R33	Jarjis 1979
^{16}O(D,p$_1$)^{17}O	135	500–3000	16ODP1_2.R33	Jarjis 1979
^{16}O(D,p$_1$)^{17}O	155	400–1100	16ODP1_1.R33	Amsel 1967
^{16}O(^{3}He,α)^{15}O	90	1600–2600	16OTA.R33	Abel
^{18}O(p,α)^{15}N	155	1500–1800	18OPA_2.R33	Alkemada
^{18}O(p,α)^{15}N	165	500–1000	18OPA_1.R33	Amsel 1967
^{18}O(D,α_0)^{16}N	165	830–2000	18ODA_1.R33	Amsel 1964
^{18}O(D,α_1)^{16}N	165	830–2000	18ODA_2.R33	Amsel 1964
^{18}O(D,α_2)^{16}N	165	830–2000	18ODA_3.R33	Amsel 1964
^{18}O(D,α_3)^{16}N	165	830–2000	18ODA_4.R33	Amsel 1964
^{19}F(p,α)^{16}O	90	700–1900	19FPA_1.R33	Dieumegard 1980
^{19}F(p,α)^{16}O	150	700–2000	19FPA_2.R33	Dieumegard 1980
^{19}F(D,α_0)^{17}O	150	700–1900	19FDA0_1.R33	Maurel 1981
^{19}F(D,α_1)^{17}O	150	1000–1900	19FDA1_1.R33	Maurel 1981
^{32}S(D,p$_0$)^{33}S	150	1000–2700	32SDP.R33	Healy 1998
^{32}S(D,p$_1$)^{33}S	150	1000–2700	32SDP1.R33	Healy 1998
^{32}S(D,p$_2$)^{33}S	150	1000–2700	32SDP2.R33	Healy 1998
^{32}S(D,p$_3$)^{33}S	150	1000–2700	32SDP3.R33	Healy 1998
^{32}S(D,p$_{456}$)^{33}S	150	1000–2700	32SDP456.R33	Healy 1998
^{32}S(D,p$_7$)^{33}S	150	1000–2700	32SDP7.R33	Healy 1998

3.7 `Calculate` menu

In the `Calculate` menu all commands for calculating spectra, scattering kinematics, stopping powers and data fitting are located. Additionally some helpful tools (density conversions, particles*sr) can be found here.

- `Calculate Spectrum`: Calculates the simulated spectrum.
- `Fit Spectrum...`: Data fitting to experimental data. See section 3.7.1 for details.
- `Kinematics...`: Calculation of scattering kinematics. Allows the calculation of the energies of backscattered particles, recoils and nuclear reaction products.
- `Stopping...`: Calculation of stopping powers for any projectile in any target element and of energy loss in the different layers.
- `Cross Section...`: Calculation of Rutherford cross sections for backscattering and recoils.
- `Density...`: Density conversions (for elements only). Mass density to atomic density and conversion from atoms/cm^2 to μg/cm^2 and nm.
- `Particles*sr...`: Calculation of particles*sr from the collected charge and detector solid angle.

3.7.1 `Fit Spectrum...`

Data fitting to backscattering spectra is a nontrivial task. In data fitting the quadratic deviation of the simulated from the measured data points

$$\chi^2 = \sum_i \frac{(N_{exp}(i) - N_{sim}(i))^2}{\sigma_i^2} \tag{3.5}$$

is minimized by varying the input parameters of the calculation. $N_{exp}(i)$ is the number of counts in channel i of the measured spectrum, $N_{sim}(i)$ the number of counts in channel i of the simulated spectrum, and σ_i the statistical error of each data point [4].

Fast fitting algorithms, such as the Levenberg-Marquardt algorithm, tend to be unstable and require the knowledge of the derivatives of χ^2. SIMNRA uses the Simplex algorithm for fitting [6, 7, 8]. The Simplex algorithm is very stable and converges (nearly) always. However, the convergence is not very fast. The Simplex algorithm always uses $n + 1$ points (called vertices) in the parameter space for fitting, where n is the number of free parameters.

You can fit:

1. Energy calibration (energy/channel and offset only, quadratic term is not changed)

[4] SIMNRA uses $\sigma_i = \sqrt{N_{exp}}$ for $N_{exp} > 4$, $\sigma_i = 2$ for $N_{exp} \leq 4$ due to Poisson statistics.

2. Particles*sr
3. Thickness of a layer
4. Composition of a layer

independently or all at once. Check which parameters should be varied. Only one layer at a time can be fitted.

- `Number of fit regions`: Number of different regions where χ^2 is calculated. Up to 10 different regions may be used. At least one region must be specified. The regions should not overlap.
- `From To`: Lower and upper channel of each fit region.
- `Max Iterations`: Maximum number of Simplex iterations. Fitting will be performed until the desired accuracy is obtained or the maximum number of iterations is reached.
- `Fit Accuracy`: Desired accuracy of the fit. The fit has converged if the relative change of all fitted parameters and of χ^2 is below `Fit Accuracy`. The relative change of a parameter A is $\Delta A/A$, where ΔA is the difference between the best vertex (the vertex with the lowest χ^2) and the worst vertex (the vertex with the highest χ^2).
- `Calculate Fit Error`: If checked an error estimate for all fitted parameters is computed. See below for details. This is a time consuming process and may require more computing time than the fit itself. Default is unchecked.

Fit error

An error bar for fitted parameters can be obtained under the following assumptions:

1. The physics model (i.e. stopping powers, cross sections etc.) is assumed to be accurate with zero error. Obviously, in reality this is not the case, and errors introduced by inaccurately known stopping powers or cross sections may largely exceed the computed errors. SIMNRA does not know whether a stopping power or cross section is accurate or not — you should know that.
2. All nonfitted parameters are assumed to be accurate with zero error. Again, usually this will be not the case, but SIMNRA is not able to quantify these errors: It does not know how accurately you determined your energy calibration or performed the ion current measurement.

The error bar Δa of a fitted parameter a is determined by the shape of the χ^2 surface near the minimum: A flat minimum of χ^2 allows a larger variation of a and will result in larger errors of a. On a confidence level of 68.3% (the usual 1σ interval) the error of a is obtained by varying a until χ^2 has increased by 1 [8]:

$$\Delta\chi^2(a_{\Delta=1}) = \chi^2(a_{\Delta=1}) - \chi^2_{min} = 1. \tag{3.6}$$

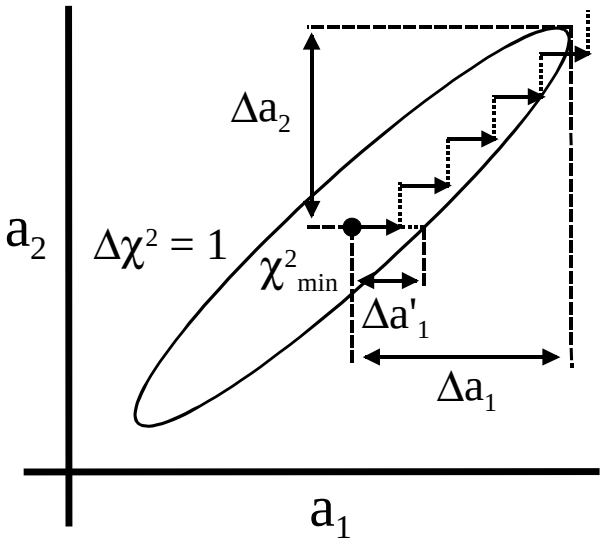

Figure 3.6: $\Delta\chi^2 = 1$ contour near the χ^2 minimum (black dot) for two fit parameters a_1 and a_2. Δa_1 and Δa_2 are the fit errors for a_1 and a_2 if fitted simultaneously, $\Delta a_1'$ the error for a_1 if only a_1 is fitted.

χ^2_{min} is the minimised χ^2 with an optimised parameter a_{min}, and the error Δa of a is $\Delta a = |a_{\Delta=1} - a_{min}|$.

If we have more than one fit parameter things get more complicated [8]. As an example we consider the case of two fit parameters a_1 and a_2. The $\Delta\chi^2 = 1$ contour now is an ellipse (fig. 3.6) due to correlations between a_1 and a_2, and for more than two fit parameters a multi-dimensional ellipsoid. To find the confidence intervals for a_1 and a_2 we have to do the following: Increase a_1 by some amount (black arrows in fig. 3.6). Now find a new minimum of χ^2 by optimising a_2, a_1 remains unchanged (dotted line in fig. 3.6). Increase a_1 and optimise a_2 again, and so on until $\Delta\chi^2 = 1$. For n fit parameters $a_1 ... a_n$ we have to increase a_1 and optimise $a_2 ... a_n$ until $\Delta\chi^2 = 1$.

As can be seen in fig. 3.6 the error bar $\Delta a_1'$ becomes nonrealistic small if only a_1 is fitted. This is a consequence of the assumption that all nonfitted parameters are accurate. To obtain realistic error bars all parameters should be fitted in one step.

A quantitative measure for the goodness-of-fit of the assumed model can be obtained from the value of χ^2_{min}. See [8, Chapter 14.1] (or any good textbook about statistics) for more information.

3.8 `Tools` menu

In the `Tools` menu several tools for spectrum evaluation are located. You can find

1. a data reader to read out the contents of a specific channel
2. a tool for integrating spectra.

These tools appear as floating windows and are updated automatically if the spectrum is recalculated or if a new spectrum is loaded from disk.

3.8.1 `Data Reader`

The data reader is displayed as a small black crosshair with white legend in the plot. The data reader control window displays the channel, the energy of this channel and the number of counts in the channel. The data reader is moved by entering the channel number or by using the spin up/spin down buttons in the control window. The data reader is updated automatically if a spectrum is recalculated or if a new spectrum is loaded from disk.

3.8.2 `Integrate Spectrum`

The `Integrate Spectrum` tool allows to integrate a specific spectrum. The integral of a spectrum is the sum of all counts between a lower and an upper channel including the boundary channels. The integration boundaries are displayed as small black vertical lines in the plot. The boundaries are moved by entering the channel numbers or by using the spin up/spin down buttons in the control window. The integral is updated automatically if a spectrum is recalculated or if a new spectrum is loaded from disk.

3.9 `Plot` menu

This section describes all plot related commands, including all commands which are not accessible via menus.

- `Autoscaling`: If checked, the plot will be scaled automatically to minimum and maximum if experimental data are imported or a new calculation is performed. If unchecked, the axis scales remain fixed.
- `Rescale x-Axis`: Scales the x-axis to minimum and maximum of all visible spectra.
- `Rescale y-Axis`: Scales the y-axis to minimum and maximum of all visible spectra.
- `Unzoom`: Undo all zoom operations.
- `x-Axis...`: Scale the x-axis manually by entering the axis minimum and maximum, set logarithmic x-axis. Same as a double-click with the left mouse button on the x-axis.
- `y-Axis...`: Scale the y-axis manually by entering the axis minimum and maximum, set logarithmic y-axis. Same as a double-click with the left mouse button on the y-axis.
- `Legend...`: Allows to alter the text of the legend. Same as a double-click with the left mouse button on the legend.
- `Delete Experimental Data`: Deletes the experimental data from the plot.
- `Delete Simulated Data`: Deletes all simulated data from the plot.
- **Zooming into the plot:** To zoom into the plot click with the left mouse button into the upper left corner of the range you want to zoom in. Keep the mouse button down and tear a rectangle to the lower right corner of the zooming range.
- **Panning:** Click with the right mouse button into the plot, keep the mouse button down and move the mouse.
- **Zooming out:** Click with the left mouse button into the plot. Keep the mouse button down and move the mouse towards the upper left corner. Or use `Plot: Unzoom`.

3.10 `Options` menu

- `Create Reaction List`: SIMNRA uses a file named CRSEC.LST in the cross-sections directory to know which cross-section data are available. `Create Reaction List` will create this file. You have to recreate the reaction list if you add or delete cross-section data files, see section 3.14.

  Note: In some cases files are not readable by SIMNRA due to format errors. These files will be ignored. The program displays a list of all ignored files.

- `Preferences...`: Allows to set global program preferences. These preferences are stored permanently.

  The `Print` tab:

  - `White background for print`: If checked, then the grey background of the graph is changed to white in the printout.
  - `Show "Print What?" dialog`: If checked, then a dialog asking what to print (experimental conditions, graph) is displayed. If unchecked, this dialog is omitted and everything is printed.

  The `Spectrum Data` tab:

  - Determines which menu entries are visible in the `File: Read Spectrum Data` menu.

  The `Saving` tab:

  - `Create BACKUP.NRA when saving`: If checked, the old NRA-file is saved to a file named BACKUP.NRA each time `File: Save` or `File: Save As...` is used. In the case of erraneous overwriting of a file you can recover the old data from this file. In each directory only one BACKUP.NRA can exist.

3.11 Help menu

- `User's Guide`: Opens the User's Guide in PDF-format using Adobe Acrobat or Adobe Acrobat Reader.
  Note 1: Adobe Acrobat or Acrobar Reader are not part of SIMNRA. Adobe Acrobat Reader can be obtained freely from the Adobe web site at `www.adobe.com`, while Adobe Acrobat is a commercial product.
  Note 2: Context sensitive help is only available with Adobe Acrobat, but not with Adobe Acrobat Reader. The Reader always starts with the first page of the User's Guide, which is due to some limitations of the Reader. SIMNRA first tries to invoke Acrobat, and if this fails Acrobat Reader.

- `About...`: Shows the version number of the program.

- `Register...`: Registration of the program.

3.12 Data exchange with other programs

3.12.1 Graphics programs: Excel, Origin, ...

SIMNRA allows to exchange data with graphics programs by two different methods:

1. Via the clipboard. With `Edit: Copy Data` the experimental and simulated spectra are copied in ASCII format to the windows clipboard. They can be pasted into any spreadsheet program. See section 3.3 for details.

2. Via ASCII file. With `File: Write Spectrum Data...` the experimental and simulated data are exported as columns into an ASCII file. You can import this file into any plot program, such as Excel, Origin or Mathematica. See section 3.2 for details.

3.12.2 RUMP

SIMNRA can read and write sample description files (*.LCM) and read RBS files (*.RBS) used by the RUMP program. Sample description files contain the composition of the sample and the absorber foil. These files can be read and written by `File: RUMP: Read Sample Description File` and `File: RUMP: Write Sample Description File`. RUMP stores experimental parameters (Type of incident particles, incident energy, scattering geometry, etc.) and spectral data in binary files with extension *.RBS. These files can be read by `File: RUMP: Read RBS File`. SIMNRA can not write RBS files.

Sample Description Files

SIMNRA supports only a subset of the RUMP sample description commands. The supported command are listed in Table 3.6. All other commands will be neglected. Note that especially the RUMP commands `Equation`, `Species` and `Fuzz` are not supported. If your sample description file contains these commands, they will be neglected and a warning will be shown.

RBS Files

SIMNRA can read RUMP's RBS file format version 1.1 from 8/94 with the following limitations:

1. Data compression level 3 (zero compressed) is not implemented. Levels 0–2 (uncompressed real, uncompressed integer, differential integer) are fully implemented.

2. Each RBS file may contain only one spectrum. Record type 20h is allowed, but may contain only one row.

3. Only one record 120h (RBS spectrum type) or 121h (FRES spectrum type) may be present, i.e. simultaneous RBS and FRES (= ERD) are not allowed.

4. Record types 01h (printed comments), 02h (unprinted comments), 101h (identifier for the data set), 102h (MCA information) and 103h (collection date/time) are recognized, but ignored.

RESET
LAYER
OPEN
NEXT
COMPOSITION[a][b]
THICKNESS[c]
ABSORBER

[a] Partly implemented. Only elements are recognised, but no isotopes. The command `Composition Si 1 O 2 /` will be recognised and the natural isotopic ratios for Si and O will be used. The command `Composition 28Si 1 16O 2 /` will not be recognised properly.

[b] RUMP allows to enter SiO_2 as Si 1 O 2. SIMNRA will convert this to Si 0.33333 O 0.66666.

[c] As units for thickness are possible: `/CM2`, `M/CM2`, `A`, `NM`. If `A` for Å or `NM` for nm are used, SIMNRA will use the weighted atomic densities of all elements in the layer to convert Å or nm to 10^{15} atoms/cm^2. It is highly recommended to use the units `/CM2` or `M/CM2` instead.

Table 3.6: RUMP sample description commands which are supported by SIMNRA.

5. Record type 111h (accelerator parameters): Beam current is ignored by SIMNRA, and pile-up is not calculated.

6. Record type 112h (data collection parameters): Starting channel of data is rounded from real to integer. This may result in differences of ±0.5 channels between RUMP and SIMNRA, if a non-integer starting channel is used.

3.12.3 IBA data furnace

The IBA data furnace (NDF) was developed at the University of Surrey and is available from http://www.ee.surrey.ac.uk/Research/SCRIBA/ndf/. This program converts energy spectra to depth profiles. The depth profiles are stored in RUMP's sample description format LCM. You can read these files with the command `File: Read RUMP`, see section 3.12.2.

3.13 Importing spectrum data in any format

SIMNRA can read experimental spectrum data in several formats including ASCII, see section 3.2. But many laboratories have their own spectrum data file formats. SIMNRA offers the possibility to import any type of experimental data by supplying a dynamic link library (DLL), which reads the data and passes them to SIMNRA. This DLL must be supplied by the user and is called if `File: Read Spectrum Data: User...` is clicked. This section describes the details of this DLL.

The DLL-name must be `user.dll`. It must be located in the `SIMNRA\UserDll` subdirectory - otherwise SIMNRA will not find it. The DLL must export a function `ReadData` (exact spelling), defined as follows[5]:

```
Function ReadData  (FileName :  PChar;
                    Var Count :  Integer;
                    Data :  Pointer):      Integer; stdcall;
```

`Filename`	Input parameter. Null terminated string with the full name including path to the file which shall be read.
`Count`	Output parameter. Pointer to a 32 bit signed integer value which indicates how many channels were actually read.
`Data`	Input parameter. Pointer to an array of 32 bit signed integer values which will take the spectrum data. The array starts at channel 0(!) and has a maximum of 8192 channels.

The return value of `ReadData` is a 32 bit signed integer. It must be 0, if the file was read successfully. Any other return value indicates an error condition.

The calling convention of `ReadData` must be `stdcall` in Borland Delphi or `WINAPI` in Microsoft C++.

A small code example in Pascal can be found in `UserDLL\sample.dpr`. A more detailed example is given in `UserDLL\sample1.dpr`.

[5]The code examples are in Pascal (Borland Delphi 4).

3.14 Adding new cross-section data

To add new cross-section data, you have to perform the following steps:

1. Create a cross-section data file in the R33 file format. The easiest way to do this is by using the R33Manager. Alternatively you can use any text editor. The file format is described below.

2. Copy this file into the directory where all other cross-section data files are (subdirectory CRSEC of your SIMNRA installation).

3. Recreate the reaction list by clicking `Options: Create Reaction List`.

   Note: If your file is ignored, SIMNRA was not able to read or understand the file. Carefully read the section about the R33 file format and try again.

3.14.1 The R33 file format

The R33 file format is described in full detail by I.C. Vickridge in the file R33Help.htm, which should be present in your SIMNRA installation directory, and in Appendix B. SIMNRA reads the updated R33 file format of April 2002, but is also able to read older R33 files which conform to the original specification from the year 1991[6].

An example for a valid file in the R33 format is shown in fig. 3.7. Each line must end with <CR><LF> (Carriage Return and Line Feed).

SIMNRA uses not only the data points, but also a part of the information supplied in the file header. The following lines are used by SIMNRA and must be present in the file. Though the lines may be arranged in any order, it is recommended to arrange them in the same order as shown in Fig. 3.7. Any other entries than the ones listed below are ignored by SIMNRA, but may be necessary to form a valid R33 file. See Appendix B or the file R33Help.htm for details.

- A line containing the string 'Source:'. The rest of the line has to contain a reference or other source for the data and will appear as description in the reaction menu.

- A line containing the string 'Reaction:'. SIMNRA will interpret the nuclear reaction string written in that line (In the example of fig. 3.7 16O(d,a0)14N) to find out which particles are involved in the nuclear reaction. The masses of the particles are ignored.

- A line containing the string 'Masses:'. SIMNRA will read the masses of the particles from this line. All masses in amu. The first mass is the mass of the incident particle, the second mass is the mass of the target particle, the third mass is the mass of the outgoing particle for which the cross-section is valid and the fourth mass is the mass of the other reaction product. The masses may be rounded to the nearest integer value - SIMNRA will replace the given masses by the exact values.

[6] The original specification can be found in DSIR Physical Sciences Report 33 by I.C. Vickridge

```
COMMENT: These cross sections have been digitised from the publication
cited below.  No error of either the energy and or the sigma is given.
Some errors may be among the data, we are recently checking them.
The Los Alamos Ion Beam Handbook also will contain these data as soon
as it is ready.  If you use this data please refer to the paper below.
Source:  A.Turos, L.Wielunski and a Batcz, NIM, 111(1973), 605
Special comment:
WARNING ! THIS IS MAINLY FOR TEST NO GUARANTY IS PROVIDED FOR EVEN
AGREEMENT WITH THE ORIGINAL PUBLICATION.
File created by R33 Manager version 0.1

Version:  R33
Source:  A.Turos, L.Wielunski and a Batcz, NIM, 111(1973), 605
Name:  Gyorgy Vizkelethy
Address1:  Department of Physics
Address2:  Idaho State University
Address3:  Campus Box 8106
Address4:  Pocatello, ID 83209-8106
Address5:  (208) 236-2626
Address6:  vizkel@physics.isu.edu
Serial Number:  0
Reaction:  16O(d,a0)14N
Distribution:  Energy
Composition:
Masses:  2.000, 16.000, 4.000, 14.000
Zeds:  1, 8, 2, 7
Qvalue:  3110.00, 0.00, 0.00, 0.00, 0.00
Theta:  145.00
Sigfactors:  1.00, 0.00
Enfactors:  1.00, 0.00, 0.00, 0.00
Units:  mb
Data:
761.0      0.0      2.92E+0000      0.0
770.0      0.0      3.65E+0000      0.0
775.0      0.0      3.99E+0000      0.0
780.0      0.0      4.41E+0000      0.0
785.0      0.0      4.55E+0000      0.0
EndData:
```

Figure 3.7: Example for a cross-section data file in the R33 file format.

In some cases, for example if the file contains elastic scattering data, the cross section values are not for a specific isotope, but for natural isotopic composition. In this case the mean target mass should be used.

- If the cross section values are for natural isotopic target composition rather than for a specific isotope a line containing the string 'Composition: Natural' has to be present. In this case the given cross section is used for all isotopes. This line has to be omitted if the cross section is for a specific isotope.

  Other compositions than 'Natural' must not be used.

- A line containing the string 'QValue:'. The Q-value is the energy released in the nuclear reaction (in keV). Q = 0.0 for elastic scattering. Up to 5 different Q-values are allowed, for example for multiple particle groups which are not resolved. SIMNRA will use the mean value of all non-zero Q-values.

- A line containing the string 'Theta:'. Theta should be given in degrees. The value of theta is not used by SIMNRA, but this line must be present and contain a value.

- Optionally a line containing the string 'Units:' may be present. Valid values are 'mb' for differential cross sections, 'tot' for total cross sections, and 'rr' for ratio to Rutherford. Differential cross sections have to be in mbarn/sr, and total cross sections in mbarn. If the 'Units' line is omitted, SIMNRA will assume 'mb', i.e. differential cross sections. The value 'tot' indicates that the cross section is integrated over all angles. Thus if 'tot' is used the value of theta has no meaning. Nevertheless, a valid real number has to be given for theta.

- A line containing either the string 'Nvalues:' or 'Data:'. The value of Nvalues is ignored. SIMNRA assumes that the data will start after this line.

- The data are organised in 4 columns: The first column is the energy in keV, the second column is the energy error in keV (ignored by SIMNRA), the third column is the cross-section in the laboratory frame, and the fourth column is the cross-section error (ignored by SIMNRA). The cross section units have to be mbarn/sr for differential cross sections and mbarn for total cross sections. SIMNRA expects the data to be arranged in order of ascending energy.

- Scale conversion factors ('EnFactors' and 'SigFactors') must not be used, as they are ignored by SIMNRA.

3.15 Energy calibration issues

3.15.1 Detector nonlinearity

A semiconductor detector, which is used in most ion beam experiments, does not measure the real particle energy, but a somewhat smaller energy. This has been called pulse height defect. The pulse height defect is due to:

1. The energy and particle dependent energy loss in the top electrode and the dead layer of the semiconductor detector [9, 10, 11].

2. Only the electronic energy loss in the active detector region is measured, while nuclear energy loss is not detected [9]. The nuclear energy loss is energy and particle dependent.

3. Heavy ions produce a high density of electron-hole pairs. The electron-hole pairs may recombine before separation by the electric field in the detector. This has been called plasma effect [9]. The plasma effect is energy and particle dependent.

The energy dependence of the pulse height defect results in a nonlinearity of the energy calibration. The energy loss in the top electrode and the dead layer can be accounted in the following way:

- You can create a foil consisting of two layers in front of the detector. Layer 2 is composed of the material of the top electrode (usually Au) and has the thickness of the electrode (usually the thickness is supplied by the manufacturer of the detector). Layer 1 is composed of silicon in the case of a silicon detector and has the thickness of the dead layer (the dead layer is the insensitive region near the electrode). The dead layer thickness can be obtained only experimentally by tilting the detector.

For swift ions (protons and He) this should be sufficient to achieve a linear energy calibration. But the nuclear energy loss and the plasma effect, which are both important for heavy ions, are not taken into account by this procedure.

An easier way to account for detector nonlinearities is to use a non-linear energy calibration with a quadratic correction term of the form

$$E\,[\mathrm{keV}] = A + B \times \mathrm{channel} + C \times \mathrm{channel}^2.$$

See section 3.4.1 for details.

3.15.2 Energy calibration for different ion species

As already shown in Section 3.15.1 the pulse height defect depends on the particle species. This requires an individual energy calibration for each ion species if different ion species are detected, as is the case in NRA and ERDA measurements with incident heavy ions. SIMNRA offers the possibility to use an individual nonlinear energy calibration for each detected species, see Section 3.4.1 for details.

3.16 Programming support

3.16.1 Command line parameters

- */regserver* — Registers the OLE automation server in the Windows Registry. This is done automatically by SIMNRA, so there should be rarely, if ever, the necessity to use this parameter.
- */unregserver* — Unregisters the OLE automation server from the Windows Registry. This can be done before uninstalling SIMNRA.
- Additionally SIMNRA accepts one optional command line parameter, which is the name with full path of a NRA-file. This file is opened upon startup. Use double quotes (") if the file name contains blanks.

  Example: `simnra "c:\test.nra"`

3.16.2 OLE automation summary

This section describes OLE 2.0 automation support in SIMNRA. SIMNRA is an OLE automation server, which allows other applications to control SIMNRA. This is useful for batch processing of a large number of spectra and the like. A short overview of the OLE objects and methods is given below, for a complete description of the parameters associated with OLE automation methods see appendix A. Some sample programs can be found in section A.10.

Objects

SIMNRA exports the following OLE automation objects:

- *Simnra.App* — The application itself.
- *Simnra.Setup* — Experimental setup.
- *Simnra.Calc* — Parameters for calculation.
- *Simnra.Target* — Target with layers and elements.
- *Simnra.Fit* — Fit parameters.
- *Simnra.Spectrum* — Experimental and simulated spectra; Plot properties.
- *Simnra.Stopping* — Stopping powers, energy loss and straggling in elements and layers.

Properties and methods

SIMNRA exports the following OLE automation properties and methods, grouped by object:

Simnra.App

- *Active* — Specifies whether SIMNRA is active and has focus.
- *BringToFront* — Brings SIMNRA to the front above all other applications.
- *CalculateSpectrum* — Calculates a simulated spectrum.
- *CopySpectrumData* — Copies experimental and simulated spectra in ASCII format to the Windows clipboard.
- *DeleteSpectrumOnCalculate* — Specifies whether the current simulated spectrum is deleted if a new calculation is performed.
- *FitSpectrum* — Fits a spectrum.
- *Hide* — Hides SIMNRA.
- *LastMessage* — Text of the last error message or warning.
- *Maximize* — Maximizes SIMNRA to fill the whole screen.
- *Minimize* — Minimizes SIMNRA to the Windows task bar.
- *Open* — Opens a NRA-file.
- *ReadSpectrumData* — Imports experimental data in different data formats.
- *Restore* — Restores the minimized application to its normal size.
- *SaveAs* — Saves a NRA-file.
- *Show* — Shows SIMNRA, if it was hidden.
- *ShowMessages* — Specifies if error messages are shown.
- *WriteSpectrumData* — Writes all spectra (experimental, simulated) in ASCII-format to a file.

Simnra.Setup

- *Alpha* — Incident angle [deg].
- *Beamspread* — Energy spread of incident beam [keV FWHM].
- *Beta* — Exit angle [deg].
- *CalibrationLinear* — Linear calibration term B for energy calibration, see eq. 3.1 [keV/channel].
- *CalibrationOffset* — Calibration offset A for energy calibration, see eq. 3.1 [keV].

- *CalibrationQuadratic* — Quadratic calibration term C for energy calibration, see eq. 3.1 [keV/channel^2].
- *DetectorResolution* — Detector resolution [keV FWHM].
- *Energy* — Energy of incident ions [keV].
- *ParticlesSr* — Number of incident particles times solid angle [sr].
- *Theta* — Scattering angle [deg].

Simnra.Calc

- *AutoStepwidthIn* — Specifies if automatic step width control for incident ions is used.
- *AutoStepwidthOut* — Specifies if automatic step width control for outgoing ions is used.
- *dEin* — Stepwidth incident ions [keV].
- *dEout* — Stepwidth outgoing ions [keV].
- *DualScattering* — Specifies if dual scattering is calculated.
- *ElementSpectra* — Specifies if individual spectra for each element in the target are calculated.
- *EMin* — Cutoff energy [keV].
- *HighEnergyStopping* — Selects high energy stopping (Andersen-Ziegler only).
- *Isotopes* — Specifies if isotopes are taken into account.
- *IsotopeSpectra* — Specifies if individual spectra for each isotope in the target are calculated.
- *MultipleScattering* — Specifies if multiple scattering is calculated.
- *NumberOfAngleVariations* — Number of angle steps in the calculation of rough substrates.
- *NumberOfDVariations* — Number of thickness steps in the calculation of rough layers.
- *Straggling* — Specifies if energy loss and geometrical straggling are taken into account.
- *ZBStopping* — Selects Ziegler-Biersack or Andersen-Ziegler stopping.

Simnra.Target

- *AddElement* — Adds an element to a layer.
- *AddLayer* — Adds a layer to the target.
- *DeleteElement* — Deletes an element from a layer.
- *DeleteLayer* — Deletes a layer from the target.
- *ElementConcentration* — Concentration of an element in a layer.
- *ElementName* — Name of an element in a layer.
- *HasLayerRoughness* — Specifies if a layer is rough.
- *HasSubstrateRoughness* — Specifies if the substrate is rough.
- *InsertLayer* — Inserts a layer.
- *LayerRoughness* — FWHM of the roughness of a layer [10^{15} atoms/cm^2].
- *LayerThickness* — Thickness of a layer [10^{15} atoms/cm^2].
- *NumberOfElements* — Number of different elements in a layer.
- *NumberOfLayers* — Total number of layers in the target.
- *SubstrateRoughness* — FWHM of the substrate roughness [deg].

Simnra.Fit

- *Accuracy* — Desired accuracy of the fit.
- *Chi2* — Quadratic deviation χ^2 between the simulated and measured data points.
- *EnergyCalibration* — Specifies if the energy calibration is fitted.
- *LayerComposition* — Specifies if the composition of a layer is fitted.
- *LayerNr* — Specifies which layer is fitted.
- *LayerThickness* — Specifies if the thickness of a layer is fitted.
- *MaxIterations* — Maximum number of fit iterations.
- *NumberOfRegions* — Number of different fit regions.
- *ParticlesSr* — Specifies if the number of incident particles times solid angle is fitted.
- *RegionMaxChannel* — Upper channels of fit regions.
- *RegionMinChannel* — Lower channels of fit regions.

Simnra.Spectrum

- *AutoScale* — Specifies if the plot is scaled automatically.
- *BottomAxisMax* — Bottom axis maximum.
- *BottomAxisMin* — Bottom axis minimum.
- *LeftAxisMax* — Left axis maximum.
- *LeftAxisMin* — Left axis minimum.
- *Data* — Data in a specific channel.
- *Integrate* — Integrates a spectrum.
- *NumberOfChannels* — Number of channels in a spectrum.

Simnra.Stopping

- *StoppingInElement* — Stopping power in an element [keV/10^{15} atoms/cm^2].
- *StoppingInLayer* — Stopping power in a target or foil layer [keV/10^{15} atoms/cm^2].
- *EnergylossInLayer* — Energy loss in a target or foil layer [keV].
- *StragglingInLayer* — FWHM of energy loss straggling in a target or foil layer [keV].

Chapter 4

Physics

4.1 Overview

During the last decade several programs for the simulation of backscattering spectra have been developed. The most common program is Doolittle's RUMP [12, 13]. However, RUMP uses several approximations to save computing time. The increase in computer power during the last years has made it possible to drop several of the approximations used by RUMP. SIMNRA offers more freedom in the use of non-Rutherford cross-sections and nuclear reactions, treats several topics such as straggling and convolution more precise and adds new possibilities such as dual scattering. This section describes the physics involved in the simulation of a backscattering spectrum as performed by SIMNRA.

The target is subdivided into shallow sublayers. Each simulated spectrum is made up of the superimposed contributions from each isotope of each sublayer of the sample target. The thickness of each sublayer is chosen in such a way that the energy loss in each sublayer is about the stepwidth of the incoming particles. When the incident particles penetrate a sublayer, they loose energy due to electronic and nuclear energy loss and the beam energy is spread due to straggling. The calculation of the energy loss is described in detail in section 4.5, and the calculation of straggling in section 4.7. SIMNRA calculates the energy of backscattered particles[1] from the front and the backside of the sublayer, and the energy of these particles when reaching the detector after passing to the target surface and traversing a foil in front of the detector, see fig. 4.1. The contribution of each isotope in each sublayer will be referred to as a brick.

To account for energy straggling and the finite energy resolution of the detector the brick shown in fig. 4.1 is convoluted with a Gaussian function $f(E, \sigma^2)$ with width

$$\sigma^2 = \sigma^2_{\text{Straggling Out}} + \sigma^2_{\text{Detector}}. \tag{4.1}$$

$\sigma^2_{\text{Straggling Out}}$ is the variance of the energy distribution of the outgoing particles due to energy loss straggling, and $\sigma^2_{\text{Detector}}$ is the energy resolution of the detector.

The final contribution to the energy spectrum of each isotope in each sublayer is given

[1] A 'backscattered' particle may be a recoil or a product in a nuclear reaction as well.

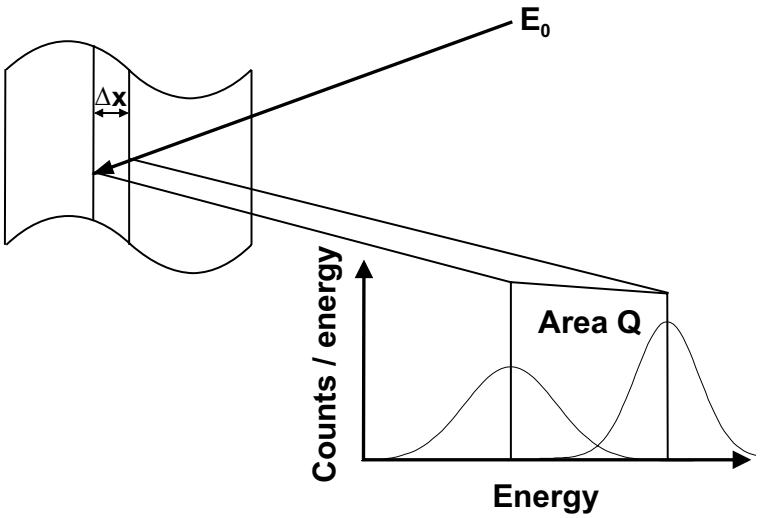

Figure 4.1: Notation used for a single brick.

by

$$S(E) = \int_0^\infty S_0(E')\, f(E', \sigma^2(E'))\, dE' \tag{4.2}$$

Here $S_0(E)$ is the energy spectrum before convolution and $S(E)$ the spectrum after the convolution. Note that the width of the Gaussian changes throughout the brick due to different straggling contributions.

The Number of counts N_i in each channel i is given by integrating $S(E)$ over the channel width from the minimum to the maximum energy of each channel:

$$N_i = \int_{E_{min}(i)}^{E_{max}(i)} S(E')\, dE' \tag{4.3}$$

Eqs. 4.2 and 4.3 can be put together into a 2-dimensional integral, which is computed by SIMNRA by means of a 2-dimensional Gauss-Legendre integration. The accuracy of the integration is about 10^{-4}.

The area Q of the brick in fig. 4.1 is calculated by SIMNRA by using the cross-section at the mean energy $\bar{E}$ in the brick.

$$Q = N\Delta\Omega \frac{d\sigma}{d\Omega}(\bar{E}) \frac{\Delta x}{\cos\alpha} \tag{4.4}$$

$N\Delta\Omega$ is the number of incident particles times the solid angle of the detector and $d\sigma/d\Omega(\bar{E})$ is the differential cross-section evaluated at the mean energy $\bar{E}$. The heights of the front and back side of the brick are adjusted to give the correct area when integrated. SIMNRA interpolates the brick linearly, as shown in fig. 4.1. This is, however, only valid if the cross-section does not vary strongly and the brick is sufficiently thin. If the cross-section has structures such as sharp resonances, the stepwidth of the incoming particles must be sufficiently smaller than the width of the resonance.

4.2 Atomic data

The masses of the elements and all isotopes used by SIMNRA have been taken from the recommended values of the 1995 update to the atomic mass evaluation [14]. The abundances of the isotopes have been taken from the recommended values of isotopic abundances in [15]. Isotopic masses and abundances are stored in the file ATOMDATA.DAT. This file contains also the data of some isotopes which do not occur naturally but may be created in nuclear reactions and are necessary for kinematic calculations.

4.3 Scattering kinematics

4.3.1 Elastic scattering

Energy of backscattered projectiles

The energy E_1 of a backscattered projectile with incident energy E_0 and mass M_1 after scattering is given in the laboratory system by

$$E_1 = E_0 \frac{M_1^2}{(M_1+M_2)^2} \left\{ \cos\theta \pm \left[\left(\frac{M_2}{M_1}\right)^2 - \sin^2\theta \right]^{1/2} \right\}^2 \tag{4.5}$$

θ is the scattering angle and M_2 the mass of the target nucleus initially at rest. For $M_1 < M_2$ only the plus sign in eq. 4.5 applies. If $M_1 > M_2$ then eq. 4.5 has two solutions, and the maximum possible scattering angle θ_{max} is given by

$$\theta_{max} = \arcsin\left(\frac{M_2}{M_1}\right). \tag{4.6}$$

The second solution for $M_1 > M_2$ is obtained because different impact parameters d result in the same scattering angle θ. Consider for example the scattering angle $\theta = 0$: This angle is obtained for a head-on collision with $d = 0$, but also for very large impact parameters $d \approx \infty$.

SIMNRA version 3.50 and higher uses both solutions of eq. 4.5, if kinematically possible. Earlier versions of SIMNRA used eq. 4.5 only with the plus sign, the solution with the minus sign was neglected.

Energy of recoils

The energy E_2 of a recoil is given in the laboratory system by

$$E_2 = E_0 \frac{4M_1M_2}{(M_1+M_2)^2} \cos^2\theta. \tag{4.7}$$

E_0 is the energy of the incident projectile, M_1 the mass of the projectile, M_2 the mass of the target nucleus initially at rest and θ the recoil angle, with $0° \le \theta \le 90°$.

4.3.2 Nuclear reactions

For the calculation of nuclear reactions kinematics we use the quantities listed in table 4.1.

We define the following quantities:

$$\begin{aligned} A_{13} &= \frac{M_1M_3}{(M_1+M_2)(M_3+M_4)} \frac{E_1}{E_T} \\ A_{14} &= \frac{M_1M_4}{(M_1+M_2)(M_3+M_4)} \frac{E_1}{E_T} \\ A_{23} &= \frac{M_2M_3}{(M_1+M_2)(M_3+M_4)} \left(1 + \frac{M_1}{M_2}\frac{Q}{E_T}\right) \end{aligned}$$

	Mass	Energy
Incident ion	M_1	E_1
Target nucleus	M_2	0
Light product	M_3	E_3
Heavy product	M_4	E_4
Energy released in reaction		Q
Total energy		$E_T = E_1 + Q = E_3 + E_4$

Table 4.1: Quantities used for the calculation of nuclear reactions kinematics. The target nucleus is initially at rest. For exotherm reactions $Q > 0$, for endotherm reactions $Q < 0$.

$$A_{24} = \frac{M_2 M_4}{(M_1 + M_2)(M_3 + M_4)} \left(1 + \frac{M_1}{M_2} \frac{Q}{E_T}\right)$$

The energy E_3 of the light product created in the nuclear reaction is then given in the laboratory system by

$$E_3 = E_T A_{13} \left[\cos\theta \pm \left(\frac{A_{24}}{A_{13}} - \sin^2\theta\right)^{1/2}\right]^2 \tag{4.8}$$

θ is the emission angle of the light product in the laboratory system. For $A_{13} < A_{24}$ only the plus sign in eq. 4.8 applies. If $A_{13} > A_{24}$ then eq. 4.8 has two solutions, and the maximum possible emission angle θ_{max} of the light product is

$$\theta_{max} = \arcsin\left(\frac{A_{24}}{A_{13}}\right)^{1/2} \tag{4.9}$$

The energy E_4 of the heavy product created in the nuclear reaction is given in the laboratory system by

$$E_4 = E_T A_{14} \left[\cos\Phi \pm \left(\frac{A_{23}}{A_{14}} - \sin^2\Phi\right)^{1/2}\right]^2 \tag{4.10}$$

Φ is the emission angle of the heavy product in the laboratory system. For $A_{14} < A_{23}$ only the plus sign in eq. 4.10 applies. If $A_{14} > A_{23}$ then eq. 4.10 has two solutions, and the maximum possible emission angle Φ_{max} of the heavy product is

$$\Phi_{max} = \arcsin\left(\frac{A_{23}}{A_{14}}\right)^{1/2} \tag{4.11}$$

SIMNRA uses eqs. 4.8 and 4.10 only with the plus sign. The second solution is neglected.

4.4 Cross-section data

4.4.1 Rutherford cross-sections

The Rutherford cross-section for backscattering is given in the laboratory system by

$$\sigma_R\ [\mathrm{mb/sr}] = 5.1837436 \times 10^6 \left(\frac{Z_1 Z_2}{E\ [\mathrm{keV}]}\right)^2 \frac{\left\{\left(M_2^2 - M_1^2 \sin^2\theta\right)^{1/2} + M_2 \cos\theta\right\}^2}{M_2 \sin^4\theta\ \left(M_2^2 - M_1^2 \sin^2\theta\right)^{1/2}} \tag{4.12}$$

θ is the scattering angle, Z_1 and M_1 are the nuclear charge and the mass of the projectile, respectively, and Z_2 and M_2 are the nuclear charge and the mass of the target atom, respectively. σ_R is the differential cross-section in the laboratory system[2]. Experimental measurements indicate that actual cross-sections deviate from Rutherford at both high and low energies for all projectile-target pairs. The low-energy departures are caused by partial screening of the nuclear charges by the electron shells surrounding both nuclei [16, 17, 18, 5]. This screening is taken into account by a correction factor F:

$$\sigma = F\sigma_R$$

For $\theta > 90°$ the correction factor by L'Ecuyer *et al.* [16] is widely used:

$$F_{\mathrm{L'Ecuyer}} = 1 - \frac{0.049\, Z_1 Z_2^{4/3}}{E_{CM}} \tag{4.13}$$

E_{CM} is the energy in the center of mass system (in keV). Tabulated values of $F_{\mathrm{L'Ecuyer}}$ can be found for example in [5]. The correction for backscattering angles $\theta > 90°$ at typical energies used in ion beam analysis usually is small. For 1 MeV ^{4}He ions on gold the correction is only about 3.5%.

The correction factor by L'Ecuyer (eq. 4.13) is a first order correction and does not take into account the influence of the scattering angle θ. For $\theta < 90°$ eq. 4.13 will underestimate the necessary correction to the Rutherford cross-section. SIMNRA uses the angular- and energy dependent correction factor by Andersen *et al.* [18]:

$$F_{\mathrm{Andersen}} = \frac{\left(1 + \frac{1}{2}\frac{V_1}{E_{CM}}\right)^2}{\left\{1 + \frac{V_1}{E_{CM}} + \left[\frac{V_1}{2E_{CM}\sin\theta_{CM}/2}\right]^2\right\}^2} \tag{4.14}$$

θ_{CM} is the scattering angle in the center of mass system. The increase in the kinetic energy V_1 is given by

$$V_1\ [\mathrm{keV}] = 0.04873\, Z_1 Z_2 \left(Z_1^{2/3} + Z_2^{2/3}\right)^{1/2}$$

[2] For $M_1 > M_2$ there may exist two different solutions of the kinematic equation 4.5. The cross-section given by eq. 4.12 applies for the solution with the plus sign. The cross-section for the second solution of eq. 4.5 is obtained by calculating the scattering angle in the centre-of-mass system θ_{CM} from $\theta_{CM} = \theta - \arcsin[M_1/M_2 \sin\theta] + \pi$, calculating the Rutherford backscattering cross-section in the centre-of-mass system and transforming into the laboratory system.

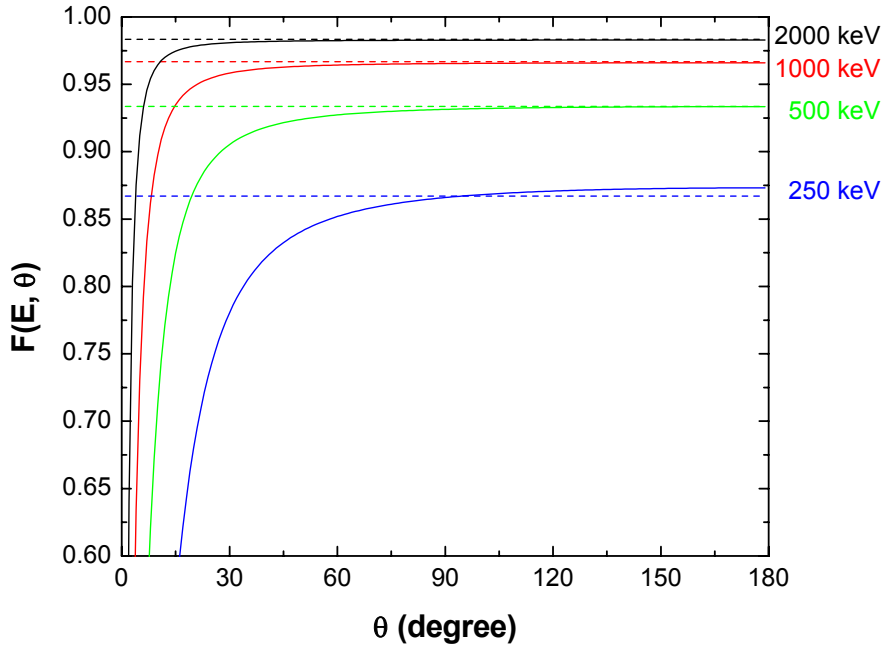

Figure 4.2: Angular dependence of the correction factors for the Rutherford cross-section by L'Ecuyer (eq. 4.13, dashed lines) and Andersen (eq. 4.14, solid lines) for ^{4}He backscattered from gold at different energies.

The dependence of the correction factor F_{Andersen} from the scattering angle θ for ^{4}He scattered from gold is shown in fig. 4.2 for different ^{4}He energies. Dashed lines are the angular independent correction factor by L'Ecuyer. For large scattering angles the correction factors by L'Ecuyer and Andersen are near to unity and similar, however, for small scattering angles the correction by Andersen becomes large and the angle-independent L'Ecuyer correction underestimates the deviations from the Rutherford cross-section.

The Rutherford cross-section for recoils is given in the laboratory system by

$$\sigma_R^{ERD}\,[\text{mb/sr}] = 2.0731 \times 10^7 \frac{[Z_1 Z_2 (M_1 + M_2)]^2}{(2 M_2 E\,[\text{keV}])^2 \cos^3\theta} \tag{4.15}$$

θ is the recoil angle in the lab system. SIMNRA applies the correction to the Rutherford cross-section from eq. 4.14 also for the recoil cross-section.

4.4.2 Non-Rutherford cross-sections

At high energies the cross-sections deviate from Rutherford due to the influence of the nuclear force. A useful formula above which energy E_{NR} deviations from Rutherford can be expected was given by Bozoian [19, 20, 21]:

$$E_{NR}\,[\text{MeV}] \quad = \quad \frac{M_1 + M_2}{M_2} \frac{Z_2}{10} \quad \text{for } Z_1 = 1$$

$$E_{NR}\,[\mathrm{MeV}] \quad = \quad \frac{M_1 + M_2}{M_2}\frac{Z_1 Z_2}{8} \quad \text{for } Z_1 > 1$$

E_{NR} is the energy at which the deviation from the Rutherford cross-section gets $> 4\%$.

SIMNRA does not check if the cross-sections at a given energy are Rutherford or not. It is in the responsibility of the user to choose the correct cross-sections. The above formulas may be useful to estimate if the cross-section is still Rutherford or not.

For non-Rutherford cross-sections SIMNRA uses experimentally determined differential cross-sections taken from SigmaBase. The use of non-Rutherford cross-sections is described in full detail in section 3.6. SIMNRA uses linear interpolation between the given data points.

4.5 Evaluation of energy loss

The energy E of a particle in the depth x is given by the integral equation

$$E(x) = E_0 - \int_0^{x/\cos\alpha} \frac{dE}{dx'}(E(x'), x')dx' \tag{4.16}$$

Here we assume that the particle starts with initial energy E_0 at the surface ($x = 0$), $dE/dx'(E(x'), x')$ is the energy and depth dependent stopping power. In principle, eq. 4.16 can be evaluated directly, but this consumes a lot of computing time.

For evaluation of the energy loss SIMNRA uses the algorithm of Doolittle instead, developed for RUMP [12]. The beam loses energy according to the differential equation

$$\frac{dE}{dx} = -\epsilon(E) \tag{4.17}$$

where this is the defining equation for $\epsilon(E)$, the energy dependent stopping cross-section. x is the pathlength into the material, measured in areal density (10^{15} atoms/cm^2). $\epsilon' = d\epsilon/dE$ is the first and $\epsilon'' = d^2\epsilon/dE^2$ the second derivative of ϵ.

If incoming or outgoing particles with incident energy E_0 traverse a layer of material with thickness Δx, then the particles energy E_1 after the layer can be expanded into a Taylor series:

$$E_1 = E_0 + \Delta x \frac{dE}{dx}(E_0) + \frac{1}{2}\Delta x^2 \frac{d^2E}{dx^2}(E_0) + \frac{1}{6}\Delta x^3 \frac{d^3E}{dx^3}(E_0) \tag{4.18}$$

The terms in eq. 4.18 look as follows:

$$\frac{dE}{dx} = -\epsilon \tag{4.19}$$

$$\frac{d^2E}{dx^2} = \frac{d}{dx}(-\epsilon) = -\frac{d\epsilon}{dE}\frac{dE}{dx} = \epsilon'\epsilon \tag{4.20}$$

$$\frac{d^3E}{dx^3} = \frac{d}{dx}(\epsilon'\epsilon) = \frac{d\epsilon'}{dx}\epsilon + \epsilon'\frac{d\epsilon}{dx} = -\epsilon''\epsilon^2 - \epsilon'^2\epsilon \tag{4.21}$$

With ϵ, ϵ' and ϵ'' evaluated at E_0

$$E_1 = E_0 - \Delta x\epsilon + \frac{1}{2}\Delta x^2\epsilon\epsilon' - \frac{1}{6}\Delta x^3\left(\epsilon''\epsilon^2 + \epsilon'^2\epsilon\right) \tag{4.22}$$

See ref. [12] for a discussion of the accuracy of the above equations.

ϵ' and ϵ'' are calculated by SIMNRA by numerical differentiation of the stopping power data. The stepwidths Δx for the incoming and outgoing particles can be adjusted in the `Setup: Calculation` menu. The stepwidth of the incoming particle should be kept small in the range of 10 keV due to the cross-section calculation, see section 4.1. The stepwidth for outgoing particles can be chosen much larger due to the accuracy of eq. 4.22. Typical values for the stepwidth of outgoing particles are around 200 keV.

4.6 Stopping power data

SIMNRA offers the possibility to use two different sets of electronic stopping power data for the stopping of swift and heavy ions in all elements: The well known electronic stopping power data by Andersen and Ziegler [1, 2] or the electronic stopping power data by Ziegler, Biersack and Littmark [3]. Generally, the Ziegler-Biersack data are more accurate and are also used by the SRIM 97 (formerly TRIM) program in calculations of stopping powers and ranges. The difference between the two data sets is typically $< 5\%$, but may be larger in some cases, especially for ions other than H or He. See [22, 23, 24] for a discussion of the accuracy of stopping powers. An up-to-date compilation of stopping power data can be found in [25].

The routines and input data for Ziegler-Biersack stopping have been taken from the SRIM 97 source code and were translated from BASIC to PASCAL.

4.6.1 Andersen-Ziegler stopping

Hydrogen

If Andersen-Ziegler stopping is selected SIMNRA uses the electronic stopping power data by Andersen and Ziegler [1] for the stopping of incident protons, deuterons and tritons in all elements. The electronic stopping power S_e in eV/(10^{15} atoms/cm^2) for an incident hydrogen ion with energy/mass E in keV/amu is given by

$$\frac{1}{S_e} = \frac{1}{S_{Low}} + \frac{1}{S_{High}} \tag{4.23}$$

with

$$S_{Low} = A_2\, E^{0.45} \tag{4.24}$$

and

$$S_{High} = \frac{A_3}{E} \ln\left[1 + \frac{A_4}{E} + A_5 E\right] \tag{4.25}$$

$A_2 - A_5$ are fitting coefficients and tabulated in [1]. They are stored in the file STOPH.DAT. Equations 4.23–4.25 are valid for 10 keV $\leq E <$ 1 MeV. For energies in the range 1 MeV–100 MeV the electronic stopping power S_e is given by

$$S_e = \frac{A_6}{\beta^2}\left[\ln\frac{A_7\beta^2}{1-\beta^2} - \beta^2 - \sum_{i=0}^{4} A_{i+8}\,(\ln E)^i\right] \tag{4.26}$$

$A_6 - A_{12}$ are tabulated in [1], $\beta = v/c$, with v the ion velocity and c the speed of light. Equation 4.26 is used only if the switch `High energy stopping` in the `Setup: Calculation` menu is checked. If unchecked, the program will use Equations 4.23–4.25 at all energies. The program default is checked. The difference between eq. 4.23 and eq. 4.26 is small in most cases. The main problem using eq. 4.26 is that the first and second derivatives of eq. 4.23 and eq. 4.26 do not fit smoothly together at 1 MeV/amu. This may result in the appearance of kinks in the spectrum.

Nuclear stopping for incident hydrogen, deuterium and tritium ions is negligible for incident energies above about 10 keV/amu [1] and is neglected by SIMNRA.

Helium

If Andersen-Ziegler stopping is selected then for incident ^{3}He and ^{4}He ions the electronic stopping power data by Ziegler [2] are used for all elements. The electronic stopping power S_e in eV/(10^{15} atoms/cm^2) for incident ^{4}He ions with energy E in keV is given by

$$\frac{1}{S_e} = \frac{1}{S_{Low}} + \frac{1}{S_{High}} \tag{4.27}$$

with

$$S_{Low} = A_1 \, E^{A_2} \tag{4.28}$$

and

$$S_{High} = \frac{A_3}{E} \ln\left[1 + \frac{A_4}{E} + A_5 E\right] \tag{4.29}$$

$A_1 - A_5$ are fitting coefficients and tabulated in [2]. They are stored in the file STOPHE.DAT. Equations 4.27–4.29 are valid for 1 keV $\leq E <$ 10 MeV. ^{4}He-stopping at higher energies (above 10 MeV) is not implemented in the program.

The stopping power of ^{3}He is identical to the stopping power of ^{4}He at the same velocity [2]. The stopping power of ^{3}He with energy E is obtained by taking the stopping power value at the energy $E(^4\text{He}) = 4/3\, E(^3\text{He})$. The stopping power for ^{3}He is valid in the energy range 10 keV $\leq E <$ 7.5 MeV.

Nuclear stopping for incident helium ions is calculated with the Krypton-Carbon (Kr-C) potential [26]. The nuclear stopping S_n in eV/10^{15} atoms/cm^2 for He-ions with incident energy E (in keV) is given by:

$$S_n = s_n \frac{8.462 \, Z_1 \, Z_2 \, M_1}{(M_1 + M_2)\left(Z_1^{2/3} + Z_2^{2/3}\right)^{1/2}} \tag{4.30}$$

s_n is the reduced nuclear stopping and Z_1, M_1 are the nuclear charge and mass of the helium ion and Z_2, M_2 are the nuclear charge and mass of the target element. The reduced nuclear stopping s_n has the simple form

$$s_n = 0.5 \, \frac{\ln(1+\epsilon)}{\epsilon + 0.10718 \, \epsilon^{0.37544}} \tag{4.31}$$

ϵ is the reduced energy and is given by

$$\epsilon = \frac{32.53 \, M_2 \, E}{Z_1 Z_2 \, (M_1 + M_2)\left(Z_1^{2/3} + Z_2^{2/3}\right)^{1/2}} \tag{4.32}$$

Nuclear stopping is only important at incident energies $E <$ 100 keV, at higher energies nuclear stopping becomes negligible.

Heavy ions

The electronic stopping power of heavy ions in all elements is derived from the stopping power of protons using Brandt-Kitagawa theory [3, 27]. The formalism is described in detail in ref. [3], a short overview is given in [27]. The screening length Λ (eq. 3-29 of ref. [3]) is multiplied by an empirical correction factor which has been digitised from fig. 3-25 of ref. [3]. The correction factor for all elements is stored in the file LCORRHI.DAT.

Note that the switch `High energy stopping` in the `Setup: Calculation` menu has influence on the calculation of the stopping power for heavy ions with incident energies above 1 MeV/amu.

Nuclear stopping for incident heavy ions is calculated with the universal potential from ref. [3]. The reduced nuclear stopping s_n with the universal potential is given by

$$s_n = \frac{\ln(1 + 1.1383\,\epsilon)}{2\left[\epsilon + 0.01321\,\epsilon^{0.21226} + 0.19593\,\epsilon^{0.5}\right]} \tag{4.33}$$

for $\epsilon \leq 30$. For $\epsilon > 30$ s_n is given by

$$s_n = \frac{\ln(\epsilon)}{2\epsilon} \tag{4.34}$$

The reduced energy ϵ in eqs. 4.33 and 4.34 is calculated using the universal screening length a_U, which is $\propto 1/(Z_1^{0.23} + Z_2^{0.23})$ instead of the Firsov screening length $a_F \propto 1/(Z_1^{2/3} + Z_2^{2/3})^{1/2}$, which is used in eq. 4.32. The difference between eq. 4.31 and 4.33 is only some percent.

The nuclear stopping component for heavy ions may be large and cannot be neglected.

4.6.2 Ziegler-Biersack stopping

Hydrogen

If Ziegler-Biersack stopping is selected SIMNRA uses the electronic stopping power data by Ziegler, Biersack and Littmark [3] for the stopping of incident protons, deuterons and tritons in all elements. The electronic stopping power S_e in eV/(10^{15} atoms/cm^2) for an incident hydrogen ion with energy/mass E in keV/amu is given by

$$S_e = \frac{S_{Low} S_{High}}{S_{Low} + S_{High}} \tag{4.35}$$

with

$$S_{Low} = C_1 E^{C_2} + C_3 E^{C_4} \tag{4.36}$$

and

$$S_{High} = \frac{C_5}{E^{C_6}} \ln\left(\frac{C_7}{E} + C_8 E\right) \tag{4.37}$$

$C_1 - C_8$ are fitting coefficients and partly tabulated in [27]. They are stored in the file SCOEF.95A for all elements. Equations 4.35–4.37 are valid in the energy range

10 keV/amu $\leq E <$ 10 MeV/amu. For energies in the range 10–100 MeV/amu the electronic stopping power S_e is given by

$$S_e = C_9 + C_{10}x + C_{11}x^2 + \frac{C_{12}}{x} \tag{4.38}$$

with $x = \ln(E)/E$. $C_9 - C_{12}$ are fitting coefficients and tabulated in the file SCOEF.95B.

For energies below 10 keV/amu the electronic stopping power S_e is given by

$$S_e(E) = S_e(10)\left(\frac{E}{10}\right)^y \tag{4.39}$$

where $S_e(10)$ is the stopping power at 10 keV/amu and $y = 0.45$ for $Z_2 > 6$ and $y = 0.35$ for $Z_2 \leq 6$.

Nuclear stopping for incident hydrogen, deuterium and tritium ions is negligible for incident energies above about 10 keV/amu [1] and is neglected by SIMNRA.

Helium

If Ziegler-Biersack stopping is selected then for incident ^{3}He and ^{4}He ions the electronic stopping power data by Ziegler, Biersack and Littmark [3] are used for all elements.

The electronic stopping of He ions in elements S_e is derived from the stopping power of protons for the same velocity S_p by using [3, 27]

$$S_e = S_p\,(\gamma_{He} Z_{He})^2 \tag{4.40}$$

Z_{He} is the helium charge and γ_{He} can be obtained from the simple polynomial fit

$$\gamma_{He}^2 = 1 - \exp\left[-\sum_{i=0}^{5} C_i E^i\right] \tag{4.41}$$

with E in keV/amu. The coefficients C_i are tabulated in [27].

Nuclear stopping for incident helium ions is calculated with the universal ZBL potential [3]. The nuclear stopping S_n in eV/10^{15} atoms/cm^2 for He-ions with incident energy E (in keV) is given by:

$$S_n = s_n \frac{8.462\,Z_1\,Z_2\,M_1}{(M_1 + M_2)\,(Z_1^{0.23} + Z_2^{0.23})} \tag{4.42}$$

s_n is the reduced nuclear stopping and Z_1, M_1 are the nuclear charge and mass of the helium ion and Z_2, M_2 are the nuclear charge and mass of the target element. The reduced nuclear stopping s_n has the simple form

$$s_n = \frac{\ln(1 + 1.1383\epsilon)}{2(\epsilon + 0.01321\,\epsilon^{0.21226} + 0.19593\,\epsilon^{0.5}} \tag{4.43}$$

for $\epsilon \leq 30$ and

$$s_n = \frac{\ln \epsilon}{2\epsilon} \tag{4.44}$$

for $\epsilon > 30$. ϵ is the reduced energy and is given by

$$\epsilon = \frac{32.53\, M_2\, E}{Z_1 Z_2\, (M_1 + M_2)\, (Z_1^{0.23} + Z_2^{0.23})} \tag{4.45}$$

Nuclear stopping is only important at incident energies $E < 100$ keV, at higher energies nuclear stopping becomes negligible.

Heavy ions

The electronic stopping power of heavy ions in all elements is derived from the stopping power of protons using Brandt-Kitagawa theory [3, 27]. The formalism is described in detail in ref. [3], a short overview is given in [27]. Fermi velocities of all target elements are stored in the file SCOEF.95A, a small correction to the Fermi velocity in the file SCOEF.95B. The ion's screening length Λ as a function of fractional charge is stored in the file SCOEF.95B.

Nuclear stopping for incident heavy ions is calculated with the universal ZBL potential from ref. [3]. The formalism is the same as for He ions, see eq. 4.42–4.45. For Z_1 and M_1 the ions nuclear charge and mass, respectively, have to be used.

The nuclear stopping component for heavy ions may be large and cannot be neglected.

Differences between SIMNRA and SRIM 97

The program SRIM (formerly TRIM) by J. Ziegler is the standard program for stopping power and range calculations. If Ziegler-Biersack stopping is selected SIMNRA uses the same stopping power routines and input data as SRIM 97 for elemental targets. The routines for stopping power calculations have been taken from the SRIM source code, the input data have been taken from the SRIM distribution. For incident hydrogen and helium ions SIMNRA therefore uses exactly the same electronic and nuclear stopping powers as the SRIM program[3]. For incident heavy ions, however, there are *small* differences between SIMNRA and SRIM. SRIM uses linear interpolation for some input data, resulting in stopping powers with a noncontinuous derivative. SIMNRA uses spline interpolation instead of linear interpolation, resulting in stopping powers with continuous second derivative. The stopping powers calculated by SIMNRA are therefore more smooth than the original stopping powers calculated by SRIM, the differences are typically below 1%.

4.6.3 Stopping in compounds

SIMNRA uses Bragg's rule [28] for the determination of the stopping power in compounds. Bragg's rule is a simple linear additivity rule of the stopping contributions of the different compound elements, assuming that the interaction of an incident ion with a target atom is independent of the surrounding target atoms. For a compound consisting of different

[3] For low energetic hydrogen ions ($E < 10$ keV) there are differences because SIMNRA neglects nuclear stopping of hydrogen.

elements i with atomic concentrations c_i ($\sum c_i = 1$) the total stopping power S is given by

$$S = \sum c_i \, S_i \tag{4.46}$$

S_i is the stopping power of each element.

Bragg's rule assumes that the interaction between the ion and the atom is independent of the environment. The chemical and physical state of the medium is, however, observed to have an effect on the energy loss. The deviations from Bragg's rule predictions are most pronounced around the stopping power maximum and for solid compounds such as oxides, nitrides and hydrocarbons. The deviations from Bragg's rule predictions may be of the order of 10–20% [27, 29]. For compounds with heavier atoms such as Fe_2O_3, NbC, NbN, Ta_2O_5, WO_3, Au alloys etc. deviations from Bragg's rule disappear (deviation $< 2\%$) [27, 30].

Ziegler and Manoyan [27] have developed the 'cores and bonds' (CAB) model, which assumes the electronic energy loss to have two contributions: The effect of the cores and the effect of the bonds, such as C-H and C-C. The CAB-model allows better predictions for the stopping in compounds, however, the bond structure has to be known. Currently the CAB-model (or any other model which allows better predictions for the stopping in compounds) is not implemented in SIMNRA. However, a correction factor f may be used for each ion species and each layer, see Section 3.5 for details. If a factor f is defined for a layer, then the program will use the stopping power $S(E)$, with E the ion energy,

$$S(E) = f \, S_{\mathrm{Bragg}}(E) \tag{4.47}$$

$S_{\mathrm{Bragg}}(E)$ is the stopping power according to Bragg's rule. Note that the factor f is energy independent.

4.7 Straggling

4.7.1 Overview

When a beam of charged particles penetrates matter, the slowing down is accompanied by a spread in the beam energy. This phenomenon is called straggling. It is due to statistical fluctuations of the energy transfer in the collision processes.

Energy loss straggling has different contributions:

1. Electronic energy loss straggling due to statistical fluctuations in the transfer of energy to electrons.

2. Nuclear energy loss straggling due to statistical fluctuations in the nuclear energy loss.

3. Geometrical straggling due to finite detector solid angle and finite beam spot size, resulting in a distribution of scattering angles and different pathlengths for outgoing particles.

4. Straggling due to multiple small angle scattering, resulting in angular and energy spread on the ingoing and outgoing paths.

5. Straggling due to surface and interlayer roughness and thickness inhomogeneities of absorber foils.

An additional contribution to the energy broadening visible in experimental spectra is the energy resolution of the detector. The different straggling contributions (excluding roughness) have been reviewed by Szilágy *et. al.* [31, 32], and can be included in SIMNRA calculations. The details are described in the following sections.

4.7.2 Electronic energy loss straggling

There are four main theories describing electronic energy loss straggling [33, 34, 35], each applicable in a different regime of energy loss. With ΔE the mean energy loss of the beam, and E the energy of the incident beam, we can distinguish:

$\Delta E/E < 10\%$	**Vavilov's Theory**[36, 34]. For thin layers and small energy losses. The energy distribution is non-Gaussian and asymmetrical. This energy range is not described properly by SIMNRA.
$10 - 20\%$	**Bohr's Theory**[37, 38]. As the number of collisions becomes large, the distribution of particle energies becomes Gaussian.
$20 - 50\%$	**Symon's Theory**[33]. This theory includes non-statistical broadening caused by the change in stopping power over the particle energy distribution. If the mean energy of the beam is higher than the energy of the stopping power maximum, then particles with a lower energy have a higher stopping power, and particles with higher energy have a smaller stopping power. This results in a nonstatistical broadening of the energy distribution. The width of the particles energy distribution in Symon's theory is significantly higher than predicted by Bohr's theory. The distribution of particle energies is still Gaussian.
$50 - 90\%$	**Payne's and Tschalärs Theory** [39, 40, 41]. When the energy losses become very large and the mean energy of the beam decreases below the energy of the stopping power maximum, the particle energy distribution again become skewed, because now particles with lower energy have a lower stopping power than particles with higher energy. The distribution is about Gaussian.

SIMNRA always assumes that the particles energy distribution is Gaussian. This is only an approximation for thin layers: In this case the energy distribution is described by the Vavilov distribution [36, 34]. However, the straggling contribution of thin layers to the total energy broadening is much smaller than the contribution of the finite energy resolution of the detector.

SIMNRA calculates the non-statistic broadening (or skewing) of the energy distribution when penetrating a layer in the following way [31]:
Assume two particles with energies E_1 and E_2

$$\begin{aligned} E_1 &= E_0 + \frac{\Delta E}{2} \\ E_2 &= E_0 - \frac{\Delta E}{2} \end{aligned}$$

centered around a mean energy E_0. The energy difference $E_1 - E_2$ of the two particles is ΔE. After penetrating a layer the particles have the energies E_1' and E_2' centered around a mean energy E_0'. The energy difference $\Delta E'$ behind the layer is given by

$$\Delta E' = \frac{\epsilon(E_0')}{\epsilon(E_0)}\Delta E = \frac{\epsilon_f}{\epsilon_i}\Delta E \tag{4.48}$$

with the stopping power $\epsilon = dE/dx$. ϵ_f is the stopping power at the exit of the layer and ϵ_i the stopping power at the entrance of the layer. If $\epsilon_f > \epsilon_i$, which is the case for all energies

above the stopping power maximum, the energy difference increases and the distribution function is broadened. If $\epsilon_f < \epsilon_i$, the energy difference decreases and the distribution function gets skewed. The shape of the distribution remains unchanged: a Gaussian distribution remains gaussian, but the width of the Gaussian is changed according to eq. 4.48[4].

To the non-statistic broadening we have to add the statistical effects. When the incident beam with initial energy E_0 and initial beam width σ_0^2 (σ^2 is the variance of the energy distribution, the full width at half maximum (FWHM) is $2\sqrt{2\ln 2}\,\sigma = 2.355\,\sigma$) penetrates a layer of matter with thickness Δx, then the beam width σ_1^2 after penetrating the layer is given by:

$$\sigma_1^2 = \left(\frac{\epsilon_f}{\epsilon_i}\sigma_0\right)^2 + \sigma^2 \tag{4.51}$$

ϵ_f and ϵ_i are the stopping powers of the material at the entrance and exit of the layer and σ^2 is the energy loss straggling in the layer. The first term in eq. 4.51 describes the non-statistical broadening of the beam according to eq. 4.48 due to the energy dependence of the stopping power, the second term adds the statistical effects.

The electronic energy loss straggling is calculated by applying Chu's theory [42, 38]:

$$\sigma_e^2 = H(E/M_1, Z_2)\sigma_{Bohr}^2 \tag{4.52}$$

σ_{Bohr}^2 is the electronic energy loss straggling in Bohr approximation and is given by [37, 38]:

$$\sigma_{Bohr}^2\ [\mathrm{keV}^2] = 0.26\, Z_1^2\, Z_2\, \Delta x\ [10^{18}\,\mathrm{atoms/cm}^2] \tag{4.53}$$

Bohr's theory of electronic energy loss straggling is valid in the limit of high ion velocities. In this case the electronic energy loss straggling is almost independent of the ion energy. For lower ion energies the Bohr straggling is multiplied by the Chu correction factor $H(E/M_1, Z_2)$, which depends only on E/M_1 and the nuclear charge of the target atoms Z_2. H takes into account the deviations from Bohr straggling caused by the electron binding in the target atoms. Chu [42, 38] has calculated H by using the Hartree-Fock-Slater charge distribution. This calculation gives straggling values which are considerably lower than those given by Bohr's theory. The correction factor H, as used by SIMNRA, is shown in fig. 4.3. The Z_2 oscillations are clearly visible. The Chu correction is mainly necessary for high Z_2 and low energies. For high energies H approaches 1 and becomes independent of Z_2 and energy. For E/M_1 values in the range 100–1000 keV/amu the

[4] SIMNRA versions before 3.30 used the equation

$$\Delta E' = \left(1 - \frac{d\epsilon_i}{dE}\Delta x\right)\Delta E \tag{4.49}$$

instead of eq. 4.48. Equation 4.49 is obtained by a taylor expansion of ϵ_f around ϵ_i considering only the linear term:

$$\epsilon_f = \epsilon_i - \frac{d\epsilon}{dE}\epsilon_i \Delta x \tag{4.50}$$

where $d\epsilon/dE$ is the derivative of the stopping power and Δx the layer thickness. $\epsilon_i \Delta x$ is the energy loss in the layer. By putting the above equation into eq. 4.48 we obtain eq. 4.49. The difference between eq. 4.48 and the previously used eq. 4.49 is only 1-2% because of the relatively small stepwidths used by SIMNRA.

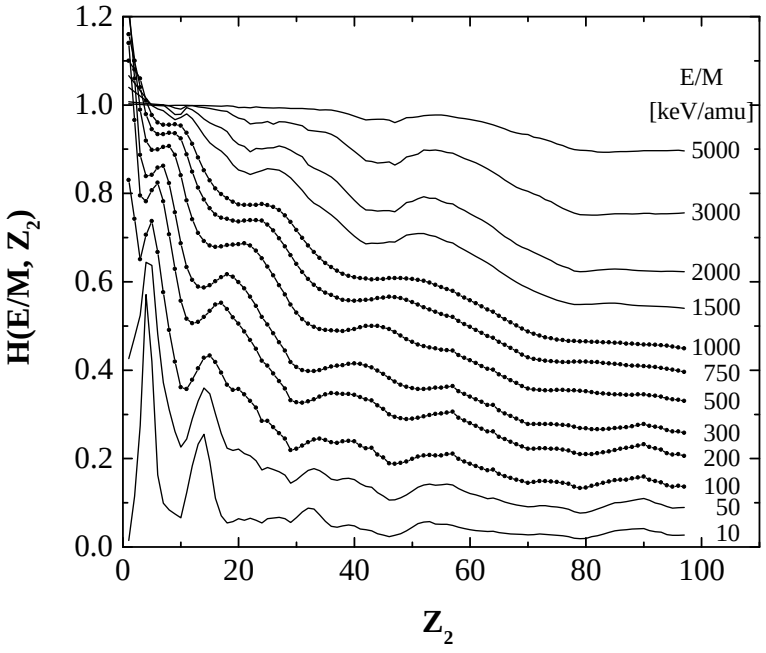

Figure 4.3: The Chu straggling correction for several values of E/M_1 as a function of the nuclear charge of the target Z_2. Dots are original data from Chu [38], solid lines are extrapolated data taken from [31].

data have been taken from ref. [38], data for lower and higher E/M_1 values are based on an extrapolation performed in ref. [31]. Tabulated values for H are stored in the file CHU_CORR.DAT. For not tabulated values SIMNRA uses linear interpolation.

Fig. 4.4 compares the beam width (FWHM) of 2.5 MeV ^{4}He ions in silicon calculated by SIMNRA using eq. 4.51 with Bohr's theory. For small energy losses the beam width calculated by SIMNRA is slightly smaller than predicted by Bohr's theory due to the Chu correction. However, this is counterbalanced by the nonstochastic broadening due to the characteristics of the stopping power curve, and for larger energy losses the beam width gets larger than in Bohr's theory. When the mean beam energy has decreased below the energy of the stopping power maximum, the beam width becomes skewed.

As can be seen from fig. 4.3 the deviation of the Chu correction from Bohr's theory is largest for high Z_2 and low energies. Fig. 4.5 shows the beam width (FWHM) of 1 MeV ^{4}He penetrating through gold. The deviation from Bohr's theory is large. The stopping power maximum is at about 960 keV. For low energy losses the beam width increases due to the statistical broadening because the nonstochastic skewing, which occurs for beam energies below the stopping power maximum, is small and the stochastic broadening wins. For larger energy losses however the beam width gets skewed.

Fig. 4.6 shows the measured RBS-spectrum for 1.0 MeV ^{4}He ions incident on a gold layer with a thickness of about 100 nm and a scattering angle of 165° compared with simulations using Bohr straggling and Chu straggling. As can be seen at the low energy edge of the layer, the Bohr straggling is broader than the experimental data. The Chu straggling

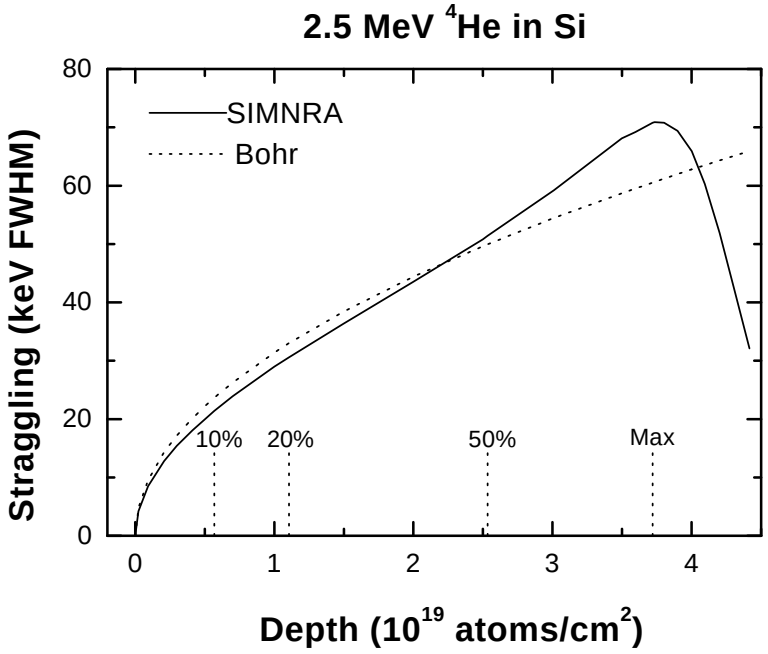

Figure 4.4: Beam width (FWHM) of 2.5 MeV ^{4}He ions penetrating through silicon. The solid line is the beam width calculated by SIMNRA using eq. 4.51, the dashed line is the prediction of Bohr's theory. The vertical lines denote the mean depth at which the beam has lost 10%, 20% and 50% of its initial energy. Max denotes the depth at which the mean energy of the beam has decreased to the energy of the stopping power maximum.

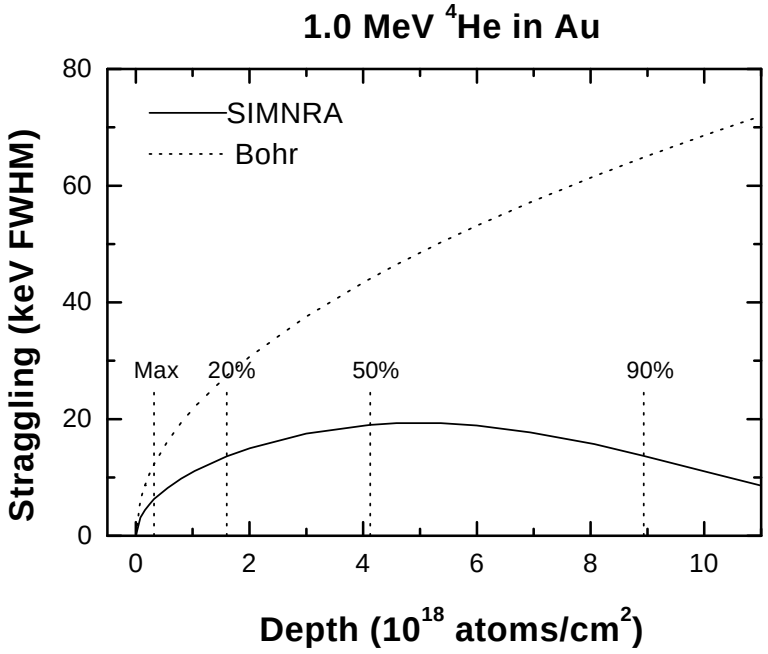

Figure 4.5: Beam width (FWHM) of 1.0 MeV ^{4}He ions penetrating through gold. The solid line is the beam width calculated by SIMNRA using eq. 4.51, the dashed line is the prediction of Bohr's theory. The vertical lines denote the mean depth at which the beam has lost 20%, 50% and 90% of its initial energy. Max denotes the depth at which the mean energy of the beam has decreased to the energy of the stopping power maximum.

fits the measured curve relatively well, except of the multiple scattering contribution.

The straggling of outgoing particles is calculated with eq. 4.51 as well. Outgoing particles always start with an energy distribution with variance σ^2_{out} which is given by

$$\sigma^2_{\text{out}} = K^2\,\sigma^2_{\text{in}} \tag{4.54}$$

with K the kinematic factor and σ^2_{in} the variance of the energy distribution of the incident beam.

4.7.3 Nuclear energy loss straggling

Fluctuations in the number of nuclear collisions lead to nuclear energy loss straggling, which can be described by Bohr's theory of nuclear straggling. The variance σ^2_n in Bohr's approximation is given by:

$$\sigma^2_n\ [\text{keV}^2] = 0.26\,Z_1^2\,Z_2^2\left(\frac{M_1}{M_1+M_2}\right)^2\,\Delta x\ [10^{18}\,\text{atoms/cm}^2] \tag{4.55}$$

For light ions, such as protons or helium ions, nuclear energy loss straggling is small compared to electronic energy loss straggling and can be neglected. For heavy ions nuclear straggling becomes more important and may exceed electronic straggling, see eqs. 4.53 and 4.55. However, it has been shown experimentally for 60 MeV ^{58}Ni ions in different target materials, that the width of the straggling distribution is only somewhat larger than electronic energy loss straggling alone [43]. The nuclear straggling energy distribution is broad with a long tail towards low energies, which cannot be described by a Gaussian distribution. However, the tail contains only a small fraction of all particles, and the width of the total energy distribution (electronic plus nuclear straggling) is still dominated by electronic energy loss straggling [43]. This justifies to neglect nuclear straggling for all ion species [5].

4.7.4 Energy loss straggling in compounds

For compounds a simple additivity rule for energy loss straggling is used [38]. The straggling in a compound consisting of elements i with atomic concentration c_i is calculated with

$$\sigma^2 = \sum_i c_i\,\sigma_i^2 \tag{4.56}$$

with σ_i^2 being the straggling in each element.

[5] SIMNRA versions before 4.70 used a quadratic addition of the nuclear and electronic energy loss straggling contributions, i. e. $\sigma^2 = \sigma_n^2 + \sigma_e^2$, with σ_n^2 the variance of the nuclear straggling and σ_e^2 the variance of the electronic straggling. Due to the different shape of the two distributions this is incorrect and results in an overestimation of the total straggling. This error is negligible for light ions (H^+, He^+), but may play a role for heavy ions.

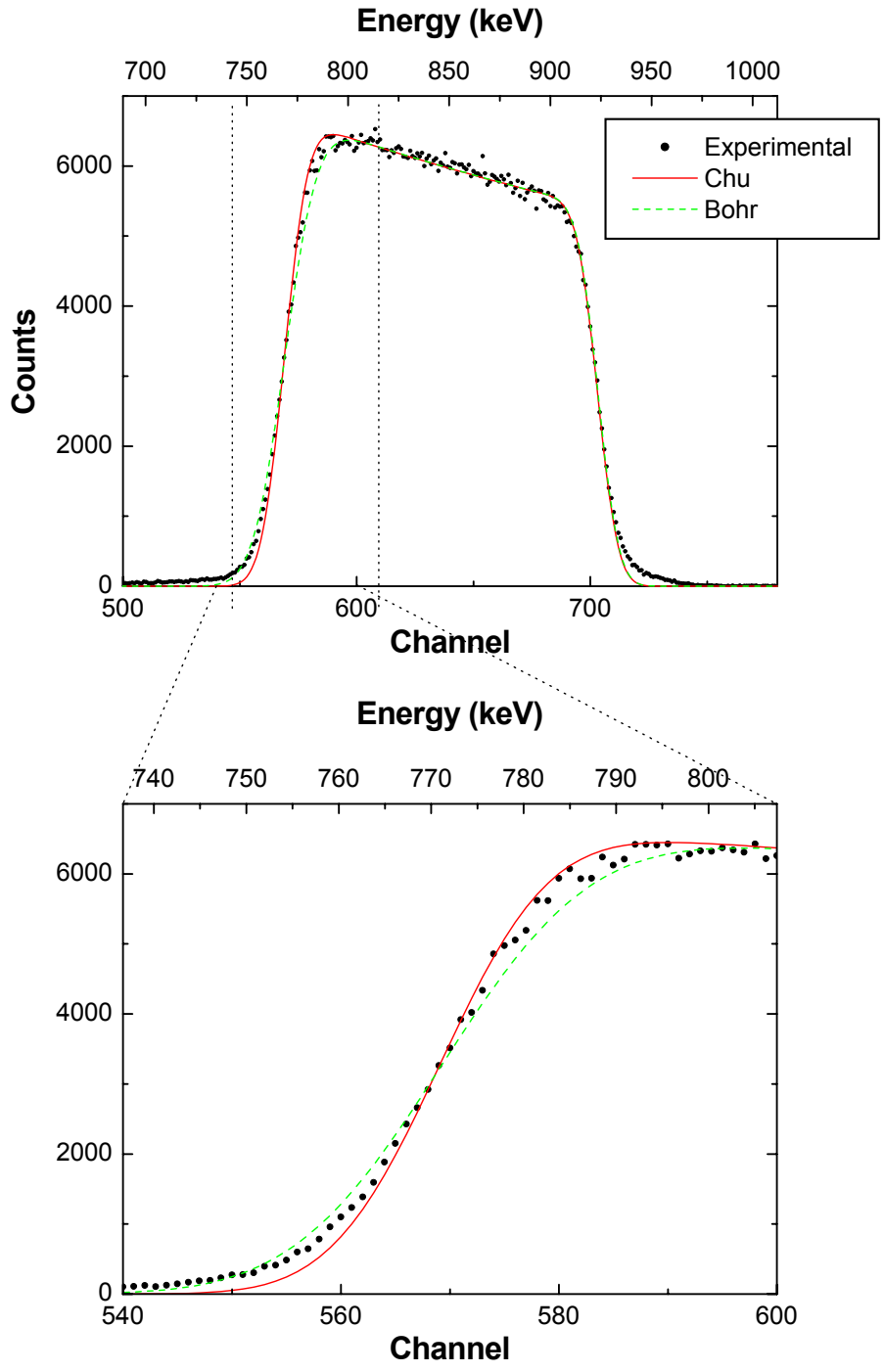

Figure 4.6: Measured and simulated spectra using Bohr and Chu straggling of 1.0 MeV ^{4}He ions incident on 100 nm Au on Si, scattering angle 165°. Bottom: Magnification of the low energy gold edge.

4.7.5 Geometrical straggling

The finite size of the incident beam and the width of the detector aperture result in a spread $\Delta\beta$ of the exit angle β for outgoing particles. This angular spread leads to differerent energies of the particles at the target surface due to

1. a spread $\Delta\theta$ of the scattering angle θ and therefore a spread of the transfered energy in the scattering process

2. different path lengths of the outgoing particles in the material.

These two contributions to geometrical straggling are not independent of each other and have to be considered simultaneously.

The spread $\Delta\beta$ of the exit angle β is given by [44, 31]:

$$(\Delta\beta)^2 = \left(\frac{g_d w}{L_D}\right)^2 + \left(\frac{g_b d \cos\beta}{L_D \cos\alpha}\right)^2 \tag{4.57}$$

where d is the diameter of the incident beam[6], w is the width of the detector aperture and L_D is the distance between the sample and the detector aperture, see fig. 3.3. g_b and g_d take into account the shapes of the beam and the detector aperture. For circular detectors or circular beams with uniform current density $g = 0.59$. $g = 0.68$ for rectangular shapes, as in the case of narrow slits [44].

SIMNRA calculates geometrical straggling by calculating the energy at the surface of particles with exit angles $\beta - \Delta\beta/2$ and $\beta + \Delta\beta/2$ and corresponding scattering angles $\theta - \Delta\theta/2$ and $\theta + \Delta\theta/2$. We therefore need the relation between $\Delta\beta$ and $\Delta\theta$.

In Cornell geometry the relation between the angles α, β and θ is given by

$$\cos\theta = \sin\alpha \, \sin\beta \, \sin\phi - \cos\alpha \, \cos\beta \tag{4.58}$$

where ϕ is the azimuth angle defined in fig. 4.15[7]. Because α, β and θ are known eq. 4.58 gives the azimuth angle ϕ. The spread of θ is given by

$$\Delta\theta = \frac{\partial\theta}{\partial\beta}\Delta\beta \tag{4.59}$$

which yields from eq. 4.58

$$\frac{\partial\theta}{\partial\beta} = -\frac{1}{\sin\theta}\left(\sin\alpha \, \cos\beta \, \sin\phi + \cos\alpha \, \sin\beta\right). \tag{4.60}$$

In IBM geometry the incident and outgoing trajectories are in the same plane (with $\phi = 90°$). Equation 4.58 simply reduces to

$$180° = \alpha + \beta + \theta \tag{4.61}$$

[6] Note that the beam spot size on the sample surface is $d/\cos\alpha$.

[7] Note that the incident particles have $\phi = -90°$.

and for the spread in θ we get from eqs. 4.59 and 4.60

$$\Delta\theta = -\Delta\beta. \tag{4.62}$$

Note the minus sign: If β increases then θ decreases and vice versa.

Energy loss straggling, geometrical straggling and the detector resolution are independent and are added quadratically.

Fig. 4.7 gives as examples the different straggling contributions at the sample surface for 2.6 MeV ^{4}He incident on $C_{0.99}D_{0.01}$ as a function of depth for typical RBS and ERDA geometries. An energy independent detector resolution of 15 keV FWHM is used. For RBS geometry the contribution of geometrical straggling is small compared to energy loss straggling and the resolution of the detector and may be neglected without penalty. For the ERDA geometry however, geometrical straggling cannot be neglected. Note that geometrical straggling first decreases until it reaches zero and then increases again. This is due to the minus-sign in eq. 4.62: If the exit angle β decreases (the outgoing path is closer to the surface normal) then the scattering angle θ increases: The backscattered or recoiled particles start with a smaller energy. However, the path length in the material is smaller due to the exit angle which is closer to normal resulting in a smaller energy loss. Near the surface the path lenght differences are small and geometrical straggling is governed by the kinematic spread. With increasing depth the two effects compensate each other more and more until in large depths the path length differences become dominant and geometrical straggling increases.

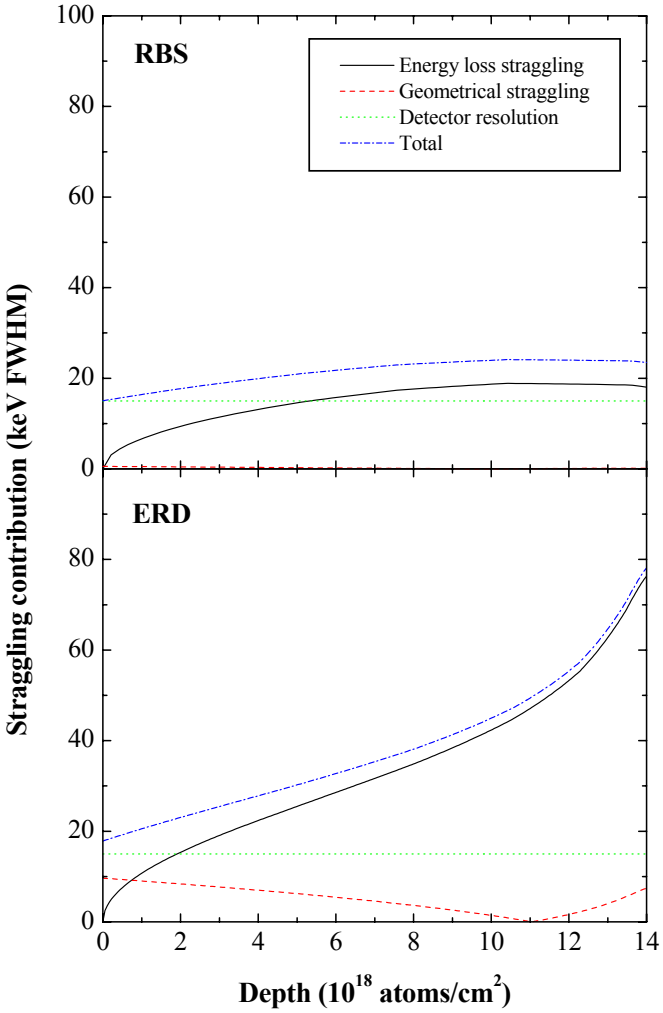

Figure 4.7: Contributions of electronic energy loss straggling, geometrical straggling and detector resolution to the total energy straggling at the sample surface for 2.6 MeV ^{4}He incident on $C_{0.99}D_{0.01}$. Beam diameter 0.5 mm, aperture width 0.5 mm, distance sample-detector aperture 100 mm, detector resolution 15 keV FWHM.
Top: RBS geometry with $\theta = 165°$, $\alpha = 0°$, $\beta = 15°$ for ^{4}He backscattered from ^{12}C.
Bottom: ERDA geometry with $\theta = 30°$, $\alpha = 75°$, $\beta = 75°$ for the deuterium recoils.

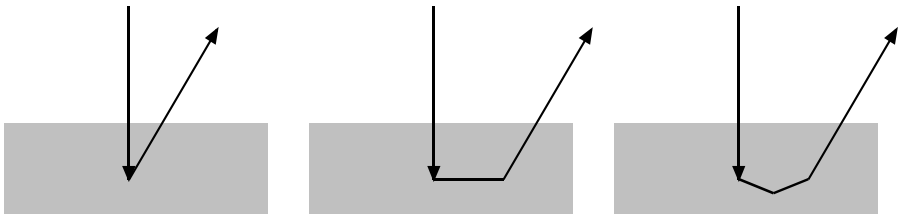

Figure 4.8: Examples of ion trajectories with one, two and three scattering events.

4.8 Multiple and plural scattering

4.8.1 Overview

SIMNRA uses straight lines as trajectories for the ingoing and outgoing particles, with one single scattering event connecting the trajectories of the particles, see fig. 4.8 left. This is only an approximation to physical reality, because the particles on the ingoing and outgoing path suffer many small angle deflections with small scattering angles (this has been called multiple scattering) and additionally may perform more than one scattering event with large scattering angle (see fig. 4.8 middle and right), before they are scattered towards the detector. This has been called plural scattering.

Multiple scattering has been recently reviewed by Szilagy *et al.* [31]. Multiple scattering results in an angular spread of the particles and therefore in a spread of path lengths. Due to the path length differences, we get an energy spread of the particles in a given depth.

Plural scattering with 2, 3, 4, ... scattering events is responsible for the background behind the low energy edge of high Z elements on top of low Z elements and the steeper increase of the spectra towards low energies than calculated with single scattering [45, 46, 47, 48, 49]. SIMNRA is able to calculate dual scattering, i. e. all particle trajectories with two scattering events.

4.8.2 Multiple (small angle) scattering

Angular and lateral spread due to multiple collisions with small deflection angles was treated analytically and numerically by Sigmund *et al.* [50, 51] for realistic screened interaction potentials of the Thomas-Fermi and Lenz-Jensen type. However, their theory is only valid for

1. Single elemental targets
2. The stopping of ions is neglected.

Due to these two assumptions the original Sigmund theory is only of limited practical use. But, as will be shown below, the Sigmund theory can be extended to multi elemental targets with stopping. The Sigmund theory is valid for small angle deflections, with each deflection $\ll 20°$.

The Sigmund theory is formulated with the reduced variables τ and $\tilde{\Phi}_s$, which are defined by

$$\tau = \pi a^2 d \tag{4.63}$$

τ is the reduced thickness, a is the Lindhard-Scharff screening radius and d the real target thickness in atoms/cm^2.

$\tilde{\Phi}_s$ is defined by

$$\tilde{\Phi}_s = \mu \Phi_s \tag{4.64}$$

with

$$\mu = \frac{Ea}{2Z_i Z_t e^2} \tag{4.65}$$

$\tilde{\Phi}_s$ is the reduced angle due to multiple scattering, Φ_s the real angle and μ the scaling factor which connects the real and reduced angles. E is the ion energy, a the screening radius as above, Z_i and Z_t the nuclear charges of the incident ions and the target atoms, respectively, and e the electron charge. The angular distribution due to multiple scattering can be described by a universal distribution function $f_s(\tilde{\Phi}_s, \tau)$, which is valid for all ion-target combinations and energies. f_s describes the absolute angular deviations from the original direction (spatial distribution).

The angular distribution due to multiple scattering is non-Gaussian. For $\Phi_s \leq \Delta\Phi_s/2$, with $\Delta\Phi_s$ the full width at half maximum (FWHM) of the angular distribution, the distribution function can be approximated by a Gaussian, see Fig. 5 of ref. [50]. A Gaussian will, however, underestimate the wings of the distribution for $\Phi_s > \Delta\Phi_s/2$. For large target thicknesses the angular distribution becomes more and more Gaussian.

Szilagyi *et al.* [31] have proposed a method how to extend the original Sigmund theory to multi-elemental targets with stopping: A multi-elemental target is divided into shallow sublayers consisting of only one element. The thickness of these sublayers is sufficiently small to allow a mean energy approximation with $\bar{E} = (E_i + E_f)/2$. $\bar{(E)}$ is the mean energy in the sublayer and E_i and E_f the energies at the entrance and exit of the sublayer. The Lindhard theory now can be applied to each sublayer. The individual angular spread contributions of two sublayer are added according to

$$(\Delta\Phi)^\nu = (\Delta\Phi_1)^\nu + (\Delta\Phi_2)^\nu \tag{4.66}$$

where $\Delta\Phi_1$ and $\Delta\Phi_2$ are the half widths in each sublayer and the exponent ν depends on the reduced thickness τ. Φ is already the projected angle instead of the spatial angle. The functions $\Delta\Phi(\tau)$ and $\nu(\tau)$ can be found in [31].

To obtain the energy distribution after penetrating a sublayer with trajectory angle α towards the surface normal SIMNRA calculates the energies of particles penetrating the sublayer with trajectory angles $\alpha \pm \Delta\Phi/2$. Additionally SIMNRA makes the following approximations:

1. The angular and energy distributions are approximated by Gaussian functions. This approximation will underestimate the wings of the multiple scattering distributions.

2. It is always assumed that the energy distribution is symmetric, i.e. that the energy of a particle penetrating the sublayer with angle $\alpha + \Delta\Phi/2$ is $E_0 - \Delta E/2$ and the energy of a particle with angle $\alpha - \Delta\Phi/2$ is $E_0 + \Delta E/2$ (Left-right symmetry), where E_0 is the energy of a particle penetrating the sublayer with angle α and ΔE the FWHM of the energy distribution. This approximation is obviously not true for normal incidence and not well fulfilled for very oblique incidence: In these cases the real energy distributions are asymmetric with respect to E_0.

Figs. 4.9–4.11 show the angular and energy spreads due to multiple scattering of 500 keV incident ^{4}He penetrating gold at an angle $\alpha = 60°$ at different depths. The model used by SIMNRA is compared to TRIM.SP calculations. TRIM.SP is a Monte-Carlo code which calculates realistic trajectories for each incident particle, taking all collisions with target atoms into account [52, 53]. 1000 incident particles were used for Figs. 4.9–4.11. The stopping power data from [2] were used in both calculations.

In Fig. 4.9 the incident beam has reached a depth of 1.6×10^{17} atoms/cm^2 and has lost about 35 keV due to electronic energy loss. The Gaussian angular- and energy distributions, which are used by SIMNRA, underestimate the wings of both distributions, however, the central part of the distributions is sufficiently well reproduced.

In Figs. 4.10 and 4.11 the incident beam has reached depths of 3.25×10^{17} atoms/cm^2 and 6.47×10^{17} atoms/cm^2, respectively. The electronic energy losses are about 70 keV and 135 keV, respectively. The angular and energy spread due to multiple scattering get broader, and the approximation with a Gaussian shape now is better fulfilled.

As already mentioned the approximations used by the program are not fulfilled for normal incidence. Figure 4.12 shows the angular and energy distributions of 500 keV incident ^{4}He in Au in a depth of 1.09×10^{18} atoms/cm^2, comparing TRIM.SP calculations and SIMNRA. The angular distribution has a minimum at 0°, which is not reproduced by SIMNRA. The energy distribution is asymmetric with a steep increase at the high energy side and a tail towards lower energies, which is also not reproduced by SIMNRA. The half width of the energy distribution is somewhat underestimated by SIMNRA. However, it should be noted that the influence of multiple scattering for normal incidence is small: The half width of the multiple scattering energy distribution shown in Fig. 4.12 is about 3 keV, which is considerably smaller than energy loss straggling (about 8.8 keV FWHM) and the energy resolution of the detector. Therefore the deviations at normal incidence between SIMNRA and physical reality are hardly ever visible.

To calculate the energy spread due to multiple scattering the energy spread contributions on the ingoing and outgoing paths have to be considered.

The energy spread contribution on the ingoing path is obtained in the following way: Particles without angular spread have a mean energy E and incident angle α in a given depth x, see Fig. 4.13 top. Particles with angular spread to one side have incident angle $\alpha + \Delta\Phi/2$, with $\Delta\Phi$ the FWHM of the angular spread and energy $E' = E - \Delta E/2$, with ΔE the FWHM of the energy spread, see Fig. 4.13 top. The scattering angle (with fixed exit angle β) for these particles is θ'. Note that E' and θ' are not independent. The same applies for particles with angular spread to the other side. These particles have the energy

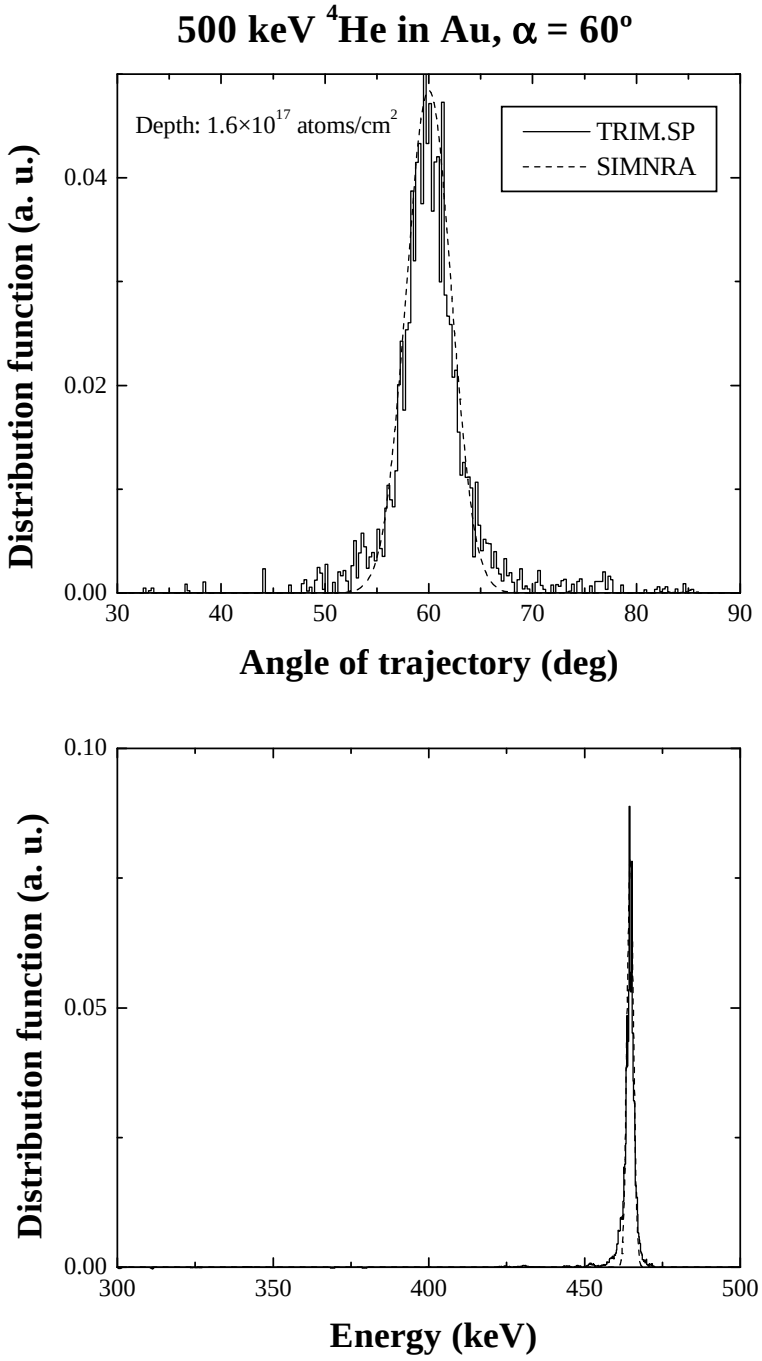

Figure 4.9: Angular and energy distributions in a depth of 1.6×10^{17} atoms/cm^2 for 500 keV incident ^{4}He in Au, incident angle $\alpha = 60°$. The angle of trajectory is measured towards the surface normal. Solid line: TRIM.SP calculation; Dashed line: SIMNRA.

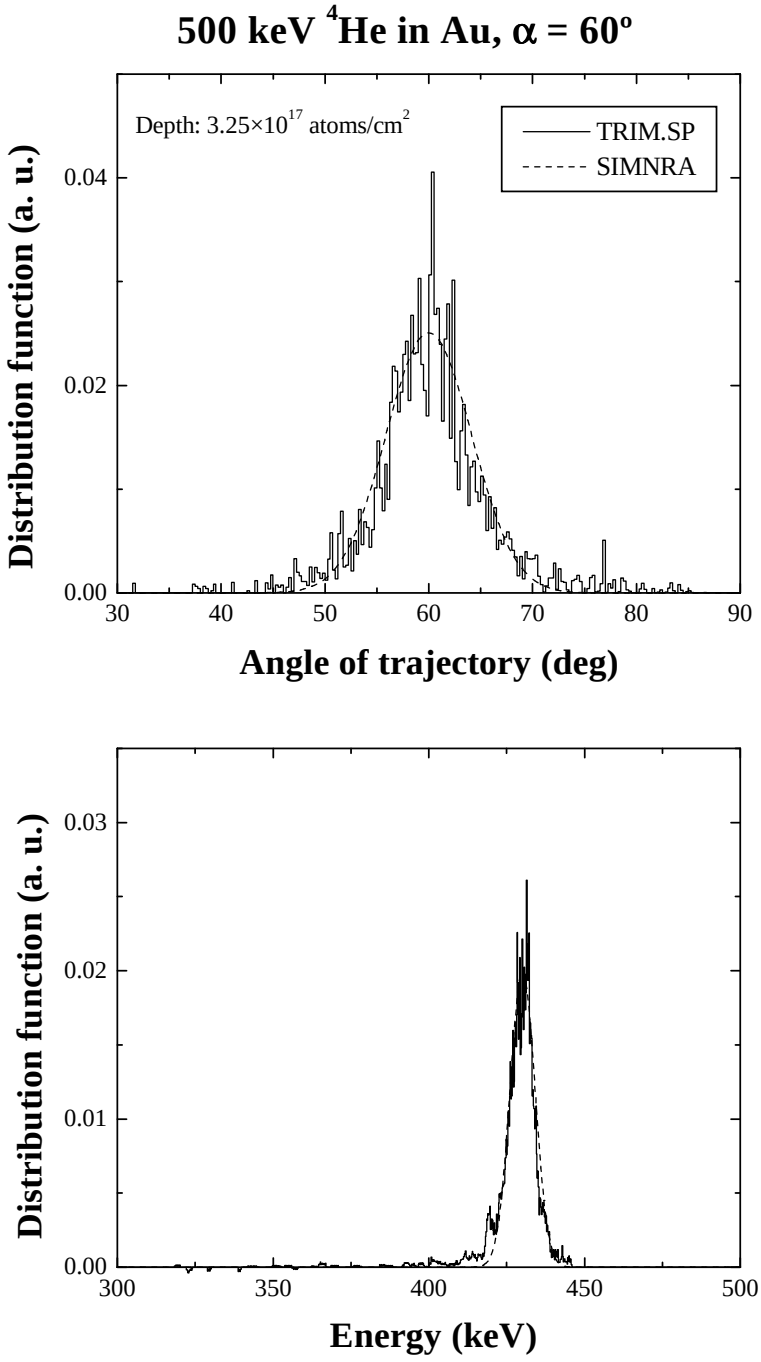

Figure 4.10: Same as Fig. 4.9, but for a depth of 3.25×10^{17} atoms/cm^2.

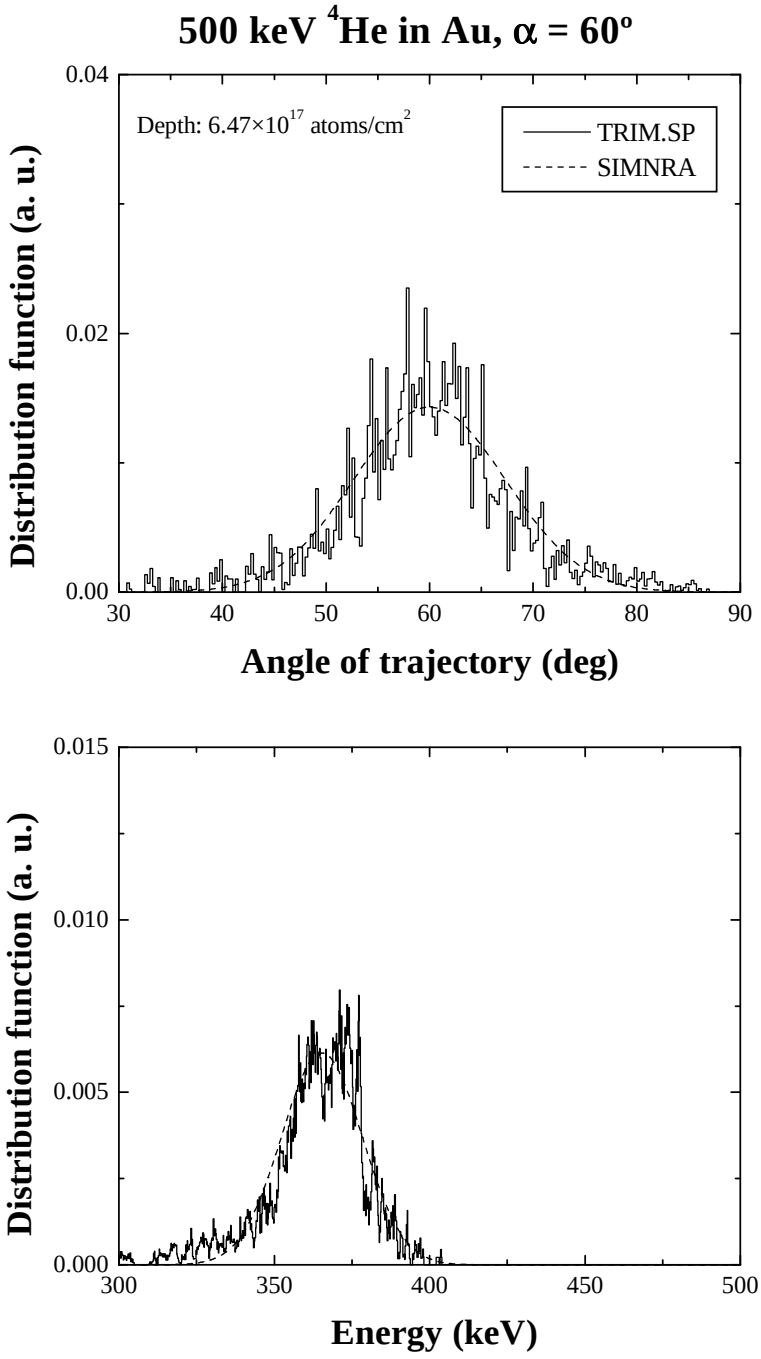

Figure 4.11: Same as Fig. 4.9, but for a depth of 6.47×10^{17} atoms/cm^2.

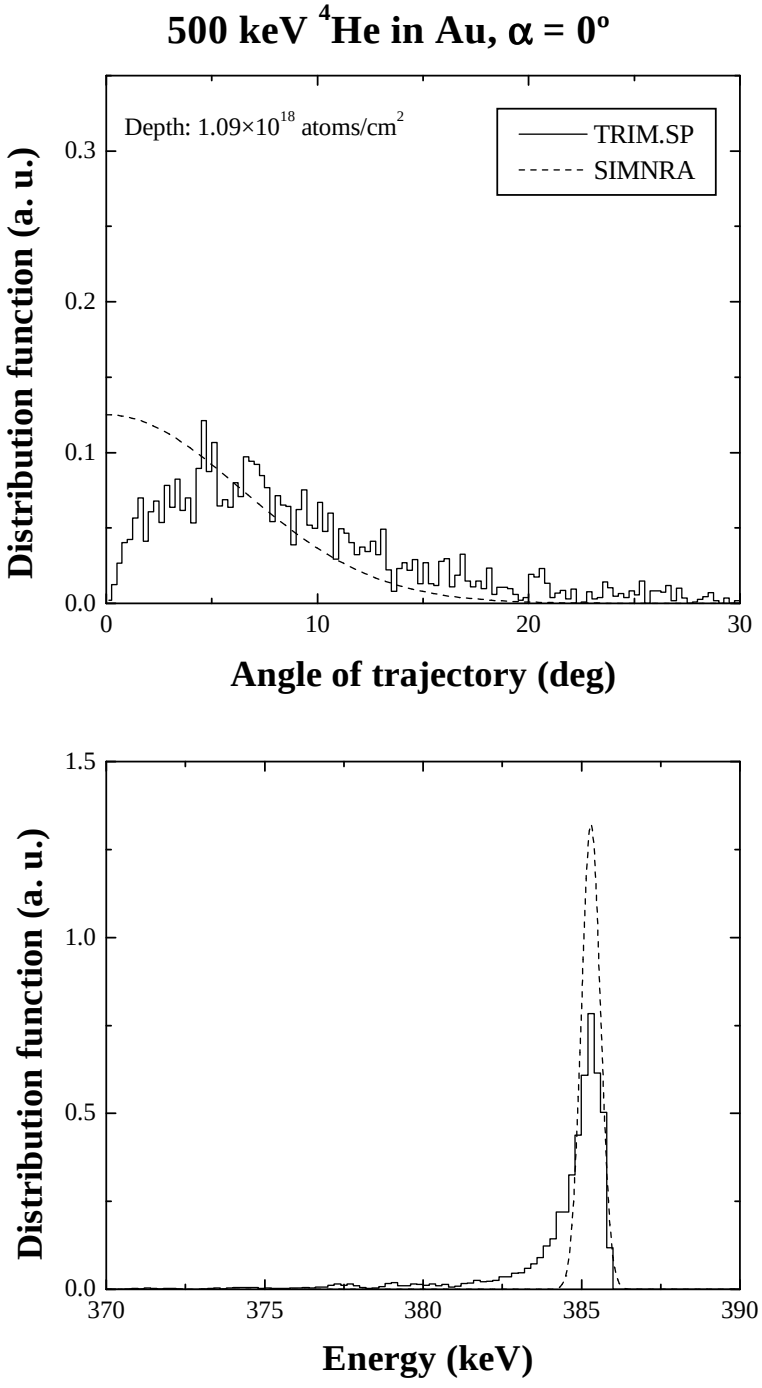

Figure 4.12: Angular and energy distributions in a depth of 1.09×10^{18} atoms/cm^2 for 500 keV incident ^{4}He in Au at normal incidence. The angle of trajectory is measured towards the surface normal. Solid line: TRIM.SP calculation; Dashed line: SIMNRA.

$E'' = E + \Delta E/2$. After scattering the particles have the energies

$$\begin{aligned} E_s &= K(\theta)E \\ E'_s &= K(\theta')E' \\ E''_s &= K(\theta'')E'' \end{aligned}$$

with K the kinematic factor. The FWHM of the energy spread contribution on the ingoing path ΔE_{in} could be obtained from

$$\Delta E_{in} = |E''_s - E'_s| \tag{4.67}$$

However, generally E''_s and E'_s are not symmetric with respect to E_s, and ΔE_{in} obtained from eq. 4.67 will neither describe the width of the high energetic part of the distribution nor the width of the low energetic part correctly. Therefore SIMNRA uses

$$\Delta E_{in} = 2|E''_s - E_s| \tag{4.68}$$

with E''_s the higher energy. This describes at least the higher energetic part of the distribution correctly.

The energy spread contribution on the outgoing path is obtained in the following way: a particle starting with some exit angle β' in the depth x may be deflected on its outgoing trajectory by multiple scattering in such a way that it has the correct angle β at the target surface to reach the detector, see Fig. 4.13 bottom. These particles have the energy E'_{out} and E''_{out} at the target surface and scattering angles θ' and θ''. Again, E'_{out} and θ' are not independent. As in the case of the energy spread contribution on the ingoing path SIMNRA uses as FWHM of the energy spread on the outgoing path ΔE_{out}

$$\Delta E_{out} = 2|E''_{out} - E_{out}| \tag{4.69}$$

with E''_{out} the higher energy. As in the case of the energy spread contribution on the ingoing path this describes the higher energetic part of the distribution correctly.

The energy spread contributions on the ingoing path ΔE_{in} and on the outgoing path ΔE_{out} are independent and can be added quadratically [31]. If an absorber foil is used, the multiple scattering induced energy spread in the foil is ΔE_{foil}. The final result for the FWHM of the total energy spread due to multiple small angle scattering ΔE_{MS} is therefore

$$\Delta E^2_{MS} = \Delta E^2_{in} + \Delta E^2_{out} + \Delta E^2_{foil} \tag{4.70}$$

Fig. 4.14 shows the contributions ΔE_{in} and ΔE_{out} for 1 MeV ^{4}He in Au as a function of the residual ^{4}He energy. For comparison the results calculated by the DEPTH code [31] are included. The agreement between the result of the two programs is good.

4.8.3 Plural (large angle) scattering

Plural large angle scattering cannot be treated analytically. SIMNRA approximates plural scattering effects by calculating all particle trajectories with two scattering events (dual

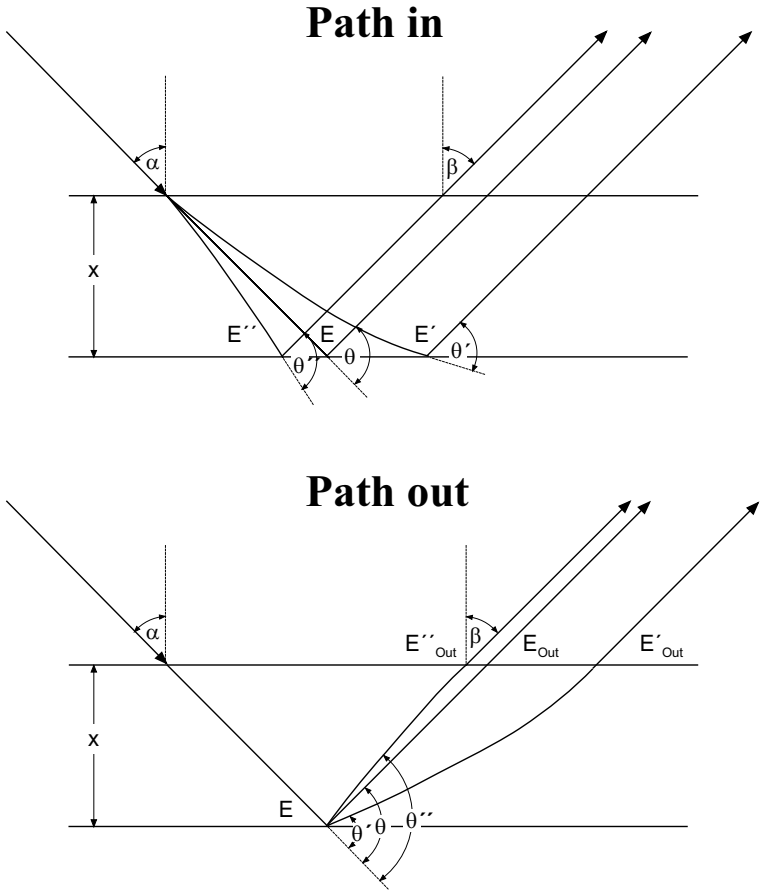

Figure 4.13: Contributions of multiple scattering on the ingoing and outgoing paths.

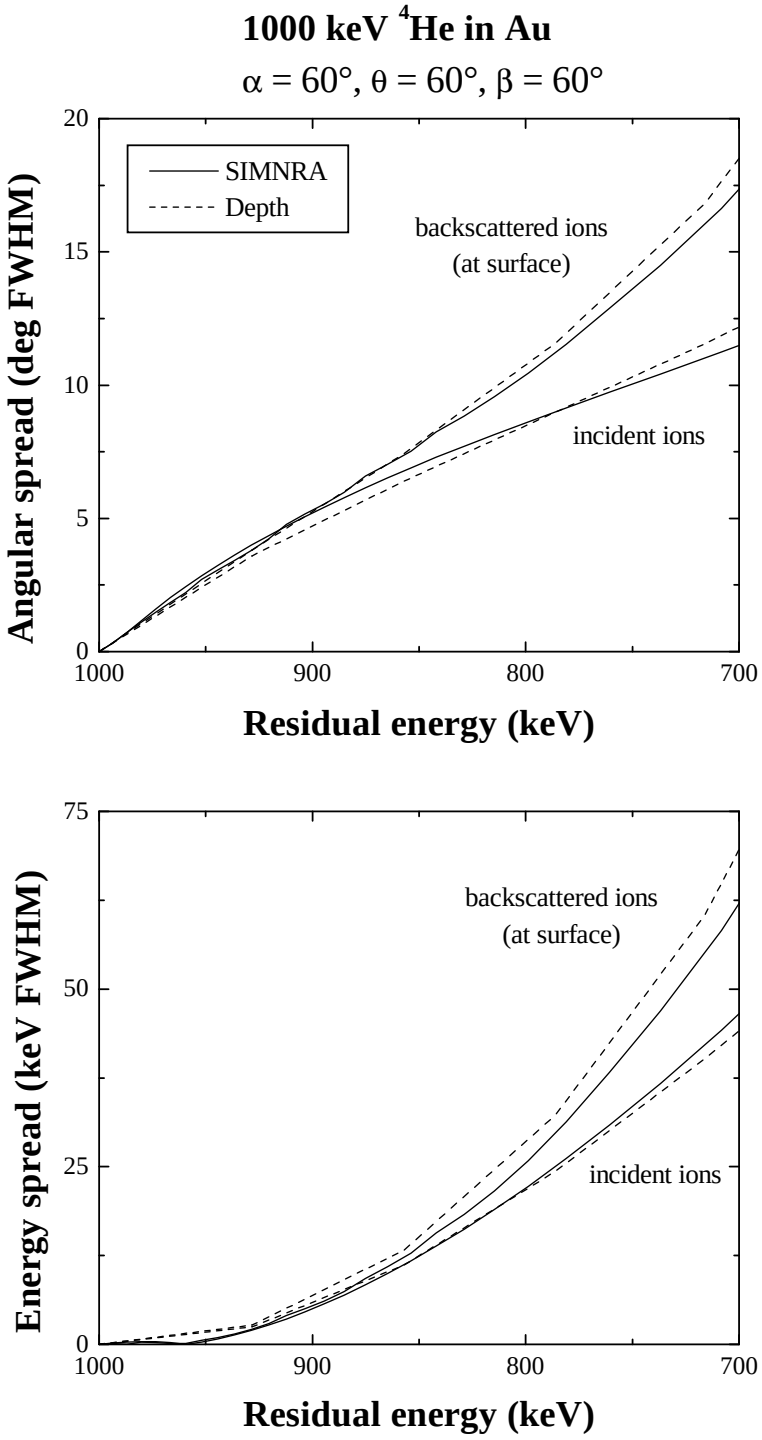

Figure 4.14: Calculated energy spread contributions on the ingoing and outgoing paths to the total energy spread due to multiple scattering. 1000 keV ^{4}He in Au, $\alpha = 60°$, $\beta = 60°$, $\theta = 60°$ (IBM geometry). Top: angular spread; bottom: energy spread. Solid lines: SIMNRA; dashed lines: DEPTH code.

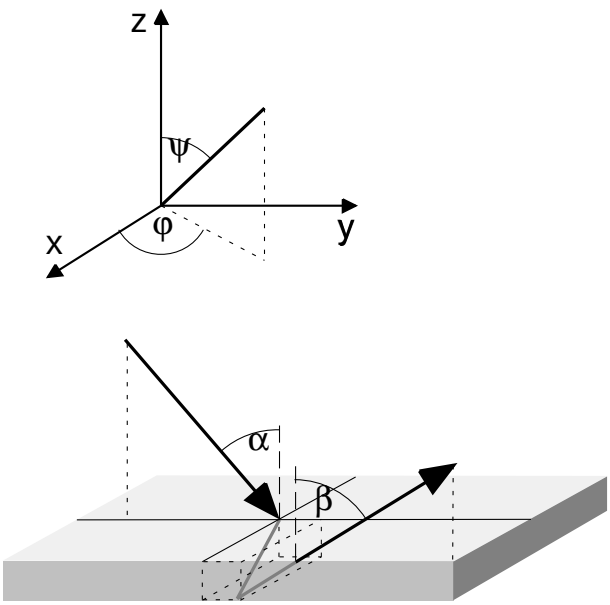

Figure 4.15: Geometry used for the calculation of dual scattering.

scattering), see Fig. 4.8. The contribution of trajectories with more than two large angle deflections is neglected. Plural (large angle) and multiple (small angle) scattering may be combined in the calculations.

SIMNRA performs the calculation of dual scattering in the following way: During each step of the incident ion particles are scattered into the whole sphere of 4π. We introduce the polar system with the polar angles ψ, ϕ, see fig. 4.15. After the first scattering event the scattered particles have the direction ψ, ϕ. The scattering angle θ_1 of the first scattering event is given by

$$\cos\theta_1 = \sin\alpha\ \sin\psi\ \sin\phi - \cos\alpha\ \cos\psi$$

SIMNRA uses the Rutherford cross-section for the calculation of the number of scattered particles in the first scattering event. The new angle α' of the particles after the first scattering is

$$\alpha' = 180^\circ - \psi$$

The scattering angle θ_2 of the second scattering event is given by

$$\cos\theta_2 = \sin\beta\ \sin\psi\ \sin\phi + \cos\beta\ \cos\psi$$

SIMNRA subdivides the whole sphere of 4π into 10 ψ-intervals and 12 ϕ-intervals, resulting in 120 solid angle intervals. SIMNRA considers only trajectories with scattering angles $\theta_1, \theta_2 > 20^\circ$ for dual scattering. Trajectories with smaller scattering angles are very similar to single scattering trajectories. For each solid angle interval a full backscattering spectrum with the starting depth of the particles equal to the depth of the incident ions and the new incident angle α' and the new scattering angle θ_2 is calculated.

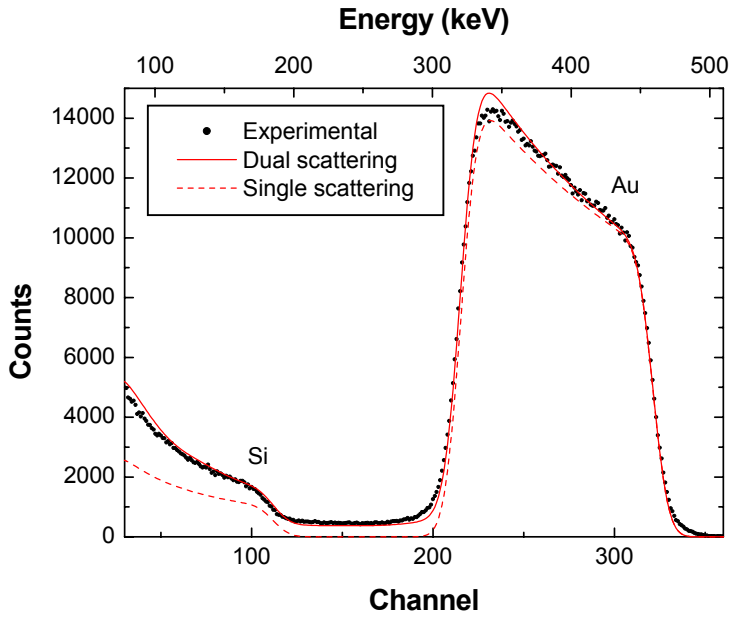

Figure 4.16: 500 keV ^{4}He ions incident on 100 nm Au on top of Si, scattering angle 165°. Circles: experimental data points, dashed line: simulation with one scattering event, solid line: simulation with two scattering events.

Fig. 4.16 compares the simulated spectra with single and dual scattering for 500 keV ^{4}He ions incident on a 100 nm gold layer on top of silicon with experimental data. With the inclusion of dual scattering the experimental results are much better approximated. Dual scattering gives the background between the low energy edge of Au and the Si edge, and the steeper increase of the gold spectrum is better described. The results with dual scattering are slightly lower than the experimental results. This is due to trajectories with more than two scattering events which are not calculated.

4.9 Surface roughness

The quantitative application of ion beam analysis methods is usually restricted to laterally homogeneous and smooth films. The experimentalist is often confronted with rough surfaces. The effects of rough surfaces of *thick* targets on RBS were investigated in some detail by Edge and Bill [54], Knudson [55], Bird *et al.* [56], and Hobbs *et al.* [57]. Wüest and Bochsler [58] and Yesil *et al.* [59, 60] attacked the problem by means of a Monte-Carlo computer simulation, taking into account correlation effects of the surface roughness and multiple surface crossings of the incident and emerging ions. It turned out that effects of rough surfaces of *thick* targets occur only for grazing angles of the incident or emerging ions. This is especially the case in ERDA on thick, rough targets, as was shown by Yesil *et al.* [59, 60] and Kitamura *et al.* [61]. Hydrogen depth profiling on rough surfaces by ERDA was studied experimentally by Behrisch *et al.* [62].

Astonishingly, the effects of rough *thin films* were studied much more scarcely. For RBS, rough films on a smooth substrate were investigated by Shorin and Sosnin [63] and Metzner *et al.* [64, 65]. Shorin and Sosnin [63] used a Monte-Carlo computer simulation. The Monte-Carlo approach suffers from long computing times of the order of hours [60], rendering these codes impractical for evaluation of experimental spectra. Moreover, the Shorin/Sosnin code treats only RBS with Rutherford cross-sections, neglecting non-Rutherford scattering, NRA and ERDA. The theoretical approach of Metzner *et al.* [64, 65] allows to extract the thickness distribution of rough films from a measured spectrum. However, this approach is only valid for RBS with Rutherford cross sections, a scattering angle of exactly 180° and constant stopping power, thus severely limiting the practical applicability of this work. The computer code RUMP [12, 13] allows to fuzz the interface between two layers by roughening the top layer. However, this is intended only for small roughness amplitudes, and the roughness distribution function is not documented.

Moreover, all work done so far treats only the case of a rough film on a smooth substrate. But in practice also the case of a film deposited on a rough substrate (Fig. 4.17(b)) is sometimes encountered. This section describes the algorithms used for the description of rough surfaces and compares results of code calculations with experimental data. The limitations of the used approximations are discussed.

4.9.1 Rough film on a smooth substrate

A rough film on a smooth substrate is shown schematically in Fig. 4.17(a). The substrate can be considered to be smooth, if its roughness is much smaller than the mean thickness $\bar{d}$ of the film. The film thickness distribution is described by a distribution function $p(d)$, with the film thickness d measured perpendicular to the substrate, see Fig. 4.17(a) and $d \geq 0$. In the literature, usually a Gaussian distribution centered at $\bar{d}$ with variance σ^2 and cut-off at zero is used for $p(d)$ [64, 65]. However, a more natural choice of a distribution function with only positive values $d \geq 0$ is the Gamma distribution, which is also fully described by its mean value $\bar{d}$ and standard deviation σ. The Gamma distribution is defined by

$$p(d) = \frac{\beta^\alpha}{\Gamma(\alpha)} d^{\alpha-1} e^{-\beta d}, d > 0 \tag{4.71}$$

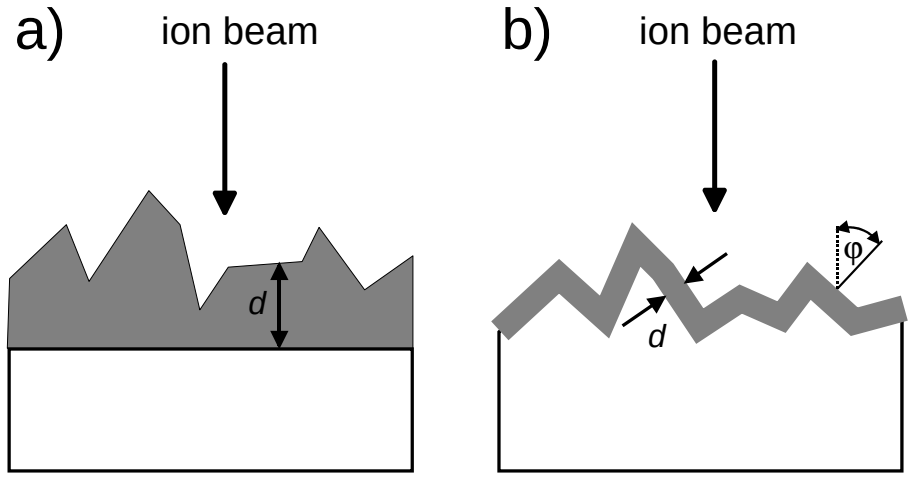

Figure 4.17: Schematic representation of a rough film on a smooth substrate (a), and of a smooth film on a rough substrate (b).

with $\alpha = \bar{d}^2/\sigma^2$ and $\beta = \bar{d}/\sigma^2$. $\Gamma(\alpha)$ is the Gamma function. The Gamma distribution is shown in Fig. 4.18 for $\bar{d} = 1$ and different standard deviations σ. The corresponding Gaussian distributions centered at 1 and identical σ are shown for comparison. If $\sigma \ll \bar{d}$, i.e. if the width of the distribution is small compared to its mean value, Gaussian and Gamma distributions are nearly identical, see the curves for $\sigma = 0.1$ in Fig. 4.18. With increasing σ the two distributions get more and more different (see the curves for $\sigma = 0.3$ and 0.7 in Fig. 4.18). For $\sigma = \bar{d}$ the Gamma distribution decreases exponentially with $p(d) = e^{-d}$, and for $\sigma > \bar{d}$ an integrable singularity develops at $d = 0$.

A RBS, NRA or ERDA spectrum of a rough film is approximated by a superposition of N spectra with different layer thicknesses d_i. N can be adjusted by the `Number of thickness steps` in the `Setup: Calculation...` menu, see section 3.4.3. Typically about $N = 20$ sub-spectra are necessary to obtain a smooth superposition, though N has to be increased to about $N = 50$ for broad distributions with $\sigma \geq \bar{d}$. The weight w_i of each sub-spectrum is determined according to the thickness distribution function. For each sub-spectrum the layer is treated to be smooth with thickness d_i. Correlation effects, such as incidence through a hump and emergence through a valley or multiple surface crossings, are neglected. This is only correct for backscattering at a scattering angle of exactly 180° and for transmission geometries. However, for scattering angles in the range 150°–180° and non-grazing incidence and emergence angles, as are used in many RBS and NRA setups, correlation effects still play only a minor role and can be neglected without severe loss of accuracy. But it should be kept in mind that the used approximation gets invalid for grazing incidence or exit angles, as is the case in ERDA - in these cases correlation effects may be dominant and can change the shape of the spectra considerably.

The effect of layer roughness on the shape of RBS spectra is shown in Fig. 4.19 for incident ^{4}He ions backscattered from a gold layer at a scattering angle of 165°. The film thickness distributions are described by the Gamma distributions shown in Fig. 4.18. If

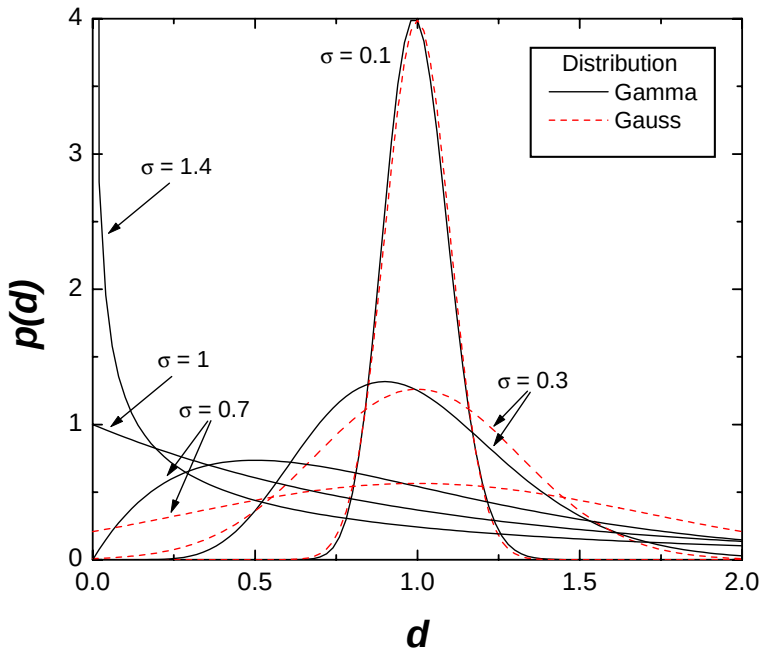

Figure 4.18: Comparison of Gaussian distribution functions centered at 1 (dashed lines) and Gamma distribution functions (solid lines) with mean value $\bar{d} = 1$ and different standard deviations σ.

the thickness variation is much smaller than the mean film thickness ($\sigma/\bar{d} = 0.1$), only the low energy edge of the film is affected by the roughness and gets broader. With increasing roughness the broadening of the low energy edge increases, until at $\sigma/\bar{d} \approx 0.6$ the high energy edge begins to decrease. The energy $E_{1/2}$, at which the low energy edge has decreased to its half height, remains fairly constant until large roughness amplitudes of the order $\sigma/\bar{d} \approx 0.6$, i.e. until the high energy edge begins to decrease. For sufficiently thick films, i.e. if the film is completely resolved, this energy is therefore a rather robust measure of the mean film thickness even for large roughnesses, as long as the high energy edge is not affected.

The energy spectrum of 1.5 MeV ^{4}He backscattered from a rough Ni-film deposited on polycrystalline carbon is shown in Fig. 4.20. The measured spectrum is well reproduced in the simulation by a mean Ni layer thickness of 2.17×10^{18} Ni-atoms/cm^2 (238 nm) and a roughness with standard deviation $\sigma = 2.12 \times 10^{17}$ Ni-atoms/cm^2 (23 nm) (solid line). The experimental data are not well reproduced by the spectrum of a smooth Ni layer (dashed line). The roughness of the Ni film was determined from line scans with a profiler. The roughness distribution, i.e. the deviation of the actual surface from the leveled one, was approximately Gaussian: For small values of $\sigma/\bar{d}$ a Gaussian and a Gamma distribution cannot be distinguished, see Fig. 4.18. The carbon substrate was already rough with a standard deviation $\sigma_{\mathrm{C}} = 18.2$ nm. The roughness of the Ni film on the substrate was $\sigma_{\mathrm{C+Ni}} = 26.5$ nm. This roughness is made up by the roughness of the carbon substrate plus the roughness of the Ni film σ_{Ni}. By assuming the two roughnesses to be independent, i.e.

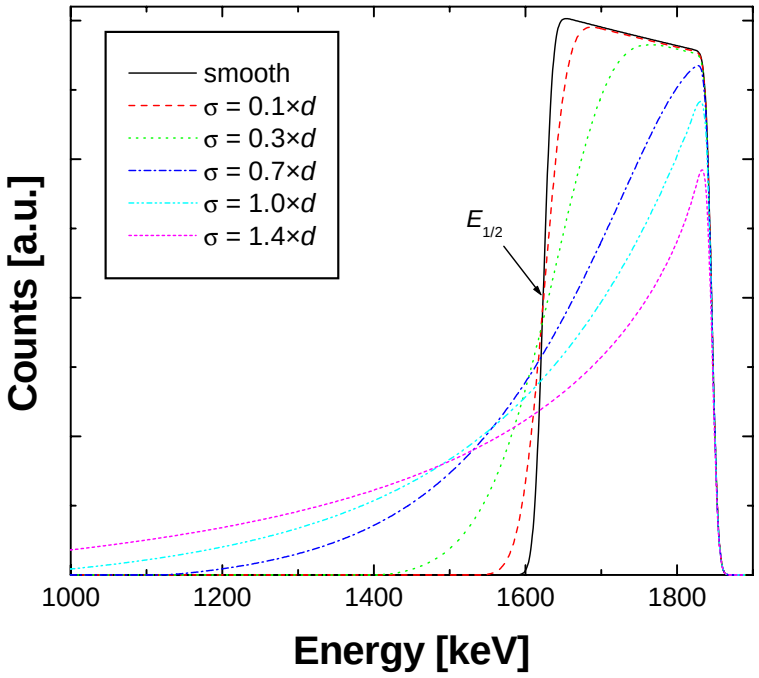

Figure 4.19: Calculated energy spectra for 2 MeV ^{4}He backscattered from a smooth and rough gold layers with mean thickness $\bar{d} = 1{\times}10^{18}$ Au-atoms/cm^2 and different roughnesses with standard deviation σ. The film thickness distributions are shown in Fig. 4.18. Incident angle $\alpha = 0°$, scattering angle 165°. $E_{1/2}$ marks the energy, at which the low energy edge has decreased to its half height.

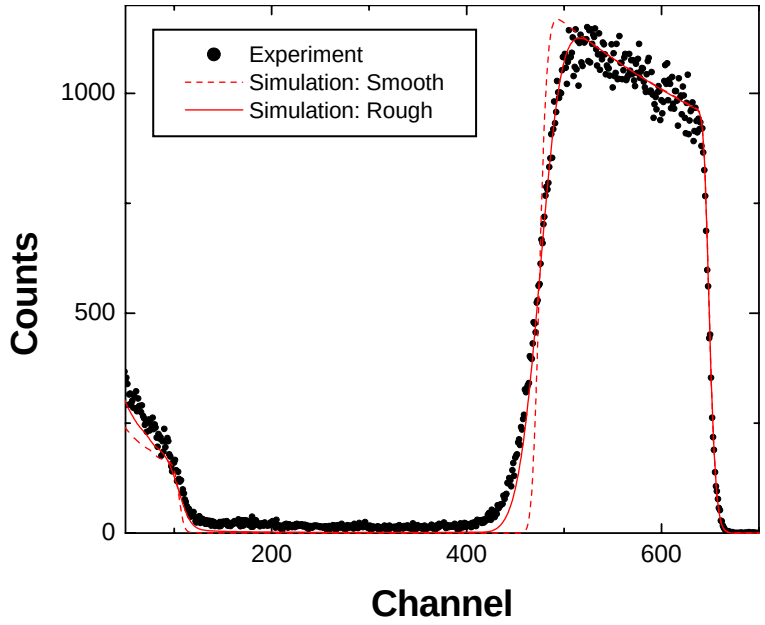

Figure 4.20: 1.5 MeV ^{4}He backscattered at 165° from a rough Ni-film with a mean thickness of 2.17×10^{18} Ni-atoms/cm^2 on carbon substrate. Dots: Experimental data; Dashed line: Simulation assuming a smooth Ni layer; Solid line: Simulation assuming a rough Ni layer with roughness $\sigma = 2.12 \times 10^{17}$ Ni-atoms/cm^2.

$\sigma^2_{\mathrm{C+Ni}} = \sigma^2_{\mathrm{C}} + \sigma^2_{\mathrm{Ni}}$, the roughness of the Ni film alone is about 19.3 nm, in good agreement with the result from He backscattering of 23 nm.

The energy spectrum of 2.0 MeV ^{4}He backscattered from a rough oxidised aluminum film on polycrystalline carbon is shown in Fig. 4.21. The carbon substrate was well polished and had a mean roughness < 25 nm [67]. The film was exposed for about 8 months as erosion monitor at the vessel wall of the nuclear fusion tokamak experiment JET [66, 67], the wall temperature was about 300°C. The initial Al layer thickness was 3.16×10^{18} atoms/cm^2 (525 nm), but decreased due to sputtering by bombardment with energetic hydrogen atoms from the nuclear fusion plasma to 7.5×10^{17} Al-atoms/cm^2. At the same time the Al film was oxidised and some nickel, which was initially eroded at an erosion dominated area of the JET vessel wall [8], was redeposited on the Al film and incorporated. The observed spectrum with the tails at the low energy sides of the O, Al and Ni peaks cannot be reproduced by assuming a smooth layer. But it is fairly well reproduced by a rough layer with a mean film thickness of 1.11×10^{18} atoms/cm^2, roughness $\sigma = 1.06 \times 10^{18}$ atoms/cm^2, and composition 68% Al, 30% O, 2% Ni (solid line in Fig. 4.21). The shape of the film thickness distribution is close to the curve with $\sigma = 1$ in Fig. 4.18. This example shows clearly, that non-Gaussian distributions of layer thicknesses are observed in practice and can be described by a Gamma distribution.

[8] The JET vessel walls consist of Inconel, a stainless steel with high nickel content.

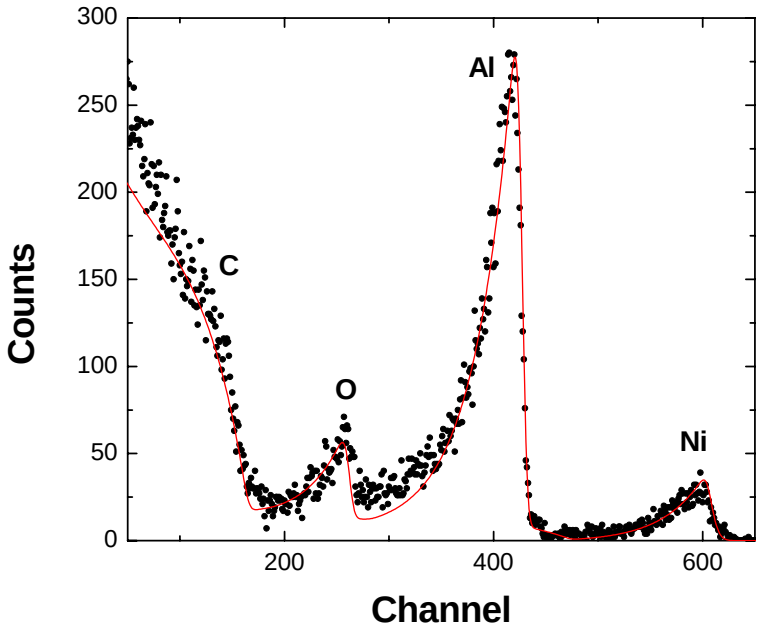

Figure 4.21: 2 MeV ^{4}He backscattered at 165° from a rough oxidised aluminum film on carbon. The film was used as long term sample in the tokamak JET and was strongly eroded by plasma impact. Additionally some Ni was deposited from the plasma. Dots: Experimental data; Solid line: Simulation with a mean film thickness of 1.11×10^{18} atoms/cm^2 and roughness $\sigma = 1.06 \times 10^{18}$ atoms/cm^2. Film composition 68% Al, 30% O, 2% Ni.

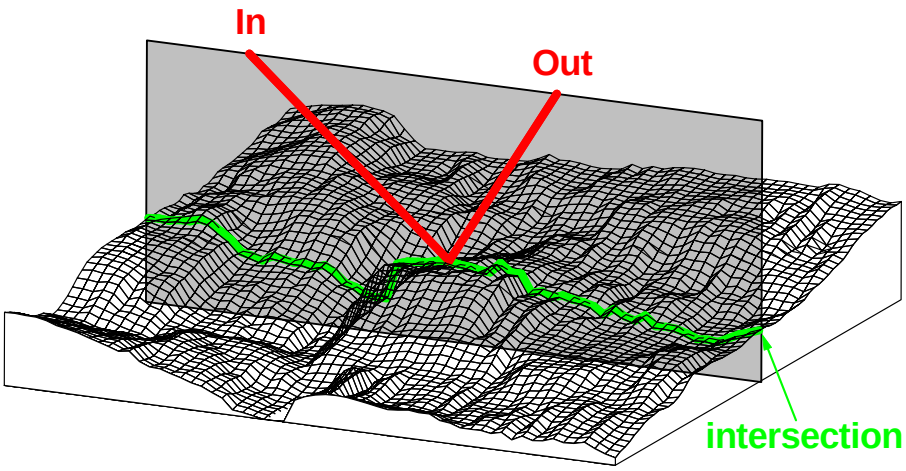

Figure 4.22: Schematic representation of a rough surface. In: Direction of the incident beam; Out: Direction of the outgoing beam; Light gray: Plane spanned by the incident and outgoing beams; Intersection: Intersection of this plane with the rough surface.

4.9.2 Smooth film on a rough substrate

A film with homogeneous thickness d on a rough substrate is shown schematically in Fig. 4.17b. The substrate is considered to be rough, if its roughness amplitude is much larger than the thickness d of the film. We assume a rough substrate to consist of inclined line segments with local inclination angle φ, and the film thickness d is measured parallel to the local surface normal. Such a rough surface is described by a distribution of local tilt angles $p(\varphi)$. The concept of a local tilt angle was already used by Küstner *et al.* for the calculation of the sputtering yield of rough surfaces by ion bombardment in the energy range 100 eV to several keV [68]. In Küstner's work the rough surface was treated as a fully 3-dimensional object, which was necessary due to the 3-dimensional nature of the collision cascades created by keV ions. In MeV ion beam analysis the trajectories of the incident and emerging ions can be approximated with good accuracy by straight lines, and we have to consider only the intersection of the plane, which is formed by the directions of the incident and emerging ions, and the target surface, see Fig. 4.22: This is only a 2-dimensional line profile as the one shown in Fig. 4.17b.

The tilt angle distribution is given by $p(\varphi)$. This distribution describes the frequency of occurence of a line segment inclined by φ. A rough surface without preferential orientation has a mean tilt angle

$$\bar{\varphi} = \int_{-90^\circ}^{90^\circ} \varphi\, p(\varphi)\, d\varphi = 0^\circ. \tag{4.72}$$

The probability distribution $\tilde{p}(\varphi)$ of hitting a surface tilted by φ by an incident ion is given by

$$\tilde{p}(\varphi) = p(\varphi)\cos(\alpha - \varphi), \tag{4.73}$$

with the incident angle α of the ion. α is measured towards the surface normal of a non-inclined surface. The factor $\cos(\alpha - \varphi)$ is due to the projection of the line segment into the

plane perpendicular to the incident ion trajectory: It is more likely to hit a segment which is perpendicular to the incident trajectory than an inclined segment - and obviously it is impossible to hit a segment which is tilted parallel to the incident beam. It is important to note that a profiler or a scanning tunneling microscope (STM), which samples the surface at a constant step width parallel to the surface, measures the distribution $\tilde{p}(\varphi)$ rather than $p(\varphi)$: Large tilt angles are under-represented, and tilt angles of 90° cannot be measured at all.

RBS, NRA and ERDA spectra of a smooth film on a rough substrate are approximated by a superposition of M spectra with different local incident angles $\tilde{\alpha}$, where

$$\tilde{\alpha} = |\alpha - \varphi| \tag{4.74}$$

and local exit angles $\tilde{\beta}$. The choice of $\tilde{\beta}$ is discussed below. M can be adjusted by the `Number of angular steps` in the `Setup: Calculation...` menu, see section 3.4.3. The weight of each sub-spectrum is determined according to the distribution function $\tilde{p}(\varphi)$. For each sub-spectrum the substrate is treated to be smooth, i.e. a spectrum for a smooth layer, but with angles $\tilde{\alpha}$ and $\tilde{\beta}$ is calculated. Incident angles $\tilde{\alpha} > 90°$ are excluded: This represents a line segment which cannot be hit by the incident beam. As in the case of a rough film on a smooth substrate, surface correlation effects like shadowing of one line segment by another, and multiple surface crossings are neglected.

By using a simple 2-dimensional model, one can choose analogue to Eq. 4.74 as local exit angle $\tilde{\beta}$

$$\tilde{\beta} = |\beta + \varphi| \tag{4.75}$$

This relation was used by SIMNRA 4.70–4.90. But it turned out that this 2-dimensional model is oversimplified and results in unrealistic spectra if a rough surfaces is bombarded at non-normal incident angles $\alpha \neq 0$. We have to take the 3-dimensional nature of a rough surface into account, which consists of inclined and rotated surface areas instead of just line segments, as in the 2-dimensional case. Each surface area can be described by a local tilt angle φ and a rotation angle ψ. Many different combinations (φ, ψ) result in identical local incident angles $\tilde{\alpha}$, but always with a different local exit angle $\tilde{\beta}$: For each $\tilde{\alpha}$ we have a distribution of $\tilde{\beta}$'s instead of just one as in the 2-dimensional case. $\tilde{\beta}$ as function of $\tilde{\alpha}$ and a control parameter ψ can be obtained as follows, see Fig. 4.23: Rotate the xy-plane around the vector $\vec{\alpha}$ by an angle ψ. This rotation can be described by a rotation matrix $\mathbf{M}_{\vec{\alpha}}(\psi)$. The normal vector of the rotated plane is $\vec{n}(\psi) = \mathbf{M}_{\vec{\alpha}}(\psi)\vec{z}$, where $\vec{z}$ is the normal vector of the non-rotated plane, which is identical to the z-axis. The exit angle $\tilde{\beta}$ is given by the scalar product of $\vec{n}(\psi)$ and $\vec{\beta}$, with $\cos\tilde{\beta}(\psi) = \vec{n}(\psi)\vec{\beta}$, where $\vec{\beta}$ is the vector which describes the exit beam. For the exact solution of the 3-dimensional problem it would be necessary to take many different $\tilde{\beta}$ for each $\tilde{\alpha}$ into account, which increases the computing time considerably. Therefore we replace the function $\tilde{\beta}(\psi)$ by its mean value

$$< \tilde{\beta} >= \int_0^{2\pi} w(\psi)\tilde{\beta}(\psi)d\psi, \tag{4.76}$$

where $w(\psi)$ is a weighting factor due to the projection of the surface element onto the incident beam, with $w(\psi) = \vec{n}(\psi)\vec{\alpha}$. This is a 2.5-dimensional model: We use the fully

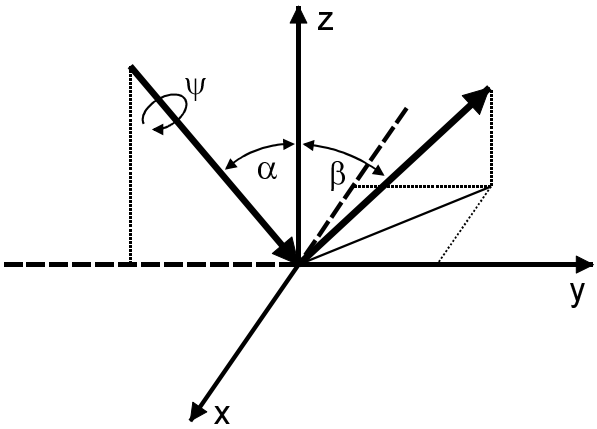

Figure 4.23: Rotation of the xy-plane around $\vec{\alpha}$ by ψ.

3-dimensional surface for the calculation of $< \tilde{\beta} >$, but we use only one local exit angle $< \tilde{\beta} >$ for each local incident angle $\tilde{\alpha}$ as in the 2-dimensional model.

If we have a local tilt angle φ, then the local incident and exit angles $\tilde{\alpha}$ and $< \tilde{\beta} >$ are calculated according to Eqs. 4.74 and 4.76. Which distribution has to be used as tilt angle distribution? A line profile of the surface of a carbon fibre composite (CFC) material manufactured by Dunlop is shown in Fig. 4.24 (top). Due to its high thermal conductivity this material is used for high heat flux components in the tokamak experiment JET. The standard deviation of the surface roughness is about $\sigma = 8.2$ μm. A histogram of the tilt angle distribution $\tilde{p}(\varphi)$, obtained with a profiler from several line scans in different sample directions, is shown in Fig. 4.24 (bottom). Tilt angles larger than about 60° are not observed due to the apex angle of the profiler tip. The tilt angle distribution is fairly well described by a Lorentz distribution for the tilt angles $p(\varphi)$ (dashed line), while a Gaussian distribution underestimates strongly the wings of the distribution (dotted line). The full width at half maximum (FWHM) of the Lorentz distribution is 26.6°.

Having the incident angle α Calculated backscattering spectra for incident ^{4}He ions backscattered from a gold layer with thickness 1×10^{18} atoms/cm^2 at a scattering angle of 165° are shown in Fig. 4.25 for a smooth and rough substrates. The rough substrates are described by a Lorentz distribution of tilt angles with different FWHM w. On a rough substrate the low energy edge gets a tail, which increases with increasing roughness. This tail extends to energies close to zero. With increasing roughness the Au peak also gets broader, and the energy $E_{1/2}$, at which the low energy edge has decreased to its half height, is no good measure for the film thickness: It depends on the roughness of the substrate. The high energy edge and the plateau are only slightly affected by substrate roughness and decrease only little at large roughnesses due to shadowing: The backscattered particles do not reach the detector any more, because the exit angle β points inside the layer. For $w = \infty$ the local tilt angles are equipartitioned, and the corresponding spectrum represents the case of maximum roughness.

A measured spectrum for 2.5 MeV protons backscattered from a tungsten layer on top

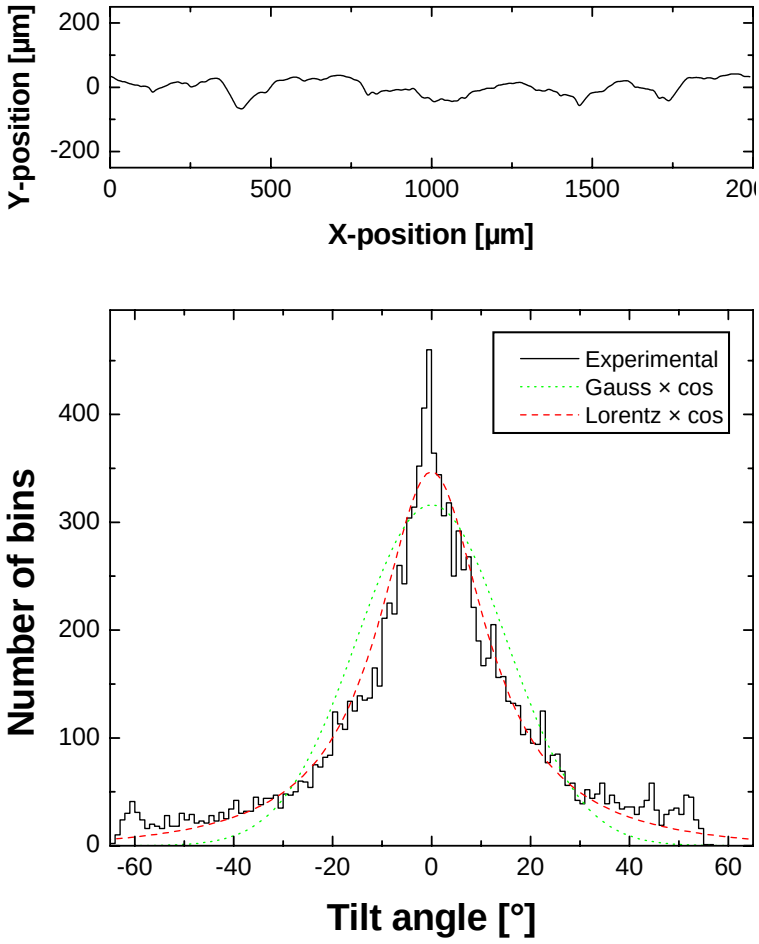

Figure 4.24: Top: Line profile of a carbon fibre composite (CFC) surface. Bottom: Histogram of the local tilt angle distribution of the CFC surface. Solid line: Experimental data; Dashed line: Lorentz distribution times cosine of the tilt angle; Dotted line: Gaussian distribution times cosine of the tilt angle.

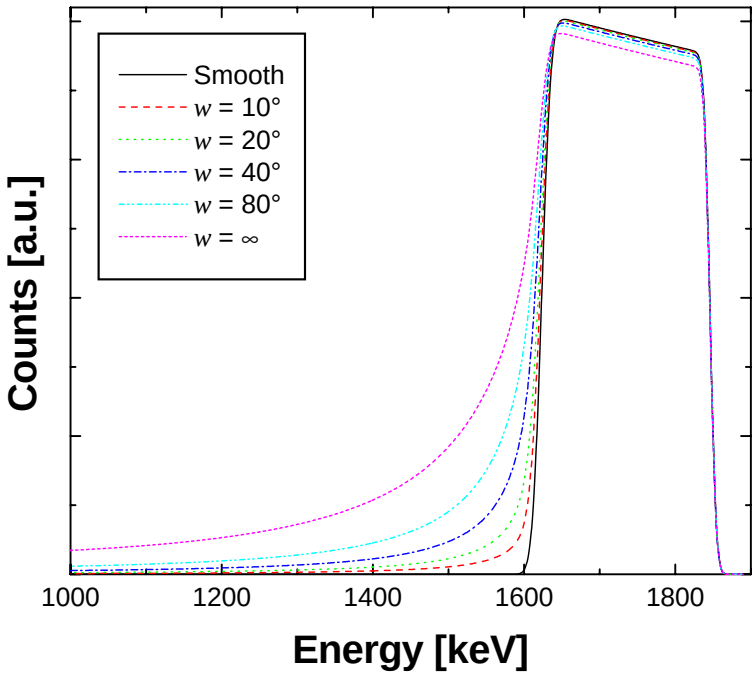

Figure 4.25: Calculated energy spectra for 2 MeV ^{4}He backscattered from a gold layer with thickness 1×10^{18} Au-atoms/cm^2 on a rough substrate with different roughnesses. The roughness is described by a Lorentz distribution of tilt angles with FWHM w. $w = \infty$ is an equipartition of tilt angles. Incident angle $\alpha = 0°$, scattering angle 165°.

of a rough carbon substrate is shown in Fig. 4.26. The non-Rutherford elastic scattering data from [69] were used for the C(p,p)C cross section. The substrate is the same CFC material, which surface is shown in Fig. 4.24. The mean W layer thickness was about 3.5 μm, while the standard deviation of the substrate roughness was about 8.2 μm, i.e. the substrate roughness was considerably larger than the thickness of the W layer. The dotted line in Fig. 4.26 is the calculated spectrum for a smooth W layer on a smooth carbon substrate. Plural scattering in the W layer was included in dual scattering approximation, see section 4.8.3. Plural scattering results for example in the small background visible between the carbon and tungsten signals in channels 500–650. This spectrum has only minor resemblance with the experimental curve, and requires a slightly thicker W layer (3.6 μm) for best fit. The dashed line is calculated for a rough W layer, characterized by a Gamma-distribution of layer thicknesses with a mean thickness of 3.5 μm and standard deviation $\sigma = 0.3$ μm on a rough carbon substrate, characterized by a Lorentz distribution of tilt angles with FWHM = 20°. The roughnesses of the layer and the substrate are assumed to be independent, and plural scattering is not taken into account. The W peak (channels > 650) is already well described, but the low energy tail below the peak is underestimated. The solid line uses the same roughness parameters, but takes additionally plural scattering into account. Now the whole experimental spectrum is reproduced well. Compared to the smooth layer the contribution of plural scattering has increased strongly, which is due to an enhancement of plural scattering at inclined incidence. The height and shape of the low energy tail below the W-peak in channels < 650 are determined by the wings of the tilt angle distribution with inclination angles $> \pm 45°$. The observed tilt angle distribution, see Fig. 4.24, is best described by a FWHM of 26.6°, while the best fit to the measured spectrum yields a FWHM of about 20°. It is assumed that inaccuracies in the measurement of the tilt angle distribution at high inclinations due to the apex angle of the profiler tip and the constant step width, together with uncertainties in the calculation of the plural scattering background, are the reason for this small discrepancy. Additionally it should be kept in mind that the used model of inclined line segments, see Fig. 4.17(b), is only an approximation to physical reality, and the real surface has an additional fine structure.

The influence of the different roughnesses on the shape of the RBS spectrum is shown in more detail in Fig. 4.27. The experimental data (black dots) and the solid line in the top and bottom figures are the same as in Fig. 4.26. The substrate roughness is kept constant in Fig. 4.27 (top), and the roughness of the W layer is varied from smooth to 0.6 μm. The roughness of the W-layer influences mainly the low energy edge of the W peak, best fit is obtained for $\sigma = 0.3$ μm. The bottom part shows the influence of the carbon substrate roughness for constant W-layer roughness. Substrate roughness influences mainly the low energy tail below the W-peak, while the low energy edge of the W-peak is less affected by substrate roughness. Best fit is obtained for about 20° FWHM. Due to the different effects of the two roughnesses on the shape of RBS spectra the two roughnesses can be easily distinguished.

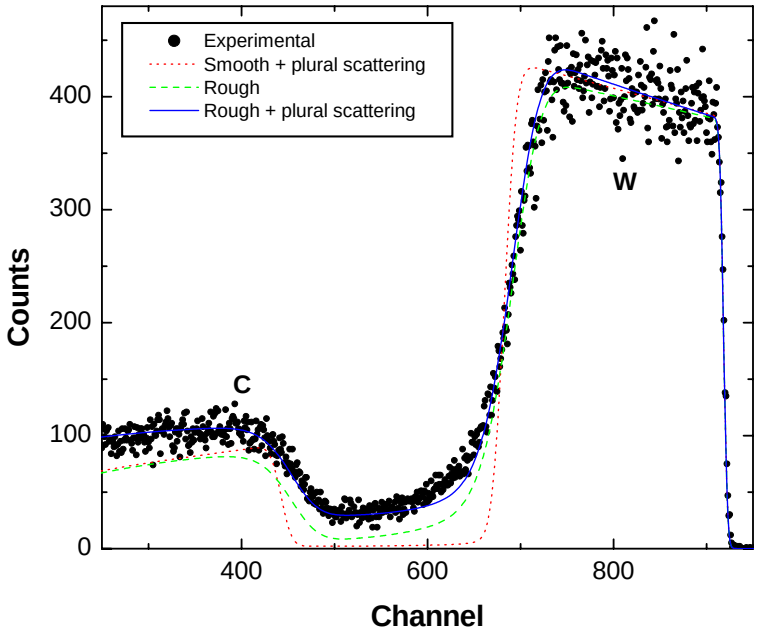

Figure 4.26: 2.5 MeV protons backscattered from 3.5 μm W on a rough carbon substrate, scattering angle 165°. Dots: Experimental data; Dotted line: Calculated spectrum for a smooth W layer (3.6 μm) on a smooth C substrate including plural scattering; Dashed line: Calculated spectrum for a rough W layer (3.5 μm, $\sigma = 0.30$ μm) on a rough substrate (FWHM 20°); Solid line: As dashed line, but including plural scattering.

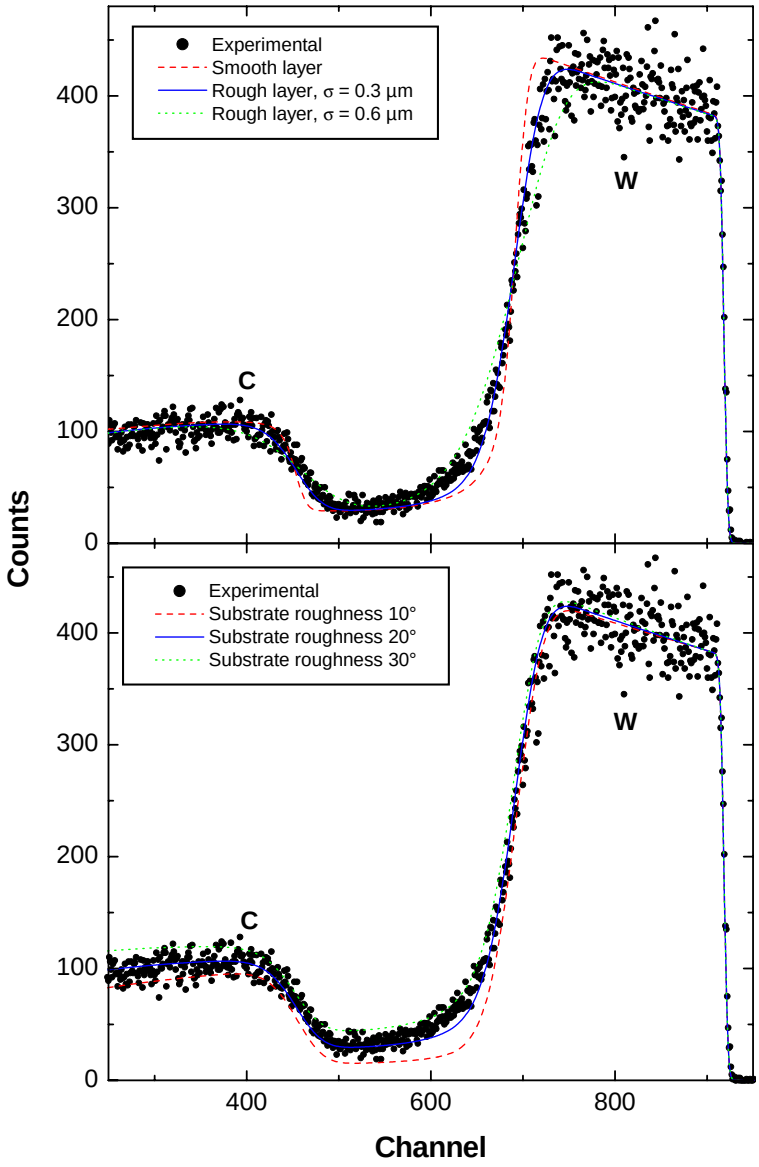

Figure 4.27: Same experimental data as in Fig. 4.26, compared to simulation calculations with different roughness parameters. Top: Calculations for a rough carbon substrate (FWHM 20°) and different W-layer roughnesses, characterized by a Gamma-distribution with standard deviation σ; Bottom: Calculations for a rough W layer ($\sigma = 0.3$ μm) and different substrate roughnesses, characterized by a Lorentz-distribution of tilt angles with different FWHM's. Mean W-layer thickness 3.5 μm, plural scattering included.

Chapter 5

Examples

This chapter gives several examples for the abilities of SIMNRA.

All backscattering spectra were measured at the IPP Garching at a scattering angle $\theta = 165°$. The solid angle of the detector was 1.08×10^{-3} sr. A standard surface barrier detector with a nominal energy resolution of 15 keV FWHM was used.

5.1 RBS: Rutherford cross-sections

Fig. 5.1 shows the measured and simulated spectra for 1.0 MeV ^{4}He incident ions on a gold layer with a thickness of about 100 nm on top of silicon. The simulated spectrum fits the measured data very well. The low background between the Si edge and the low energy Au edge is due to plural scattering (this means the backscattered particles have suffered more than one scattering event with large scattering angle) [47, 48, 49], which was not simulated for this example. The deviation between experiment and simulation at low energies in the Si spectrum is due to the same reason.

Fig. 5.2 compares simulated spectra with single and dual scattering for 500 keV ^{4}He ions incident on a 100 nm gold layer on top of silicon with experimental data. At this low energy plural scattering is important. With the inclusion of dual scattering the experimental results are much better approximated. Dual scattering gives the background between the low energy edge of Au and the Si edge, and the steeper increase of the gold spectrum is better described. The results with dual scattering are slightly lower than the experimental results. This is due to trajectories with more than two scattering events, which are not calculated.

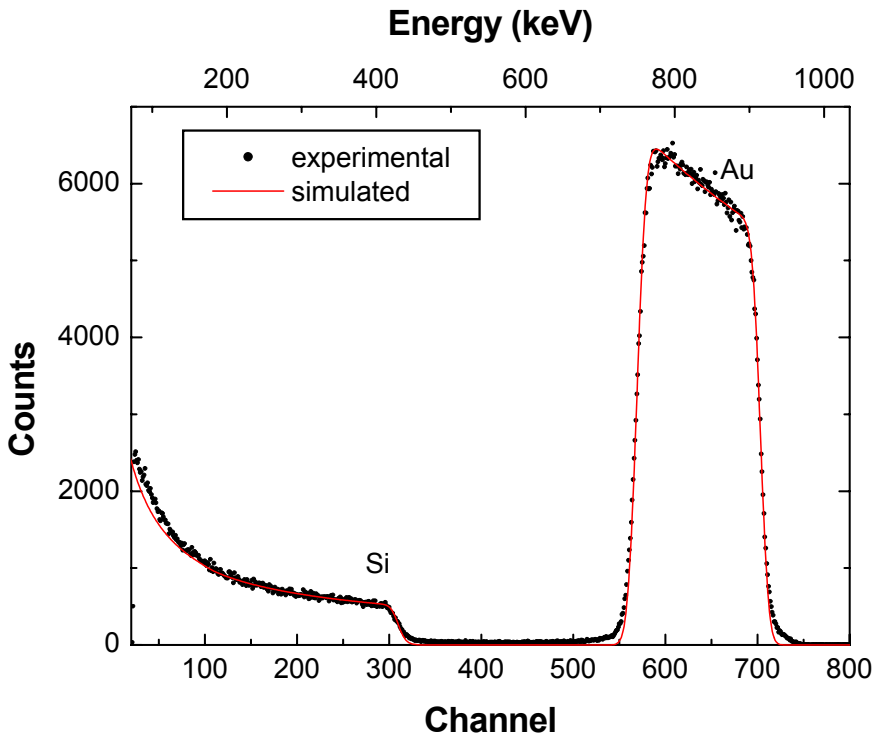

Figure 5.1: 1000 keV ^{4}He incident on Au on top of silicon, $\theta = 165°$.

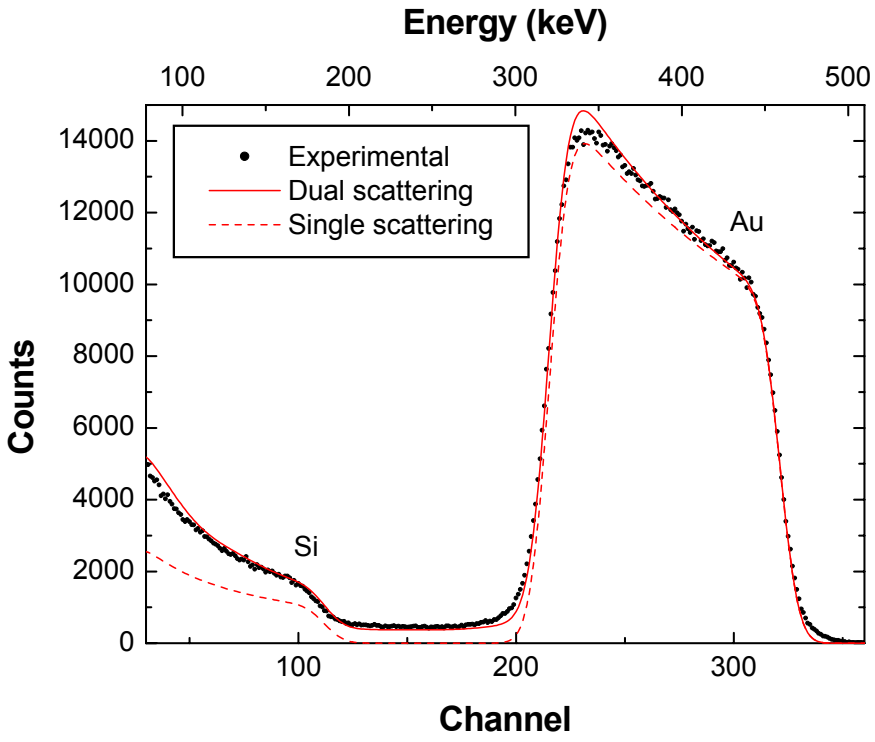

Figure 5.2: 500 keV ^{4}He ions incident on 100 nm Au on top of Si, scattering angle 165°. Circles: experimental data points, dashed line: simulation with one scattering event, solid line: simulation with two scattering events.

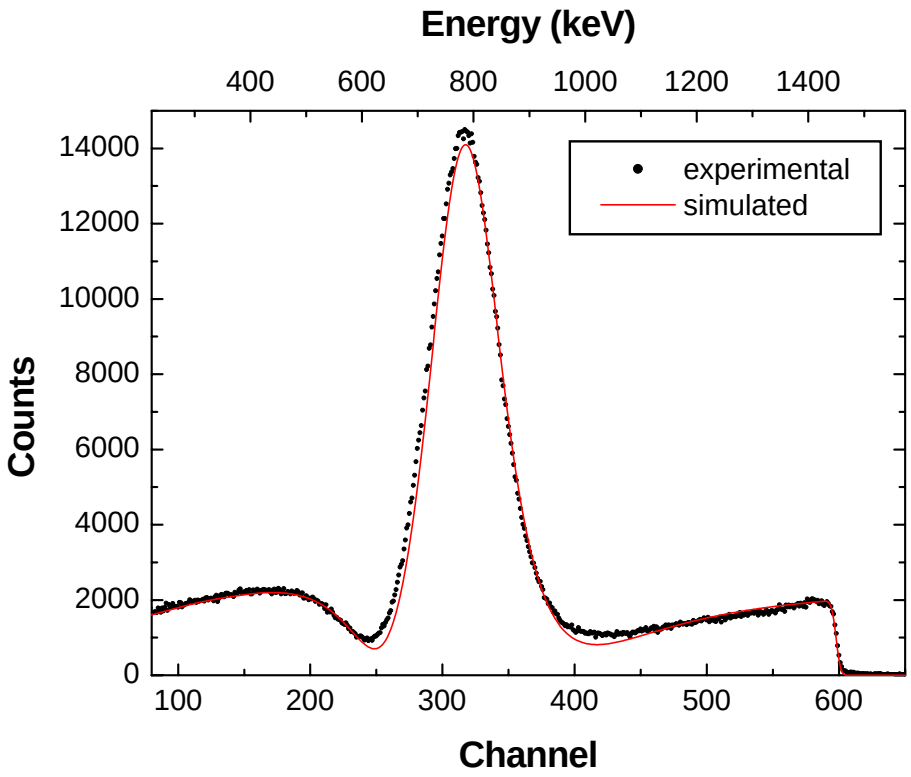

Figure 5.3: 2000 keV protons on carbon (HOPG), $\alpha = 5°$, $\theta = 165°$.

5.2 RBS: Non-Rutherford cross-sections

Fig. 5.3 shows the measured and simulated spectra for 2.0 MeV protons incident on highly oriented pyrolytic graphite (HOPG). To avoid channelling the incident angle α was 5°. The cross-section is non-Rutherford, and the cross-section data of Amirikas *et. al.* [69] were used for the simulation. The pronounced peak in the spectrum is due to the resonance in the ^{12}C(p,p)^{12}C cross-section at 1732 keV. The measured and simulated spectra agree very well.

Fig. 5.4 shows the measured and simulated spectra for 2.0 MeV protons incident on silicon. To avoid channelling the incident angle α was 5°. The cross-section is non-Rutherford, and the cross-section data of Vorona *et. al.* [70] were used for the simulation. As in the case of carbon the measured and simulated spectra agree very well. The structures in the simulated spectrum between channel 500 and 700 are due to the experimentally determined cross-section data, which contain these structures.

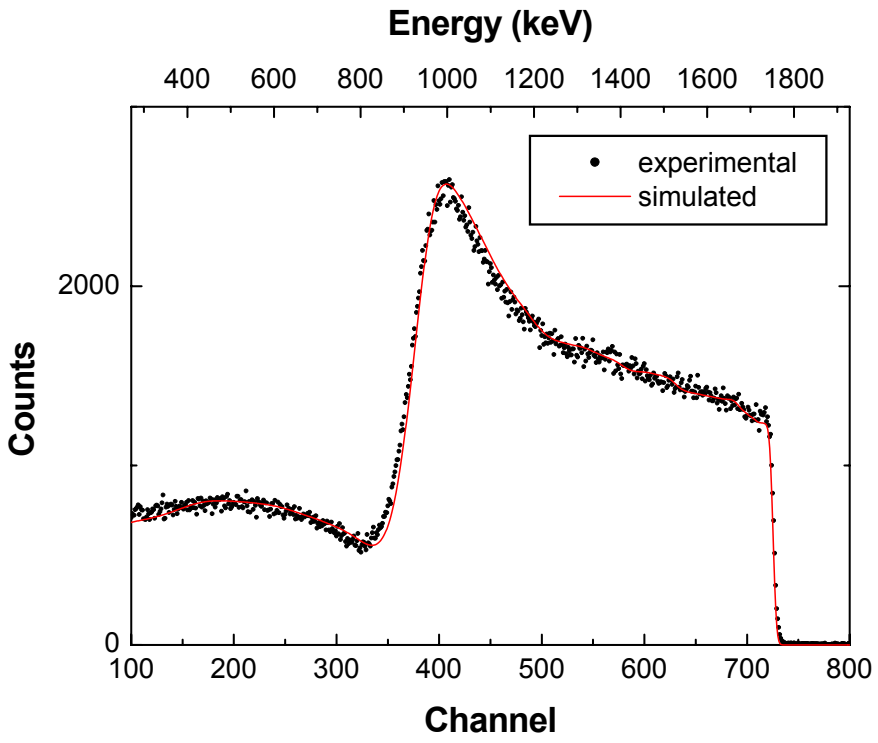

Figure 5.4: 2000 keV protons backscattered from silicon, $\alpha = 5°$, $\theta = 165°$.

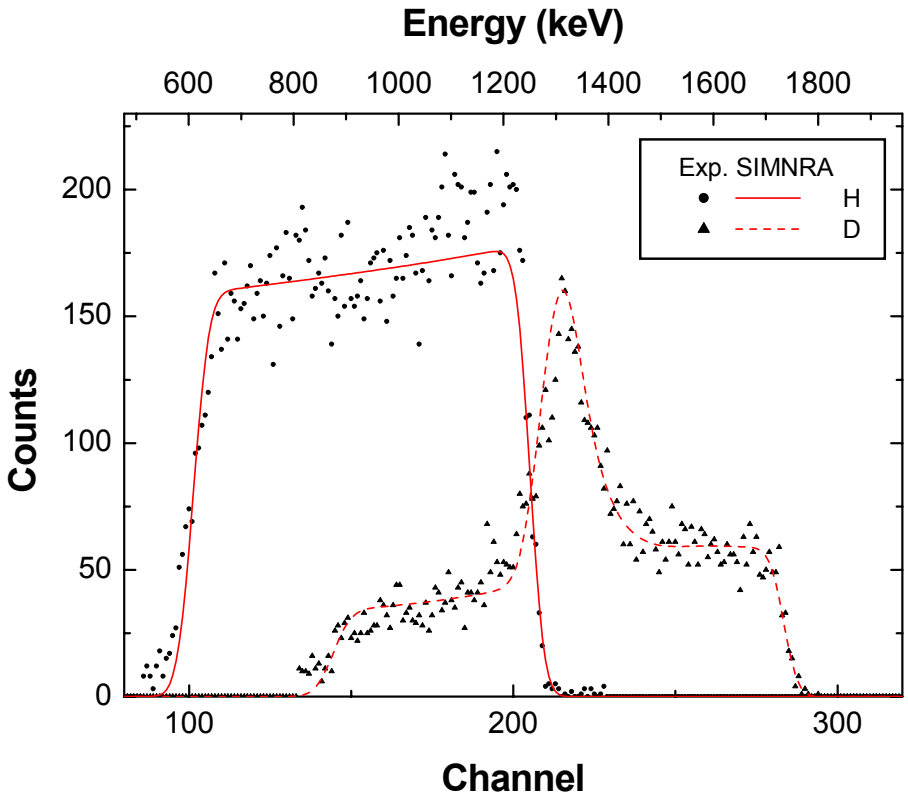

Figure 5.5: ERDA with 2.6 MeV ^{4}He ions incident on a soft amorphous hydrocarbon layer (a:C-H layer) containing both H and D. The recoiling H and D atoms were separated with a ΔE-E telescope detector, the backscattered ^{4}He ions are not shown. $\alpha = \beta = 75°$, $\theta = 30°$.

5.3 ERDA: Non-Rutherford cross-sections

Fig 5.5 shows the measured and simulated spectra for ERDA with 2.6 MeV incident ^{4}He ions on a soft amorphous hydrocarbon layer (a:C-H layer) containing both H and D. The recoiling H and D atoms were separated with a ΔE-E telescope detector [71]. Both recoil cross-sections are non-Rutherford. The cross-section data of Baglin *et al.* [72] for H(^{4}He,H)^{4}He and of Besenbacher *et al.* [73] for D(^{4}He,D)^{4}He were used for the simulation. The peak in the deuterium spectrum is due to a resonance at a ^{4}He energy of 2130 keV. The measured and simulated data agree very well.

Chapter 6

Acknowledgements

Many cross-section data files included with SIMNRA have been taken from SigmaBase (http://ibaserver.physics.isu.edu/sigmabase), which is maintained by I. Vickridge. See the file http://ibaserver.physics.isu.edu/sigmabase/newuser.html for more information about SigmaBase.

The stopping power data and subroutines for Ziegler-Biersack stopping have been taken from Ziegler's SRIM 97 program, but were translated from BASIC to PASCAL.

The routines for reading RUMP's RBS file format were obtained from Peter Revesz, Cornell University, USA. They were translated from C to PASCAL.

The graphics subsystem for SIMNRA versions prior to 4.5 was developed by Achim von Keudell, Max-Planck-Institut für Plasmaphysik, Garching, Germany.

Valuable input and many bug reports were obtained from Joachim Roth and Hans Maier (Max-Planck-Institut für Plasmaphysik, Garching, Germany), Jörg Röhrich and Swen Lindner (Hahn Meitner Institut, Berlin, Germany), Günther Dollinger (Technische Universität, München, Germany), and Peter Revesz (Cornell University, USA).

Many additional cross section data were obtained from Iva Bogdanović Radović (Rudjer Bošković Institute, Zagreb, Croatia), B. Diaz-Herrera (Max-Planck-Institut für Plasmaphysik, Garching, Germany), and L.Y. Kim (Max-Planck-Institut für Plasmaphysik, Garching, Germany).

SIMNRA was developed at the Max-Planck-Institut für Plasmaphysik, Garching, Germany.

The R33 file format and the R33Manager were developed by Ian Vickridge, Université Paris, France. The text of Appendix was written by I. Vickridge and has been taken from the file R33Help.htm.

Appendix A

OLE automation reference

This section describes OLE automation support in SIMNRA in full detail. A short overview of the OLE objects and methods can be found in section 3.16.2, some sample programs are shown in section A.10. The properties and methods are grouped by object.

A.1 Data types

SIMNRA is written in Borland Delphi and uses only automation compatible data types. The data types used by Delphi, the corresponding types in Microsoft's Interface Definition Language IDL, and the corresponding types used in Variants are summarized below.

Delphi type	IDL type	Variant type	Description
Boolean	VARIANT_BOOL	VT_BOOL	True = -1, False = 0
Double	double	VT_R8	8-byte real
Integer	long	VT_I4	4-byte signed integer
WideString	BSTR	VT_BSTR	binary string

A.2 Simnra.App

The `Simnra.App` object represents the application itself.

A.2.1 Properties

Active

```
[Get] Property Active :  Boolean;
```

Description

Specifies whether SIMNRA is active and has focus. Active is True while SIMNRA is active and False if it is not. SIMNRA is active if it has focus, and becomes inactive when a window from a different application is about to become activated. Active is readonly.

Related Properties and Methods

App.BringToFront 113
App.Minimize 116
App.Restore 118

DeleteSpectrumOnCalculate

```
[Get/Set] Property DeleteSpectrumOnCalculate :  Boolean;
```

Default Value

true

Description

If `DeleteSpectrumOnCalculate` is `true`, the current simulated spectrum is deleted before a new spectrum is calculated. If `false`, the current simulated spectrum is conserved, and the new spectrum is added to the current one. Default is `true`.
Example:

```
'  Spectrum for scattering angle 160°
Setup.Theta = 160
App.CalculateSpectrum

' Spectrum for scattering angle 170° is now added
' to the previous spectrum
App.DeleteSpectrumOnCalculate = false
Setup.Theta = 170
App.CalculateSpectrum
```

Related Properties and Methods

App.CalculateSpectrum 114

LastMessage

```
[Get] Property LastMessage :  WideString;
```

Description

Text of the last error message or warning. `LastMessage` is retained until a new error or warning is issued or it is read with `LastMessage`. `LastMessage` is readonly. See section A.9 for more details about error handling.

Related Properties and Methods

App.ShowMessages 113

ShowMessages

```
[Get/Set] Property ShowMessages :  Boolean;
```

Default Value

false

Description

Specifies if error messages are shown or suppressed. If `ShowMessages` is `true`, program execution is stopped if an error is encountered, and a message box with an error description or warning is shown. Program execution is resumed after pressing the `OK` button. If `ShowMessages` is `false`, the message box is suppressed and program execution continues. The routine which produced the error, like `App.Open` or `App.CalculateSpectrum`, returns an error flag. The text of the error message can be retrieved with `LastMessage`. See section A.9 for more details about error handling.

Related Properties and Methods

App.LastMessage 113

A.2.2 Methods

BringToFront

```
Procedure BringToFront;
```

Description

Brings SIMNRA to the front above all other applications.

Parameters

None

Return Value

None

Related Properties and Methods

App.Active 111
App.Minimize 116
App.Restore 118

CalculateSpectrum

```
Function CalculateSpectrum :  Boolean;
```

Description

Calculates a simulated spectrum.

Parameters

None

Return Value

Returns `true` if the calculation succeeded.

Related Properties and Methods

App.DeleteSpectrumOnCalculate 112

CopySpectrumData

```
Procedure CopySpectrumData;
```

Description

Copies experimental and simulated spectra in ASCII format to the Windows clipboard. See `Edit: Copy Data` in section 3.3 for a description of the format.

Parameters

None

Return Value

None

Related Properties and Methods

App.WriteSpectrumData 119

FitSpectrum

```
Function FitSpectrum :  Boolean;
```

Description

Fits a spectrum. You have to adjust the fit parameters in the `Simnra.Fit` 133 object first, before the fit can be performed with `FitSpectrum`.

Parameters

None

Return Value

Returns `true` if the fit succeeded.

Hide

```
Procedure Hide;
```

Description

Hides SIMNRA. The program is still running, but not visible.

Parameters

None

Return Value

None

Related Properties and Methods

App.Minimize 116
App.Show 119

Maximize

```
Procedure Maximize;
```

Description

Maximizes SIMNRA to fill the whole screen. SIMNRA must be visible, i.e. not minimized or hidden, otherwise `Maximize` has no effect.

Parameters

None

Return Value

None

Related Properties and Methods

App.Minimize 116

Minimize

```
Procedure Minimize;
```

Description

Minimizes SIMNRA to the Windows task bar.

Parameters

None

Return Value

None

Related Properties and Methods

App.Maximize 116
App.Restore 118
App.Active 111
App.BringToFront 113

Open

```
Function Open(FileName :  WideString) :  Boolean;
```

Description

Opens a NRA-file.

Parameters

`FileName`	The name of the NRA-file including path.

Return Value

Returns `true` if the file was opened successfully.

Related Properties and Methods

App.SaveAs 118

ReadSpectrumData

```
Function ReadSpectrumData(FileName :  WideString; Format :
Integer) :  Boolean;
```

Description

Imports experimental data in different formats.

Parameters

`FileName`	The name of the spectrum data file including path.
`Format`	Format of the spectrum data file. Allowed values for `Format` are: 1: Data in ASCII file format 2: Data in Canberra's CAM file format 4: Data in RUMP's RBS file format 5: Data in user defined format. Requires a used supplied dll. See section 3.13 for more details.

Return Value

Returns `true` if the file was imported successfully.

Related Properties and Methods

App.WriteSpectrumData 119

Restore

```
Procedure Restore;
```

Description

Restores the minimized application to its normal size.

Parameters

None

Return Value

None

Related Properties and Methods

App.Active 111
App.BringToFront 113
App.Minimize 116

SaveAs

```
Function SaveAs(FileName :  WideString) :  Boolean;
```

Description

Save a NRA-file.

Parameters

`FileName`	The name of the NRA-file including path. If the file already exists it will be overwritten.

Return Value

Returns `true` if the file was saved successfully.

Related Properties and Methods

App.Open 117

Show

```
Procedure Show;
```

Description

Shows SIMNRA, if it was hidden.

Parameters

None

Return Value

None

Related Properties and Methods

App.Hide 115

WriteSpectrumData

```
Function WriteSpectrumData(FileName :  WideString) :  Boolean;
```

Description

Writes all spectra (experimental, simulated) in ASCII-format to a file. See `File: Write Spectrum Data...` in section 3.2 for a description of the file format.

Parameters

`FileName`	The name of the data file including path. If the file already exists it will be overwritten.

Return Value

Returns `true` if the file was written successfully.

Related Properties and Methods

App.ReadSpectrumData 117
App.CopySpectrumData 114

A.3 Simnra.Setup

The `Simnra.Setup` object represents the experimental setup.

A.3.1 Properties

Alpha

```
[Get/Set] Property Alpha :  Double;
```

Description

Incident angle α [deg].

Related Properties and Methods

Setup.Beta 120
Setup.Theta 122

Beamspread

```
[Get/Set] Property Beamspread :  Double;
```

Description

Energy spread of incident beam [keV FWHM].

Related Properties and Methods

Setup.Energy 122

Beta

```
[Get/Set] Property Beta :  Double;
```

Description

Exit angle β [deg].

Related Properties and Methods

Setup.Alpha 120
Setup.Theta 122

CalibrationLinear

```
[Get/Set] Property CalibrationLinear :  Double;
```

Description

Linear calibration term B for energy calibration, see eq. 3.1 [keV/channel].

Related Properties and Methods

Setup.CalibrationOffset 121
Setup.CalibrationQuadratic 121

CalibrationOffset

```
[Get/Set] Property CalibrationOffset :  Double;
```

Description

Calibration offset A for energy calibration, see eq. 3.1 [keV].

Related Properties and Methods

Setup.CalibrationLinear 121
Setup.CalibrationQuadratic 121

CalibrationQuadratic

```
[Get/Set] Property CalibrationQuadratic :  Double;
```

Description

Quadratic calibration term C for energy calibration, see eq. 3.1 [keV/channel^2].

Related Properties and Methods

Setup.CalibrationLinear 121
Setup.CalibrationOffset 121

DetectorResolution

```
[Get/Set] Property DetectorResolution :  Double;
```

Description

Detector resolution [keV FWHM].

Energy

```
[Get/Set] Property Energy :  Double;
```

Description

Energy of incident ions [keV].

Related Properties and Methods

Setup.Beamspread 120

ParticlesSr

```
[Get/Set] Property ParticlesSr :  Double;
```

Description

Number of incident particles times solid angle [sr].

Theta

```
[Get/Set] Property Theta :  Double;
```

Description

Scattering angle θ [deg].

Related Properties and Methods

Setup.Alpha 120
Setup.Beta 120

A.4 Simnra.Calc

The `Simnra.Calc` object represents the parameters of the calculation.

A.4.1 Properties

AutoStepwidthIn

```
[Get/Set] Property AutoStepwidthIn :  Boolean;
```

Description

Specifies if automatic step width control for incident ions is used.

Related Properties and Methods

Calc.AutoStepwidthOut 123

AutoStepwidthOut

```
[Get/Set] Property AutoStepwidthOut :  Boolean;
```

Description

Specifies if automatic step width control for outgoing ions is used.

Related Properties and Methods

Calc.AutoStepwidthIn 123

---

dEin

```
[Get/Set] Property dEin :  Double;
```

Description

Stepwidth incident ions [keV].

Related Properties and Methods

Calc.dEout 124

---

dEout

```
[Get/Set] Property dEout :  Double;
```

Description

Stepwidth outgoing ions [keV].

Related Properties and Methods

Calc.dEin 123

DualScattering

```
[Get/Set] Property DualScattering :  Boolean;
```

Description

Specifies if dual scattering is calculated.

ElementSpectra

```
[Get/Set] Property ElementSpectra :  Boolean;
```

Description

Specifies if individual spectra for each element in the target are calculated.

Related Properties and Methods

Calc.IsotopeSpectra 125

EMin

```
[Get/Set] Property EMin :  Double;
```

Description

Cutoff energy [keV].

HighEnergyStopping

```
[Get/Set] Property HighEnergyStopping :  Boolean;
```

Description

Selects if high energy stopping power data are used or not. This switch is only used together with the stopping power data by Andersen-Ziegler and has no influence if Ziegler-Biersack stopping is selected. See section 3.4.3 for more details.

Related Properties and Methods

Calc.ZBStopping 126

Isotopes

```
[Get/Set] Property Isotopes :  Boolean;
```

Description

Specifies if isotopes are taken into account.

IsotopeSpectra

```
[Get/Set] Property IsotopeSpectra :  Boolean;
```

Description

Specifies if individual spectra for each isotope in the target are calculated.

Related Properties and Methods

Calc.ElementSpectra 124

MultipleScattering

```
[Get/Set] Property MultipleScattering :  Boolean;
```

Description

Specifies if multiple scattering is calculated.

NumberOfAngleVariations

```
[Get/Set] Property NumberOfAngleVariations :  Integer;
```

Description

Number of angle steps in the calculation of rough substrates.

Related Properties and Methods

Calc.NumberOfDVariations 126

NumberOfDVariations

```
[Get/Set] Property NumberOfDVariations :  Integer;
```

Description

Number of thickness steps in the calculation of rough layers.

Related Properties and Methods

Calc.NumberOfAngleVariations 126

Straggling

```
[Get/Set] Property Straggling :  Boolean;
```

Description

Specifies if energy loss and geometrical straggling are taken into account.

ZBStopping

```
[Get/Set] Property ZBStopping :  Boolean;
```

Description

Selects Ziegler-Biersack or Andersen-Ziegler stopping. If `ZBStopping` is `true`, Ziegler-Biersack stopping is used, while Andersen-Ziegler is selected if `ZBStopping` is set to `false`. See section 3.4.3 for more details about stopping power data.

Related Properties and Methods

A.5 Simnra.Target

The `Simnra.Target` object represents the target with all layers and elements.

A.5.1 Properties

ElementConcentration

```
[Get/Set] Property ElementConcentration[lay, el :  Integer] :
Double;
```

Description

Concentration of element number `el` in layer number `lay`. The sum of concentrations of all elements in a layer must be equal to 1. This is not checked by SIMNRA. If `ElementConcentration` is changed, it is the responsibility of the programmer to assure that the sum of the concentrations is equal to 1.

Parameters

`lay`	Number of the layer, with $1 \leq$ `lay` $\leq$ `NumberOfLayers`.
`el`	Number of the element, with $1 \leq$ `el` $\leq$ `NumberOfElements[lay]`.

ElementName

```
[Get/Set] Property ElementName[lay, el :  Integer] :
WideString;
```

Description

Name of element number `el` in layer number `lay`. Returns `'XX'` if the element is unknown.
Attention: Do not use `ElementName` to add new elements to the target: The element should already be present in at least one layer. If you add new elements, they will have undefined cross sections.

Parameters

`lay`	Number of the layer, with $1 \leq$ `lay` $\leq$ `NumberOfLayers`.

`el`	Number of the element, with $1 \leq$ `el` $\leq$ `NumberOfElements[lay]`.

HasLayerRoughness

```
[Get/Set] Property HasLayerRoughness[lay : Integer] : Boolean;
```

Description

Specifies if the layer number `lay` is rough or not. The FWHM of the roughness is specified by `Target.LayerRoughness`. If `HasLayerRoughness` is `false`, the layer is treated as smooth, and `Target.LayerRoughness` is ignored.

Parameters

`lay`	Number of the layer, with $1 \leq$ `lay` $\leq$ `NumberOfLayers`.

Related Properties and Methods

Target.LayerRougness 128

HasSubstrateRoughness

```
[Get/Set] Property HasSubstrateRoughness : Boolean;
```

Description

Specifies if the substrate is rough or not. The FWHM of the roughness is specified by `Target.SubstrateRoughness`. If `HasSubstrateRoughness` is `false`, the substrate is treated as smooth, and `Target.SubstrateRoughness` is ignored.

Related Properties and Methods

Target.SubstrateRougness 130

LayerRoughness

```
[Get/Set] Property LayerRoughness[lay : Integer] : Double;
```

Description

FWHM of the roughness of layer number `lay` [10^{15} atoms/cm^2]. `Target.HasLayerRoughness[lay]` must be `true`, otherwise `LayerRoughness` has no effect.

Parameters

`lay`	Number of the layer, with $1 \leq$ `lay` $\leq$ `NumberOfLayers`.

Related Properties and Methods

Target.HasLayerRougness 128

LayerThickness

```
[Get/Set] Property LayerThickness[lay : Integer] : Double;
```

Description

Thickness of layer number `lay` [10^{15} atoms/cm^2].

Parameters

`lay`	Number of the layer, with $1 \leq$ `lay` $\leq$ `NumberOfLayers`.

NumberOfElements

```
[Get] Property NumberOfElements[lay : Integer] : Integer;
```

Description

Number of different elements in layer number `lay`. `NumberOfElements` is readonly.

Parameters

`lay`	Number of the layer, with $1 \leq$ `lay` $\leq$ `NumberOfLayers`.

NumberOfLayers

```
[Get] Property NumberOfLayers : Integer;
```

Description

Total number of layers in the target. `NumberOfLayers` is readonly.

SubstrateRoughness

```
[Get/Set] Property SubstrateRoughness :  Double;
```

Description

FWHM of the substrate roughness [deg]. `Target.HasSubstrateRoughness` must be `true`, otherwise `SubstrateRoughness` has no effect.

Related Properties and Methods

Target.HasSubstrateRougness 128

A.5.2 Methods

AddElement

```
Function AddElement(lay :  Integer):  Boolean;
```

Description

Adds an element to layer number `lay`. The element has no name and zero concentration. After adding the elements properties have to be set with `ElementName` and `ElementConcentration`.
Attention: Do not use `AddElement` to add new elements to the target. See `ElementName` for details.

Parameters

`lay`	Number of the layer, with $1 \leq$ `lay` $\leq$ `NumberOfLayers`.

Return Value

Returns `true` if the element was added successfully.

Related Properties and Methods

Target.AddLayer 131
Target.ElementConcentration 127
Target.ElementName 127

AddLayer

```
Function AddLayer :  Boolean;
```

Description

Adds a new layer. The layer is the last layer in the stack, has zero thickness and contains no elements. After adding a layer at least one element has to be added with `AddElement` and layer properties like thickness, roughness etc. have to be set.

Parameters

None

Return Value

Returns `true` if the layer was added successfully.

Related Properties and Methods

Target.AddElement 130
Target.InsertLayer 132

DeleteElement

```
Function DeleteElement(lay, el :  Integer) :  Boolean;
```

Description

Deletes element number `el` in layer number `lay`.

Parameters

`lay`	Number of the layer, with $1 \leq$ `lay` $\leq$ `NumberOfLayers`.
`el`	Number of the element, with $1 \leq$ `el` $\leq$ `NumberOfElements[lay]`.

Return Value

Returns `true` if the element was deleted successfully.

Related Properties and Methods

Target.DeleteLayer 132

DeleteLayer

```
Function DeleteLayer(lay :  Integer) :  Boolean;
```

Description

Deletes layer number `lay`.

Parameters

`lay`	Number of the layer to delete, with $1 \leq$ `lay` $\leq$ `NumberOfLayers`.

Return Value

Returns `true` if the layer was deleted successfully.

Related Properties and Methods

Target.DeleteElement 131

InsertLayer

```
Function InsertLayer(lay :  Integer) :  Boolean;
```

Description

Inserts a new layer in front of layer number `lay`. The layer has zero thickness and contains no elements. After inserting a layer at least one element has to be added with `AddElement` and layer properties like thickness, roughness etc. have to be set.

Parameters

`lay`	Number of the layer, with $1 \leq$ `lay` $\leq$ `NumberOfLayers`.

Return Value

Returns `true` if the layer was inserted successfully.

Related Properties and Methods

Target.AddLayer 131

A.6 Simnra.Fit

The `Simnra.Fit` object represents the fit parameters, i.e. what to fit, number of fit regions, maximum number of iterations etc. You have to adjust the fit parameters in the `Simnra.Fit` object first, before the fit can be performed with the `App.FitSpectrum` 115 method.

A.6.1 Properties

Accuracy

```
[Get/Set] Property Accuracy :  Double;
```

Default Value

0.01

Description

Desired accuracy of the fit, see section 3.7.1. Fitting will be performed until the desired accuracy is obtained or the maximum number of iterations is reached.

Related Properties and Methods

Fit.MaxIterations 135

EnergyCalibration

```
[Get/Set] Property EnergyCalibration :  Boolean;
```

Default Value

false

Description

Specifies if the energy calibration (offset and linear term) is fitted. The energy calibration is fitted, if `EnergyCalibration` is `true`.

LayerComposition

```
[Get/Set] Property LayerComposition :  Boolean;
```

Default Value

false

Description

Specifies if the composition of a target layer is fitted. The number of the layer is specified by the `LayerNr` property. The composition of layer number `LayerNr` is fitted, if `LayerComposition` is `true`. Only one layer can be fitted at the same time.

Related Properties and Methods

Fit.LayerNr 134
Fit.LayerThickness 134

LayerNr

```
[Get/Set] Property LayerNr :  Integer;
```

Default Value

1

Description

Specifies the number of the target layer, which thickness or composition is fitted. Only one layer can be fitted at the same time. `Fit.LayerComposition` and/or `Fit.LayerThickness` must be `true`, otherwise `layerNr` has no effect.

Related Properties and Methods

Fit.LayerComposition 134
Fit.LayerThickness 134

LayerThickness

```
[Get/Set] Property LayerThickness :  Boolean;
```

Default Value

false

Description

Specifies if the thickness of a target layer is fitted. The number of the layer is specified by the `LayerNr` property. The thickness of layer number `LayerNr` is fitted, if `LayerThickness` is `true`. Only one layer can be fitted at the same time.

Related Properties and Methods

Fit.LayerNr 134
Fit.LayerComposition 134

MaxIterations

```
[Get/Set] Property MaxIterations :  Integer;
```

Default Value

20

Description

Maximum number of fit iterations. Fitting will be performed until the desired accuracy is obtained or the maximum number of iterations is reached.

Related Properties and Methods

Fit.Accuracy 133

NumberOfRegions

```
[Get/Set] Property NumberOfRegions :  Integer;
```

Default Value

1

Description

Number of different regions where χ^2 is calculated, see section 3.7.1. At least one region must exist, and the regions should not overlap. The lower and upper channels of the regions are specified by the `Fit.RegionMinChannel` and `Fit.RegionMaxChannel` properties.

Related Properties and Methods

Fit.RegionMaxChannel 136
Fit.RegionMinChannel 136

ParticlesSr

```
[Get/Set] Property ParticlesSr :  Boolean;
```

Default Value

false

Description

Specifies if the number of incident particles times solid angle is fitted. The number of incident particles times solid angle is fitted, if `ParticlesSr` is `true`.

RegionMaxChannel

```
[Get/Set] Property RegionMaxChannel[reg :  Integer] :  Integer;
```

Default Value

8192

Description

Upper channel of fit region number `reg`.

Related Properties and Methods

Fit.NumberOfRegions 135
Fit.RegionMinChannel 136

RegionMinChannel

```
[Get/Set] Property RegionMinChannel[reg :  Integer] :  Integer;
```

Default Value

1

Description

Lower channel of fit region number `reg`.

Related Properties and Methods

Fit.NumberOfRegions 135
Fit.RegionMaxChannel 136

A.6.2 Methods

Chi2

```
Function Chi2 :  Double;
```

Description

Quadratic deviation χ^2 between the simulated and measured data points, see Section 3.7.1. χ^2 is weighted with the statistical error of the experimental data. χ^2 is calculated only in the fit regions defined by `NumberOfRegions`, `RegionMaxChannel` and `RegionMinChannel`. `Chi2` can be used to develop your own fit algorithms.

Parameters

None

Return Value

Returns χ^2.

Related Properties and Methods

Fit.NumberOfRegion 135
Fit.RegionMaxChannel 136
Fit.RegionMinChannel 136

A.7 Simnra.Spectrum

The `Simnra.Spectrum` object represents experimental and simulated spectra, and allows to change plot parameters.

A.7.1 Input parameter

The properties and methods of `Simnra.Spectrum` require the input parameter `spID`, which specifies if the experimental or simulated spectrum is accessed. The possible values for `spID` are:

spID	Selected spectrum
1	Experimental data
2	Simulated data

Other values are not allowed.

A.7.2 Properties

AutoScale

```
[Get/Set] Property AutoScale :  Boolean;
```

Default Value

true

Description

If `AutoScale` is `true` the plot is scaled automatically, if experimental data are imported or a new calculation is performed. If `false`, the axis scales remain fixed.

BottomAxisMax

```
[Get/Set] Property BottomAxisMax :  Double;
```

Description

Bottom axis maximum.

Related Properties and Methods

BottomAxisMin 138

BottomAxisMin

```
[Get/Set] Property BottomAxisMin :  Double;
```

Description

Bottom axis minimum.

Related Properties and Methods

BottomAxisMax 138

LeftAxisMax

```
[Get/Set] Property LeftAxisMax :  Double;
```

Description

Left axis maximum.

Related Properties and Methods

LeftAxisMin 139

LeftAxisMin

```
[Get/Set] Property LeftAxisMin :  Double;
```

Description

Left axis minimum.

Related Properties and Methods

LeftAxisMax 139

NumberOfChannels

```
[Get] Property NumberOfChannels[spID : Integer] :  Integer;
```

Description

Number of channels in the experimental or simulated spectrum. `NumberOfChannels` is readonly.

Related Properties and Methods

spID 137

A.7.3 Methods

Data

```
Function Data(spID, chan :  Integer) :  Double;
```

Description

Value of experimental or simulated data in channel `chan`.

Parameters

`spID`	Selects the experimental or simulated spectrum.
`chan`	Channel number, with $0 \leq$ `chan` $\leq$ `NumberOfChannels`.

Return Value

Returns the value in channel `chan`.

Related Properties and Methods

spID 137

Integrate

```
Function Integrate(spID, lowChannel, upChannel :  Integer) :
Double;
```

Description

Sum of counts of the experimental or simulated spectrum in the range from `lowChannel` to `upChannel`.

Parameters

`spID`	Selects the experimental or simulated spectrum.
`lowChannel`	Lower channel, with $0 \leq$ `lowChannel` $\leq$ `NumberOfChannels`.
`upChannel`	Upper channel, with $0 \leq$ `upChannel` $\leq$ `NumberOfChannels`.

Return Value

Returns the sum of counts.

Related Properties and Methods

spID 137

A.8 Simnra.Stopping

The `Simnra.Stopping` object allows to calculate stopping powers, energy losses and energy loss straggling in elements, target and foil layers.

A.8.1 Input parameter

The methods of `Simnra.Stopping` require the input parameter `TargetID`, which specifies if a layer is in the target or foil. The possible values for `TargetID` are:

`TargetID`	
1	Target
2	Foil

Other values are not allowed.

A.8.2 Methods

EnergylossInLayer

```
Function EnergylossInLayer(Z1 :  Integer; M1 :  Double; E :
Double; TargetID : Integer; lay :  Integer) :  Double;
```

Description

Energy loss of an ion `Z1` in a target or foil layer. The layer is traversed perpendicularly, incident angle α and exit angle β are ignored. The stopping power model is selected with `Calc.ZBStopping` (p. 126) and `Calc.HighEnergyStopping` (p. 125), and may be additionally modified by a correction factor to the stopping power, see Section 3.5. The accuracy of the energy loss calculation is influenced by the settings of `Calc.AutoStepwidthOut` (p. 123) and `Calc.dEOut` (p. 124).

Parameters

`Z1`	Nuclear charge of the ion.
`M1`	Mass of the ion [amu].

`E`	Incident energy [keV].
`TargetID`	Selects target or foil.
`lay`	Number of the target or foil layer.

Return Value

Returns the energy loss in the layer [keV].

Related Properties and Methods

TargetID 141
Stopping.StoppingInLayer 143

StoppingInElement

```
Function StoppingInElement(Z1 :  Integer; M1 :  Double; E :
Double; Z2 :  Integer) :  Double;
```

Description

Stopping power of an ion `Z1` in element `Z2`. The stopping power model is selected with `Calc.ZBStopping` (p. 126) and `Calc.HighEnergyStopping` (p. 125).

Parameters

`Z1`	Nuclear charge of the ion.
`M1`	Mass of the ion [amu].
`E`	Incident energy [keV].
`Z2`	Nuclear charge of the target element.

Return Value

Returns the stopping power in element `Z2` [keV/10^{15} atoms/cm^2].

Related Properties and Methods

Calc.ZBStopping 126
Calc.HighEnergyStopping 125

StoppingInLayer

```
Function StoppingInLayer(Z1 :  Integer; M1 :  Double; E :
Double; TargetID : Integer; lay :  Integer) :  Double;
```

Description

Stopping power of an ion `Z1` in a target or foil layer. The stopping power model is selected with `Calc.ZBStopping` (p. 126) and `Calc.HighEnergyStopping` (p. 125), and may be additionally modified by a correction factor to the stopping power, see Section 3.5.

Parameters

`Z1`	Nuclear charge of the ion.
`M1`	Mass of the ion [amu].
`E`	Incident energy [keV].
`TargetID`	Selects target or foil.
`lay`	Number of the target or foil layer.

Return Value

Returns the stopping power in the layer [keV/10^{15} atoms/cm^2].

Related Properties and Methods

TargetID 141
Stopping.EnergyLossInLayer 141

StragglingInLayer

```
Function StragglingInLayer(Z1 :  Integer; M1 :  Double; E :
Double; TargetID : Integer; lay :  Integer) :  Double;
```

Description

Energy loss straggling of an ion `Z1` in a target or foil layer. The layer is traversed perpendicularly, incident angle α and exit angle β are ignored. See `Stopping.EnergylossInLayer` for a listing of all switches, which influence the straggling calculation.

Parameters

`Z1`	Nuclear charge of the ion.
`M1`	Mass of the ion [amu].
`E`	Incident energy [keV].
`TargetID`	Selects target or foil.
`lay`	Number of the target or foil layer.

Return Value

Returns the full width at half maximum (FWHM) of the energy loss straggling in the layer [keV].

Related Properties and Methods

TargetID 141
Stopping.EnergylossInLayer 141

A.9 Error handling

If SIMNRA is run as stand alone application, i.e. not as OLE server, it reports errors by showing message boxes with error messages or warnings, and program execution is stopped until the `OK` button of the message box is pressed by the user. This behaviour is reasonable for an interactive application, but it is not wishful for an OLE server: The server is controlled by another application or script, and the display of a message box to a script is useless. Therefore, if SIMNRA is running as server, it handles errors in a different

way: Message boxes are suppressed and program execution continues, even if an error is encountered. The error is reported by an error flag as return value of the routine which produced it. The text of the last error message can be retrieved with `App.LastMessage`.

This behaviour can be changed by setting `App.ShowMessages = true`: In this case error messages will be shown as message boxes, and program execution is stopped until the `OK` button of the box is pressed. SIMNRA is able to detect if it is running as stand alone application or as server, and `App.ShowMessages` is set to `false` automatically, if invoked as server.

The following code in Visual Basic Script shows the use of the error handling routines:

```
' Create the application object
Set App = CreateObject("Simnra.App")

' Wait 1000 ms: May be necessary for the server to start
WScript.Sleep 1000

' Open a NRA-file
Success = App.Open("c:\temp\test.nra")

' Some error reported by App.Open: Display last error message and exit
If Not Success Then
WScript.Echo App.LastMessage
Exit
End If

' Calculate a spectrum
Success = App.CalculateSpectrum
```

A.10 Programming examples

Sample program in Borland Delphi showing the use of the OLE automation objects.

```
Var App : Variant;
Result : Boolean;
Begin
{ Create the application object }
App := CreateOLEObject('Simnra.App');

{ Wait 1000 ms: May be necessary for the server to start }
Sleep(1000);

{ Open a NRA-file }
Result := App.Open('c:\temp\test.nra');

{ Calculate a spectrum }
Result := App.CalculateSpectrum;
```

```
{ Save the NRA-file }
Result := App.SaveAs('c:\temp\test.nra');
End;
```

Sample program in Visual Basic Script showing the use of the OLE automation objects.

```
' Create the application object
Set App = CreateObject("Simnra.App")

' Wait 1000 ms: May be necessary for the server to start
WScript.Sleep 1000

' Open a NRA-file
Result = App.Open("c:\temp\test.nra")

' Calculate a spectrum
Result = App.CalculateSpectrum

' Save the NRA-file
Result = App.SaveAs("c:\temp\test.nra")
```

Sample program in Visual Basic Script showing the use of the Fit object.

```
' Create the application object
Set App = CreateObject("Simnra.App")

' Create the fit object
Set Fit = CreateObject("Simnra.Fit")

' Wait 1000 ms: May be necessary for the server to start
WScript.Sleep 1000

' Open a NRA-file
Result = App.Open("c:\temp\test.nra")

' Fit thickness and composition of layer number 2
Fit.LayerNr = 2
Fit.LayerThickness = True
Fit.LayerComposition = True

' One fit region from channel 100 to 200
Fit.NumberOfRegions = 1
Fit.RegionMinChannel(1) = 100
Fit.RegionMaxChannel(1) = 200

' Perform the fit
Result = App.FitSpectrum
```

Sample program in Visual Basic Script showing how to add layers and elements.

```
' Create the application object
Set App = CreateObject("Simnra.App")

' Create the target object
Set Target = CreateObject("Simnra.Target")

' Wait 1000 ms: May be necessary for the server to start
WScript.Sleep 1000

' Open a NRA-file
Result = App.Open("c:\temp\test.nra")

' Add an empty layer: Will be the last layer
Target.AddLayer
lay = Target.NumberOfLayers

' Set the layer thickness to 1000 × 10^15 atoms/cm^2
Target.LayerThickness(lay) = 1000

' Add one element: Will be the last element
Target.AddElement(lay)
el = Target.NumberOfElements(lay)

' Set the element properties
' Attention: Au already has to be present in an already existing layer!
Target.ElementName(lay, el) = "Au"
Target.ElementConcentration(lay, el) = 1.0

' Calculate the spectrum
Result = App.CalculateSpectrum
```

Appendix B

The R33 cross section file format

The R33 cross section file format
April 2002
By I. C. Vickridge
Groupe de Physique des Solides, UMR 7588 du CNRS
Tour 23, Universits de Paris 7 et 6
2, Place Jussieu
75251 Paris

B.1 Introduction

In September 1991, in response to the workshop on cross sections for Ion Beam Analysis (IBA) held in Namur (July 1991, Nuclear Instruments and Methods B66(1992)), a simple ascii format was proposed to facilitate transfer and collation of nuclear reaction cross section data for Ion Beam Analysis (IBA) and especially for Nuclear Reaction Analysis (NRA). Although intended only as a discussion document, the ascii format - referred to as the R33 (DSIR Report 33) format - has become a de facto standard. In the decade since this first proposal there have been spectacular advances in computing power and in software usability, however the simplicity and cross-platform compatibility of the ascii character set has ensured that the need for an ascii format remains.

Nuclear reaction cross section data for Nuclear Reaction analysis has been collected and archived on the Sigmabase websites (google : Sigmabase) for about the last 7 years. This data has largely been entered in the R33 format, although there is a series of elastic cross sections that are expressed as the ratio to the corresponding Rutherford cross sections that have been entered in a format referred to as RTR (ratio to Rutherford). During this time the R33 format has been modified and added to - firstly to take into account angular distributions, which were not catered for in the first proposal, and more recently to cater for elastic cross sections expressed as the ratio-to-Rutherford, which it is useful to have for some elastic scattering programs. It is thus timely to formally update the R33 format.

There exists also the large nuclear cross section data collections of the Nuclear Data Network - the OECD NEA Nuclear data section, the IAEA Nuclear data section, and the Brookhaven National Laboratory National Nuclear Data Centre amongst others. The R33 format is proposed to become a legal computational format for the Nuclear Data Network ('Nuclear Data Needs in Ion Beam Analysis'. I.C. Vickridge. In Long Term Needs for Nuclear Data Development, Report

INDC(NDS)-428, August 2001, International Atomic Energy Agency, Vienna.). It is thus also necessary to provide an updated formal definition of the R33 format in order to provide the necessary specification for adoption of R33 as an accepted computational format.

Guiding considerations. In defining the updated R33 format I have required that previous valid R33 files should also conform to the updated format. This is so that R33 reading programs that conform to the updated specification will be able to read the existing R33 files - providing backward compatibility. There is also some redundancy in the format. This is partly from intellectual laziness, but also provides some checking of internal consistency to weed out errors.

B.2 The new R33 Format definition.

An R33 data file contains one cross section either as a function of (laboratory) incident energy, or as a function of (laboratory) detection angle. The file is made up of entries, and the data section. Each entry consists of a legal keyword followed by a colon followed by a space, followed by data in Ascii format. The keyword may be in any mixture of upper and lower case characters. Legal separators for numerical data are space, comma, colon, and semi-colon characters. Decimal points are represented only by full stops, and not by commas (as can be the case in some European countries). The legal ascii character set for the purposes of R33 files is ascii 0 to ascii FF. Apart from the 'Comment' entry and the optional 'Version' entry, entries may be in any order. Each entry ends with a carriage-return line-feed sequence. Some entries are optional [O], most are required [R], and some are mutually exclusive [Mx] where all entries for which the value of x is the same are mutually exclusive. See below for special conditions that apply to the keywords 'Comment', 'Nvalues', and 'Data', and 'EndData'. Default values are suggested for R33 reading routines, so that if an optional entry is omitted, or if a required entry is unreadable or missing illegally, the value of the corresponding variable in the reader is well-defined. All energies are expressed for the laboratory frame in keV and all angles in the laboratory frame in degrees. English is the preferred language.

Special note on data entry order: The original R33 specification called for data to be listed as x, y, xerrror, yerror, however the R33 files originally generated for the Sigmabase contained data entries in the order : x, xerror, y, yerror. The original specification was intended to allow for files containing no error information to be smaller, since the two final entries could simply be omitted. However given that the Sigmabase data fits easily on a single floppy, without compression, the file size arguments are not compelling and insisting on following the original specification will involve disrupting several existing readers, as well as introducing confusion through the existence of two families of R33 files since copies of the erroneous files will probably lie around for years in different places. So, the new specification legalises the previous erroneous usage.

B.2.1 Syntax of an R33 Entry

The syntax for the list of legal keywords and the associated data is :

Keyword: [Mx, O/R] (Default) <data type>

Note: Additional notes and guidelines concerning use of the entry. Data type may be:

string (an arbitrary series of ascii characters)

n (integer) a series of ascii characters without decimal point representing a signed integer number

r (real) a series of ascii characters that represent a signed real number. Format is fairly flexible - but only decimal points (and NOT decimal commas) are accepted. Any format that can be read in a Borland Pascal readln(r) statement is acceptable.

B.2.2 List of legal entries

Comment: [R] ('None') <String>
Note: An unlimited number of ascii characters, including single CR LF sequences, but terminating by a double CR LF sequence. There is no requirement to embed CR LF sequences within the Comment, however it is recommended to place CR LF sequences at convenient places at least every 80 characters so that if the file is printed, the comment field is printed on successive lines that are not longer than 80 characters. The double CR LF sequence that signals the end of the comment is simply a blank line. It is not felt necessary to specify an upper limit to the size of the comment, however it is expected that a useful comment would not be longer than a few tens of lines - or a few thousand characters. Note that Unix systems place only a LF character to signal an end-of-line. This is illegal for R33 files. There are freeware and shareware utilities that can add the necessary CR characters if R33 files are generated under Unix.

Version: [O] ('R33') <String>
Note: Allowed values are (case-insensitive) 'R33' and ' R33a'. This entry can be used to signal that the file conforms to the special subset of R33 files proposed by M. O. Thompson for elastic scattering cross sections for use in RUMP. Sigmabase files will always be DSIR R33, but the 'R33a' variant is detailed here for completeness. All R33a files are legal R33 files, but R33a files have the following additional conditions:
1) The Version entry is required, and must be the first entry after the Comment.
2) Only elastic cross sections can be in valid R33a files.
3) Nvalues must either not be present (so that Data and EndData entries are used), or have a value of less-than-or-equal-to zero.

Source: [R]('Unknown')<String>
Note: A concise bibliographic source (preferable) or another indication of where the data has come from (avoid if possible). This field should contain the most authoritative original source for the data. This will usually be the original publication, or thesis reference. In some cases data has been input by experimenters before or without publication. In this case this entry should contain something like 'Measured and input by D. Withrington'. It should be kept small - an upper limit of 256 characters is suggested, but not required. It would be expected that further details pertaining to Mrs Withrington would be found in the Comment.

Name: [R]('unknown')<String>

Note: The name of person or institution responsible for creating the R33 file. For R33 files automatically created from Exfor files, this would be IAEA, or NNDC, or International Nuclear Data Network or whatever. No provision is made here for including update histories, however this may be accommodated in the Comment field.

Address1: [O] (' ')<String>

⋮

Address9: [O] (' ') <String>
Note: The address of the person or institution responsible for creating the R33 file. Up to nine lines of address information may be included. This can include telephone numbers, emails and so on.

Serial Number: [R] (0) <n>
Note: The serial number will be a number providing a unique link back to the Exfor dataset from which the R33 file was generated. The default value of zero means that this number has not been assigned.

Reaction: [R] (' ') <String>
Note: the reaction string is written in a standard format that can be parsed without too much difficulty. It conforms to the usual notation of:

target nucleus(incident ion, light product)product nucleus

Nuclei are specified by their chemical symbol preceded by A : e.g. 28Si, or 6Li. The mass number is required. Some common light species may also be represented by shorthand notation, with lower case being required.
n=neutron
p=proton
d=deuterium
t=triton
a=alpha particle
h=3He
x=x-ray
g=gamma

The light product may correspond to a particular energy level of the product nucleus. This is signalled by a 'postfix' on the light product. For example, 16O(d,p1)17O is the (d,p) reaction which leaves the residual 17 oxygen in the 1st excited state. Some cross sections may be sums of several particle groups corresponding to different excited states of the compound or product nucleus. Usually such a cross section would be used when the particle groups are not resolved by the detection method employed. In this case, the postfix lists the states concerned, separated by plus signs. E.g. 14N(d,p5+6)15N. Some elastic cross sections correspond to targets having several isotopes. In this case, it is necessary to use the 'composition' keyword.

Masses: [R] (1,1,1,1)] <r,r,r,r>

Note: Four mass values in amu corresponding to the four nuclei specified in the reaction string, separated by legal separators. The order is m1, m2, m3, m4 for a reaction in which m1+m2->m3+m4. The specification of which of the two initial and final masses are m1 and m3 respectively is given by the reaction string in which we always have : m2(m1,m3,)m4, so that m1 corresponds to the projectile and m3 to the light product. At present there is no intention to cater for the few cases in which there are three or more products - for example 11B(p,a)2a. In principle the masses could be deduced directly from the reaction string, however in the interests of simplicity it seems worthwhile adding them to the R33 file to avoid having to write a reaction string parser in R33 readers. In the special case where the composition keyword is used, the values there override any contained in the Masses entry.

Zeds: [R] (1,1,1,1) <n,n,n,n>
Note: Four integers representing the atomic number of the four nuclei specified in the reaction string, in the same order as the mass entries. The Zs could also be deduced directly from the reaction string, but see the comment in the Masses entry.

Composition: [O] ('Natural') <string, r, string, r,>
Note: This entry caters for elastic cross sections measured from targets that contain a mixture of isotopes from which the elastically particles are not resolved. It consists of a list of isotopes and atom-proportions, or the value 'natural' (case insensitive) which means that a target of naturally occurring isotopic composition has been used. Isotopes are specified as for the reaction string, without shorthand notation. Example:

Target: 12C, 23.0, 13C, 26.0

If the proportions do not sum to 100, then it is assumed that they are relative amounts. In the example given, 23/49 of the atoms are 12C, and 26/49 are 13C. If the 'Composition' entry exists and has a legal value, then the values in the 'masses' entry should correspond to the appropriate weighted sum indicated in the 'composition' keyword. For example, if the target for an elastic cross section is natural silicon, then the mass given should be 28.086 - the weighted sum of stable Si isotopes in natural abundance.

Qvalue: [R] (0.0) <r, r, r, r, r>
Note: A list of up to five Q values, expressed in keV, separated by legal separators. As explained in the Reaction entry, some cross sections are for multiple particle groups, for example when the groups are not resolved experimentally. In this case a Q value is required for each particle contributing to the cross section.

Distribution: [R] ('Energy') <String>
Note: Allowed values are 'Energy', and 'Angle' . This entry says whether the data contained in this file are for a cross-section as a function of laboratory energy ('Energy') or laboratory angle ('Angle').

Theta: [M1, R] (0.0) <r>
Energy: [M1,R](1.0) <r>
Note: Theta gives the laboratory angle with respect to the incident beam, so that backscattering would be 180. Energy gives the laboratory energy of the incident beam. If both entries are present (an illegal condition) then only the entry corresponding to the keyword in the 'Distribution' entry will be used.

Sigfactors: [O] (1.0, 0.0) <r,r>
Note: Scale conversion factor and its associated error common to all the cross section data. See original R33 publication in Appendix 1 for discussion.

Units: [O] ('mb') <String>
Note: Valid values are 'mb', 'rr' and 'tot'. R33 files are always in mb/sr, or units proportional to mb/sr for differential cross sections, and mb for total cross sections. The constant of proportionality given in the enfactors entry is independent of energy. Some users find it preferable to have elastic scattering cross sections relative to the Rutherford cross section. Since the conversion factor is no longer energy-independent, the enfactors entry can no longer cater for this. In this case, the units entry should specify 'rr' for ratio to Rutherford. Nevertheless, it is recommended that elastic cross sections be stored as cross sections just like the inelastic scattering cross sections - i.e. in mb/sr. The value 'tot' indicates that the cross section is integrated over all angles, and is expressed as a function of energy. Thus if 'tot' is used as a unit then the distribution must be 'energy' and the value of theta has no meaning. Nevertheless, it is suggested that a valid real number be given for theta so that reading routines don't have to cater for non-numerical values for theta (such as 'Theta: irrelevant'!).

Enfactors: [O] (1.0, 0.0, 0.0, 0.0) <r,r,r,r>
Note: Scale conversion factors and associated errors common to all the energy or angle data. See original R33 publication in Appendix 1 for discussion.

Nvalues: [M2,R] (0)<n>
Data: [M2,R]
Enddata: [O]
Note: two methods are allowed for representing the data. The first corresponds to the original R33 specification. The data immediately following the 'Nvalues' entry consists of the cross section data, one point per line, and each point represented by four values (X, dX, Y, dY):
energy(or angle), energy(or angle) random error, sigma, sigma random error
The data ends after Nvalues lines of data.
Alternatively (and recommended), the data may be bracketed by 'Data' and 'Enddata' entries. An entry of 'Nvalues: 0' is equivalent to a 'Data' entry. The data immediately follow the Data entry, one point per line as for the Nvalues option, and the file terminates with the end of the file, or with the optional EndData entry. Nvalues is maintained for backward compatibility, but in practice most routines will simply read and count the number of lines read until the end of the file or an EndData entry is reached, so this is the preferred option. The use of the Enddata entry simply allows a check that all of the data values are contained in the file and have been read. Data entries must be arranged in order of increasing energy or angle. Duplicate energy or angle values are not allowed (the cross section must be single-valued).

Bibliography

[1] H.H. Andersen and J.F. Ziegler. *Hydrogen - Stopping Powers and Ranges in All Elements*, vol. 3 of *The Stopping and Ranges of Ions in Matter*. Pergamon Press, New York, 1977. 16, 18, 61, 61, 61, 61, 61, 64

[2] J.F. Ziegler. *Helium - Stopping Powers and Ranges in All Elements*, vol. 4 of *The Stopping and Ranges of Ions in Matter*. Pergamon Press, New York, 1977. 16, 61, 62, 62, 62, 80

[3] J.F. Ziegler, J.P. Biersack, and U. Littmark. *The Stopping and Range of Ions in Solids*, vol. 1 of *The Stopping and Ranges of Ions in Matter*. Pergamon Press, New York, 1985. 16, 16, 61, 63, 63, 63, 63, 63, 63, 64, 64, 64, 65, 65, 65

[4] J.F. Ziegler. private communication. 1997. 16

[5] J.R. Tesmer and M. Nastasi, Eds. *Handbook of Modern Ion Beam Materials Analysis*. Materials Research Society, Pittsburgh, Pennsylvania, 1995. 23, 23, 57, 57

[6] J.A. Nelder and R. Mead. Computer Journal 7 (1965) 308. 33

[7] M.S. Caceci and W.P. Cacheris. Byte, 5 (1984) 340. 33

[8] W.H. Press, B.P. Flannery, S.A. Teukolsky, and W.T. Vetterling. *Numerical Recipes*. Cambridge University Press, Cambridge, New York, 1988. 33, 34, 35, 35

[9] L. Cliche, S.C. Gujrathi, and L.A. Hamel. Nucl. Instr. Meth. B45 (1990) 270. 46, 46, 46

[10] W. Hösler and R. Darji. Nucl. Instr. Meth. B85 (1994) 602. 46

[11] E. Steinbauer, P. Bauer, M. Geretschläger, G. Bortels, J.P. Biersack, and P. Burger. Nucl. Instr. Meth. B 85 (1994) 642. 46

[12] R. Doolittle. Nucl. Instr. Meth. B9 (1985) 344. 52, 60, 60, 90

[13] R. Doolittle. Nucl. Instr. Meth. B15 (1986) 227. 52, 90

[14] G. Audi and A.H. Wapstra. Nuclear Physics A595 (1995) 409. 54

[15] P. De Bievre and P.D.P. Tylor. Int. J. Mass. Spectrom. Ion Phys. 123 (1993) 149. 54

[16] J. L'Ecuyer, J.A. Davies, and N. Matsunami. Nucl. Instr. Meth. 160 (1979) 337. 57, 57

[17] M. Hautala and M. Luomajärvi. Rad. Effects 45 (1980) 159. 57

[18] H.H. Andersen, F. Besenbacher, P. Loftager, and W. Möller. Phys. Rev. A21, 6 (1980) 1891. 57, 57

[19] M. Bozoian, K.M. Hubbard, and M. Nastasi. Nucl. Instr. Meth. B51 (1990) 311. 58

[20] M. Bozoian. Nucl. Instr. Meth. B58 (1991) 127. 58

[21] M. Bozoian. Nucl. Instr. Meth. B82 (1993) 602. 58

[22] J. Liu, Z. Zheng, and W.K. Chu. Nucl. Instr. Meth. B118 (1996) 24. 61

[23] J.F. Ziegler. Nucl. Instr. Meth. B136-138 (1998) 141. 61

[24] H. Paul, A. Schinner, and P. Sigmund. Nucl. Instr. Meth. B164-165 (2000) 212. 61

[25] H. Paul. http://www.exphys.uni-linz.ac.at/stopping/. 61

[26] J.F. Ziegler. *Stopping Cross-Sections for Energetic Ions in all Elements*, vol. 5 of *The Stopping and Ranges of Ions in Matter*. Pergamon Press, New York, 1980. 62

[27] J.F. Ziegler and J.M. Manoyan. Nucl. Instr. Meth. B35 (1988) 215. 63, 63, 63, 64, 64, 65, 65, 66, 66, 66

[28] W.H. Bragg and R. Kleeman. Philos. Mag. 10 (1905) 318. 65

[29] D. Boutard, W. Möller, and B.M.U. Scherzer. Phys. Rev. B38, 5 (1988) 2988. 66

[30] D.I. Thwaites. Nucl. Instr. Meth. B27 (1987) 293. 66

[31] E. Szilágy, F. Pászti, and G. Amsel. Nucl. Instr. Meth. B100 (1995) 103. 67, 68, 70, 70, 75, 78, 79, 79, 85, 85

[32] E. Szilágy. Nucl. Instr. Meth. B161-163 (2000) 37. 67

[33] M.A. Kumakhov and F.F. Komarov. *Energy Loss and Ion Ranges in Solids*. Gordon and Breach Science Publishers, New York, London, Paris, 1981. 68, 68

[34] J.R. Bird and J.S. Williams, Eds. *Ion Beams for Materials Analysis*. Academic Press, Sydney, New York, Tokyo, 1989. 68, 68, 68

[35] J. Tirira, Y. Serruys, and P. Trocellier. *Forward Recoil Spectrometry*. Plenum Press, New York, London, 1996. 68

[36] P.V. Vavilov. Soviet Physics J.E.T.P. 5 (1957) 749. 68, 68

[37] N. Bohr. Mat. Fys. Medd. Dan. Vid. Selsk. 18, 8 (1948) . 68, 69

[38] J.W. Mayer and E. Rimini. *Ion Handbook for Material Analysis*. Academic Press, New York, San Francisco, London, 1977. 68, 69, 69, 69, 70, 70, 73

[39] M.G. Payne. Phys. Rev. 185, 2 (1969) 611. 68

[40] C. Tschalär. Nucl. Instr. Meth. 61 (1968) 141. 68

[41] C. Tschalär. Nucl. Instr. Meth. 64 (1968) 237. 68

[42] W.K. Chu. Phys. Rev. 13 (1976) 2057. 69, 69

[43] O. Schmelmer, G. Dollinger, C.M. Frey, A. Bergmaier, and S. Karsch. Nucl. Instr. Meth. B145 (1998) 261. 73, 73

[44] D. Dieumegard, D. Dubreuil, and G. Amsel. Nucl. Instr. Meth. 166 (1979) 431. 75, 75

[45] A. Weber, H. Mommsen, W. Sarter, and A. Weller. Nucl. Instr. Meth. 198 (1982) 527. 78

[46] A. Weber and H. Mommsen. Nucl. Instr. Meth. 204 (1983) 559. 78

[47] E. Steinbauer, P. Bauer, and J.P. Biersack. Nucl. Instr. Meth. B 45 (1990) 171. 78, 104

[48] P.Bauer, E. Steinbauer, and J.P. Biersack. Nucl. Instr. Meth. B79 (1993) 443. 78, 104

[49] W. Eckstein and M. Mayer. Nucl. Instr. Meth. B153 (1999) 337. 78, 104

[50] P. Sigmund and K.B. Winterbon. Nucl. Instr. Meth. 119 (1974) 541. 78, 79

[51] A.D. Marwick and P. Sigmund. Nucl. Instr. Meth. 126 (1975) 317. 78

[52] J.P. Biersack and W. Eckstein. Appl. Phys. A34 (1984) 73. 80

[53] W. Eckstein. *Computer Simulation of Ion-Solid Interactions*, vol. 10 of *Materials Science*. Springer, Berlin, Heidelberg, New York, 1991. 80

[54] R.D. Edge and U. Bill. Nucl. Instr. Meth. 168 (1980) 157. 90

[55] A.R. Knudson. Nucl. Instr. Meth. 168 (1980) 163. 90

[56] J.R. Bird, P. Duerden, D.D. Cohen, G.B. Smith, and P. Hillery. Nucl. Instr. Meth. 218 (1983) 53. 90

[57] C.P. Hobbs, J.W. McMillan, and D.W. Palmer. Nucl. Instr. Meth. B30 (1988) 342. 90

[58] M. Wüest and P. Bochsler. Nucl. Instr. Meth. B71 (1992) 314. 90

[59] I.M. Yesil. Einfluß der Oberflächenrauhigkeit auf ERDA-Tiefen-Profile. Master's thesis, Ludwig Maximilian Universität, München, 1995. In german. 90, 90

[60] I.M. Yesil, W. Assmann, H. Huber, and K.E.G. Löbner. Nucl. Instr. Meth. B136-138 (1998) 623. 90, 90, 90

[61] A. Kitamura, T. Tamai, A. Taniike, Y. Furuyama, T. Maeda, N. Ogiwara, and M. Saidoh. Nucl. Instr. Meth. B134 (1998) 98. 90

[62] R. Behrisch, S. Grigull, U. Kreissig, and R. Grötschel. Nucl. Instr. Meth. B136-138 (1998) 628. 90

[63] V.S. Shorin and A.N. Sosnin. Nucl. Instr. Meth. B72 (1992) 452. 90, 90

[64] H. Metzner, M. Gossla, and Th. Hahn. Nucl. Instr. Meth. B124 (1997) 567. 90, 90, 90

[65] H. Metzner, Th. Hahn, M. Gossla, J. Conrad, and J.-H. Bremer. Nucl. Instr. Meth. B134 (1998) 249. 90, 90, 90

[66] M. Mayer, R. Behrisch, P. Andrew, and A.T. Peacock. J. Nucl. Mater. 241-243 (1997) 469. 94

[67] M. Mayer, R. Behrisch, C. Gowers, P. Andrew, and A.T. Peacock. Change of the optical reflectivity of mirror surfaces exposed to JET plasmas. In *Diagnostics for Experimental Thermonuclear Fusion Reactors 2*, P. Stott, G. Gorini, P. Prandoni, and E. Sindoni, Eds. Plenum Press, New York, London, 1998, p. 279. 94, 94

[68] M. Küstner, W. Eckstein, E. Hechtl, and J. Roth. J. Nucl. Mater. 265 (1999) 22. 96

[69] R. Amirikas, D.N. Jamieson, and S.P. Dooley. Nucl. Instr. Meth. B77 (1993) 110. 101, 107

[70] J. Vorona, J.W. Olness, W. Haeberli, and H.W. Lewis. Phys. Rev. 116 (1959) 1563. 107

[71] M. Wielunski, M. Mayer, R. Behrisch, J. Roth, and B.M.U. Scherzer. Nucl. Instr. Meth. B122 (1997) 113. 109

[72] J.E.E. Baglin, A.J. Kellog, M.A. Crockett, and A.H. Shih. Nucl. Instr. Meth. B64 (1992) 469. 109

[73] F. Besenbacher, I. Stensgaard, and P. Vase. Nucl. Instr. Meth. B15 (1986) 459. 109